CHEMISORPTION AND ANODIC OXIDATION OF AROMATIC MOLECULES ON PD ELECTRODE SURFACES: STUDIES BY UHV-EC-STM

A Dissertation

by

XIAOLE CHEN

Submitted to the Office of Graduate Studies of
Texas A&M University
in partial fulfillment of the requirements for the degree of

DOCTOR OF PHILOSOPHY

December 2004

Major Subject: Chemistry

CHEMISORPTION AND ANODIC OXIDATION OF AROMATIC MOLECULES ON PD ELECTRODE SURFACES: STUDIES BY UHV-EC-STM

A Dissertation

by

XIAOLE CHEN

Submitted to Texas A&M University
in partial fulfillment of the requirements
for the degree of

DOCTOR OF PHILOSOPHY

Approved as to style and content by:

_____	_____
Manuel P. Soriaga (Chair of Committee)	Marvin W. Rowe (Member)
_____	_____
D. Wayne Goodman (Member)	A. John. Appleby (Member)
	_____
	Emile A. Schweikert (Head of Department)

December 2004

Major Subject: Chemistry

ABSTRACT

Chemisorption and Anodic Oxidation of Aromatic Molecules on Pd Electrode Surfaces: Studies by UHV-EC-STM. (December 2004)

Xiaole Chen, B.S., Hunan Normal University; M.S., Beijing Normal University

Chair of Advisory Committee: Dr. Manuel P. Soriaga

The chemisorption and anodic oxidation of hydroquinone (H_2Q) and benzoquinone (BQ) at palladium electrode surfaces was studied by a combination of electrochemistry (EC), Auger electron spectroscopy (AES), high-resolution electron-energy loss spectroscopy (HREELS) and electrochemical-scanning tunneling microscopy (EC-STM) on a smooth polycrystalline and well-defined (single-crystalline) Pd(100) electrode surface. The results point to the following more critical conclusions: (*i*) Chemisorption of H_2Q from dilute (≤ 0.1 m*M*) aqueous solutions forms surface-coordinated BQ oriented parallel albeit with a slight tilt. (*ii*) At high concentrations (≥ 1 m*M*), chemisorption yields an edge-vertical oriented diphenolic species. (*iii*) The extent of anodic oxidation of the chemisorbed organic strongly depends upon its initial orientation; only the flat-adsorbed species are oxidized completely to carbon dioxide. (*iv*) The rate of anodic oxidation is likewise dependent upon the initial adsorbate orientation; the rate for vertically-oriented species is more than twice that of flat-adsorbed species. (*v*) The chemisorbed species are not oxidized (to the same extent)

simultaneously; instead, oxidation occurs one molecule at a time. That is, molecules that survive the anodic oxidation and remain on the surface retain their original identities.

ACKNOWLEDGMENTS

I would like to thank my advisor and committee chair, Professor M. P. Soriaga, for his incessant support throughout the years of my stay at Texas A&M University. His guidance and encouragement have always been an inspiration to me. I would also like to express my great gratitude to my committee members: Dr. Gy. Vigh, Dr. W. Goodman, Dr. A. J. Appleby and Dr. M. Rowe. Their advice has been essential in the completion of this research.

Many thanks go to the previous and current members of Dr. Soriaga's group: Dr. C. Wang, Dr. Y.-G. Kim, Yeon-Su, Juan, and Akhtar. Special thanks go to Dr. J. Soto who has been my mentor, and to J. Sanabria and J. Baricuatro for all the assistance in my experiments. I would like to thank all of them for the help and excellent teamwork. Working with them has been really an enjoyable and mind-opening experience.

I dedicate this dissertation to my beautiful baby girl, Angela Liu, who was born during the busy days of my research. Love and thanks go to my husband, Fenghua Liu, and my parents, Keheng Chen and Fangying Wan. I cannot imagine how I could reach this stage without their love and support.

This research was financially supported by the National Science Foundation and Robert A. Welch Foundation. I am very grateful for having been given the chance to work on this remarkable research project.

TABLE OF CONTENTS

Page

LIST OF FIGURES

FIGURE Page

FIGURE Page

FIGURE Page

FIGURE Page

FIGURE Page

LIST OF TABLES

INTRODUCTION

In electrochemical surface science, electrode/electrolyte interfaces are of fundamental interest. All electron-transfer processes originate at electrified interfaces. Examples are: metal corrosion, electrochemical sensors, batteries and fuel cells, and digital etching. It is clear that a complete understanding of the mechanisms and dynamics of complex electrochemical processes must include a sound knowledge of the nature of the electrode/electrolyte interface. Limitations of surface-sensitive analytical tools initially hindered progress in the study on the interface in the past. Recent advances in surface science techniques, in combination with classical electrochemical methods, have allowed successful ventures into atomic-level studies of the electrode/electrolyte interface.

As early as in 1879, the first model of the electrode/electrolyte interface was proposed by Helmholz. The Gouy-Chapman-Stern model of the electrical double-layer was later presented based on the Helmholz model [1]. Although these models helped delineate the physics and chemistry of the spatial region where electron transfer takes place, they are not sufficient in describing real systems because they do not take into account: (i) the influence of geometric and electronic surface structure, and (ii) the nature of interfacial ionic and/or molecular interactions. A more practical model is shown in Figure 1. This model includes the atomic structure of the electrode, the specifically adsorbed species and water molecules in the interface structure [2].

This dissertation follows the style of *Electroanalysis*.

Palladium has long been used as a catalyst for heterogeneous hydrogenation processes [3]. Its catalytic effect on the oxidation of both primary and secondary benzylic and aliphatic alcohols has been documented [4,5,6]. Compared to its congeners, Pt and Ni, Pd has a lower dissociation and atomization enthalpy; in effect, Pd has the weakest intermetallic bonds in its group [7]. The formation of Pd-adsorbate bonds is in turn made easier, making Pd a good catalyst in many chemical reactions. Pd has also been extensively used as an ideal electrode material because of its desirable electrocatalytic properties and relatively noble nature [8]. For example, Pd has been reported to be a good electrocatalyst for electrochemical selective carbonylation of methanol to dimethyl carbonate and dimethyl oxalate, two very important chemicals for the current chemical industry [9]. Electrochemical oxidation of formic acid using electrochemically deposited Pd electrode has also been recorded [10]. While most of these studies focused on the practical applications of Pd as a catalyst, fundamental studies on the mechanism of reactions occurring on the Pd surfaces are rare. The motivation of this project is to help map out the mechanism of an electrochemical reaction of a model organic compound. The organic compounds under study are the redox pair, hydroquinone and benzoquinone.

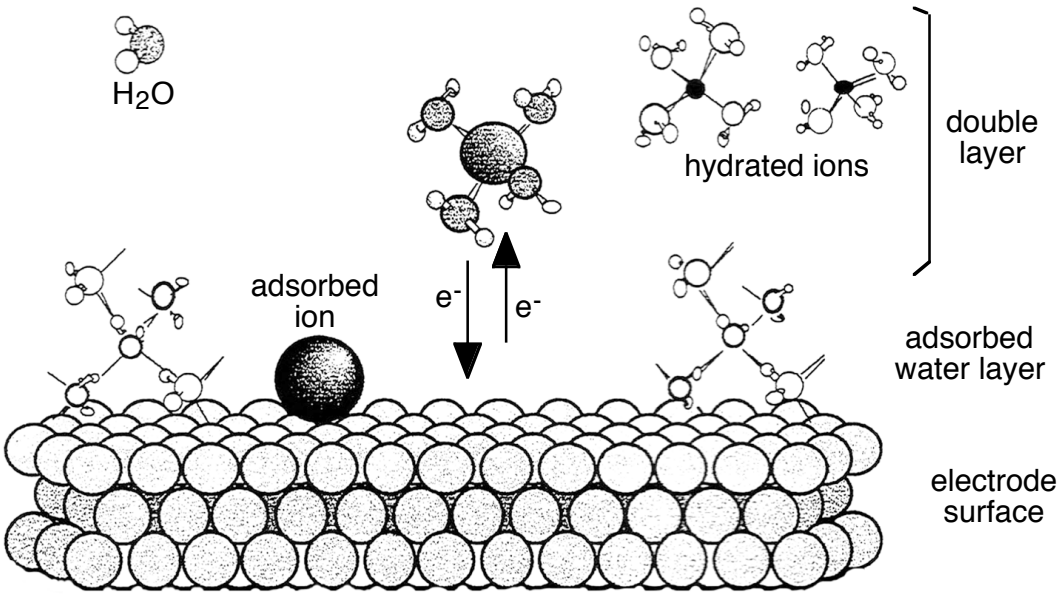

Figure 1. Contemporary atomic-scale model of the electrode/electrolyte interface [2].

Background

Chemisorption of hydroquinone (H_2Q) and benzoquinone (BQ) on polycrystalline Pt electrodes was first studied using thin-layer electrochemistry (TLE) by Soriaga et al [11, 12]. It was found that both H_2Q and BQ undergo spontaneous and irreversible chemisorption on Pt electrodes. A stepwise chemisorption isotherm was obtained. (Figure 2). Two plateaus in the isotherm were found to be related to (non-random) orientations of the adsorbates as indicated by a molecular model based on covalent and van der Waals radii (Figure 3) [13]. In this model, the orientation-dependent molecular cross-section (σ) of each molecule was represented by the area shadowed by a rectangular solid unit cell in which the organic molecule is enclosed. The cross-sections at flat (η^6), edge-vertical (η^2), and end-vertical (η^1) orientations were calculated and compared to the cross-section obtained from the TLE experiment using the equation:

$$\sigma\ (\text{Å}^2/\text{molecule}) = 10^{16}/(N_A\Gamma) \qquad (1)$$

where Γ is the packing density (mol/cm^2) and N_A is Avogadro's constant. It was revealed that the lower plateau (σ_{exp} = 52.7 $Å^2$) in the isotherm corresponded to a flat (η^6) orientation (σ_{model} = 53.8 $Å^2$), while the upper plateau (σ_{exp} = 27.9 $Å^2$) indicated the presence of an edge-vertical (η^2)- oriented (σ_{model} = 28.6 $Å^2$) adlayer.

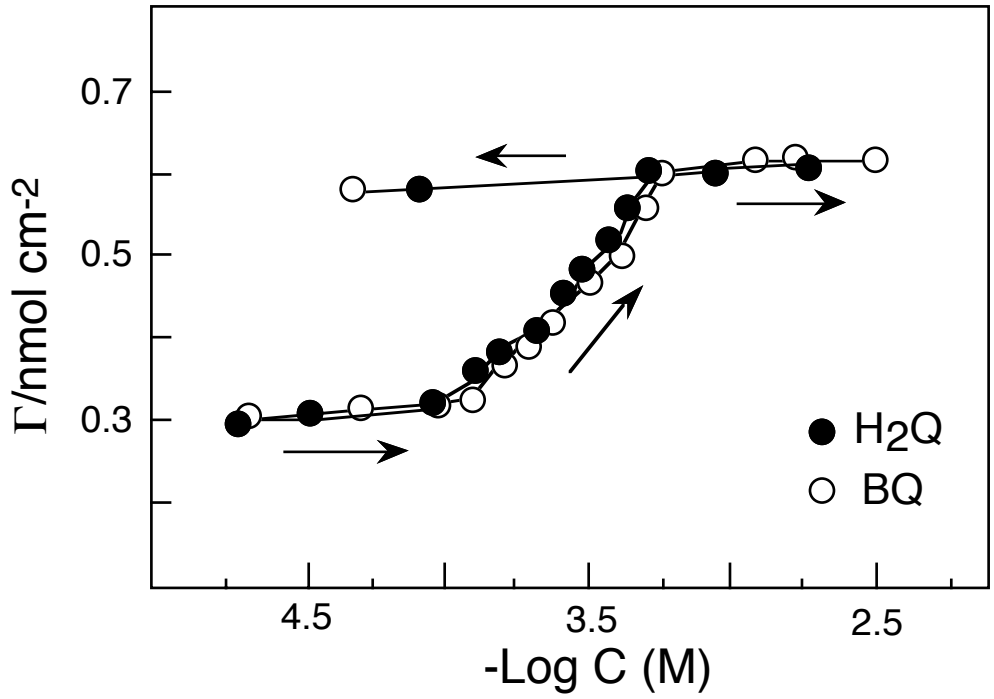

Figure 2. Chemisorption isotherms, Γ vs. -log C plots, from H_2Q and BQ solutions at a smooth polycrystalline Pt electrode.

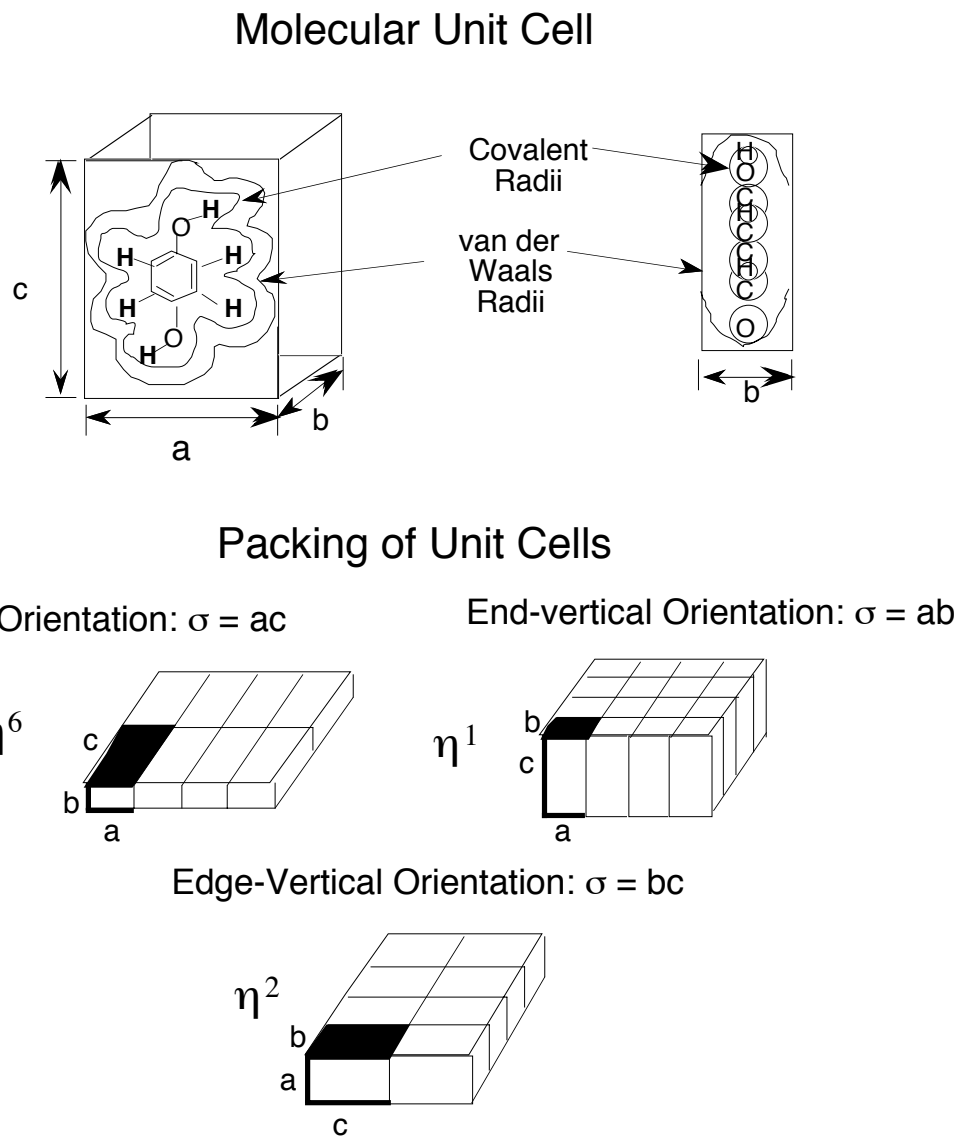

Figure 3. Molecular unit cells adopted in the calculations of the adsorbed molecule cross-sections [11].

The orientation assignments were supported by infrared reflection-absorption spectroscopy [14]. It was additionally shown that spectra obtained when H_2Q or BQ was chemisorbed were identical; this implied that, regardless of the starting material, the same species was formed on the surface:

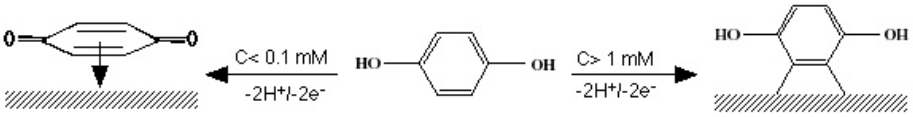

(2)

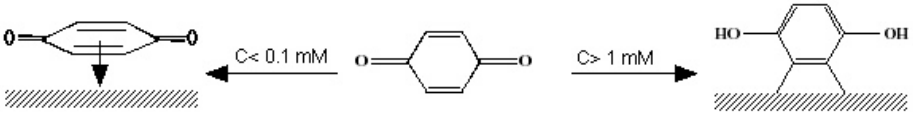

(3)

Molecular orientation was found to play a vital role in catalytic oxidation of chemisorbed H_2Q or BQ [15,16]. The oxidation process was characterized by n_{ox}, the number of electrons transferred to oxidize and desorb an adsorbed molecule. n_{ox} was determined using the following equation:

$$n_{ox} = \frac{Q_{ox}}{FA\Gamma} \tag{4}$$

where Q_{ox} is the anodic oxidation electrolytic charge and A is the area of the electrode. Results showed that the magnitude of n_{ox} was strongly dependent on the initial molecular orientation.

Electrocatalytic hydrogenation of chemisorbed η^6-BQ and η^2-H_2Q on Pt was also studied [17]. The number of electrons (n_H) transferred during hydrogenative desorption was used to characterize the hydrogenation process:

$$n_H = \frac{Q_H}{FA\Gamma} \tag{5}$$

As with n_{ox}, n_H was found to vary with orientation of adsorbed molecules [17]. The orientation-dependent electrocatalytic oxidation and hydrogenation of chemisorbed H_2Q and BQ at polycrystalline Pt may be summarized as [18]:

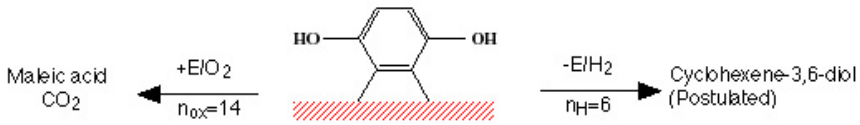

(6)

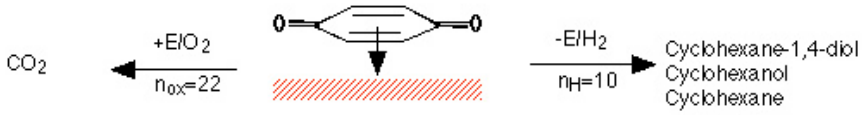

(7)

Studies on the chemisorption of H_2Q and BQ were extended to Pt(111) electrodes [19] and Pd(111) electrodes [20] using ultrahigh vacuum techniques. However, no detailed investigation has been undertaken to understand the nature of the adsorbed species in the progress of the oxidation and/or hydrogenation reactions.

Objective

The primary objective of this research is to document the critical surface science aspects of electrocatalysis at Pd surfaces. Specifically, electrochemical oxidation of a prototypical aromatic compound, hydroquinone, and its redox pair, benzoquinone, at Pd electrode surfaces was studied.

EXPERIMENTAL

Thin Layer Electrochemistry (TLE)

In thin layer electrochemistry (TLE), the entire quantity of reactants and electrolyte is confined within a thin layer of solution (2 - 50 μm). There are a few attractive features associated with TLE. (*i*) The absence of diffusional mass transport from the bulk solution facilitates interpretation of the voltammetric (current-vs.-potential) curve; (*ii*) Small volume inside the thin-layer cavity offers high sensitivity and little contamination; (*iii*) Large surface area-to-volume ratio amplifies the surface reactions. In this study, TLE served to survey processes that were later studied in great detail by surface spectroscopy and microscopy.

The thin-layer cell design used in this study is shown in Figure 4-A. In cells of this design, the electrolyte is contained inside a thin space between a cylindrical polycrystalline Pd electrode and the glass wall that surrounds it. Located near the bottom tip of the cell are two tiny pinholes through which the spent solution is removed when pressurized N_2 is passed through it. The thin-layer cavity is refilled with fresh solution by capillary action after the N_2 flow is stopped.

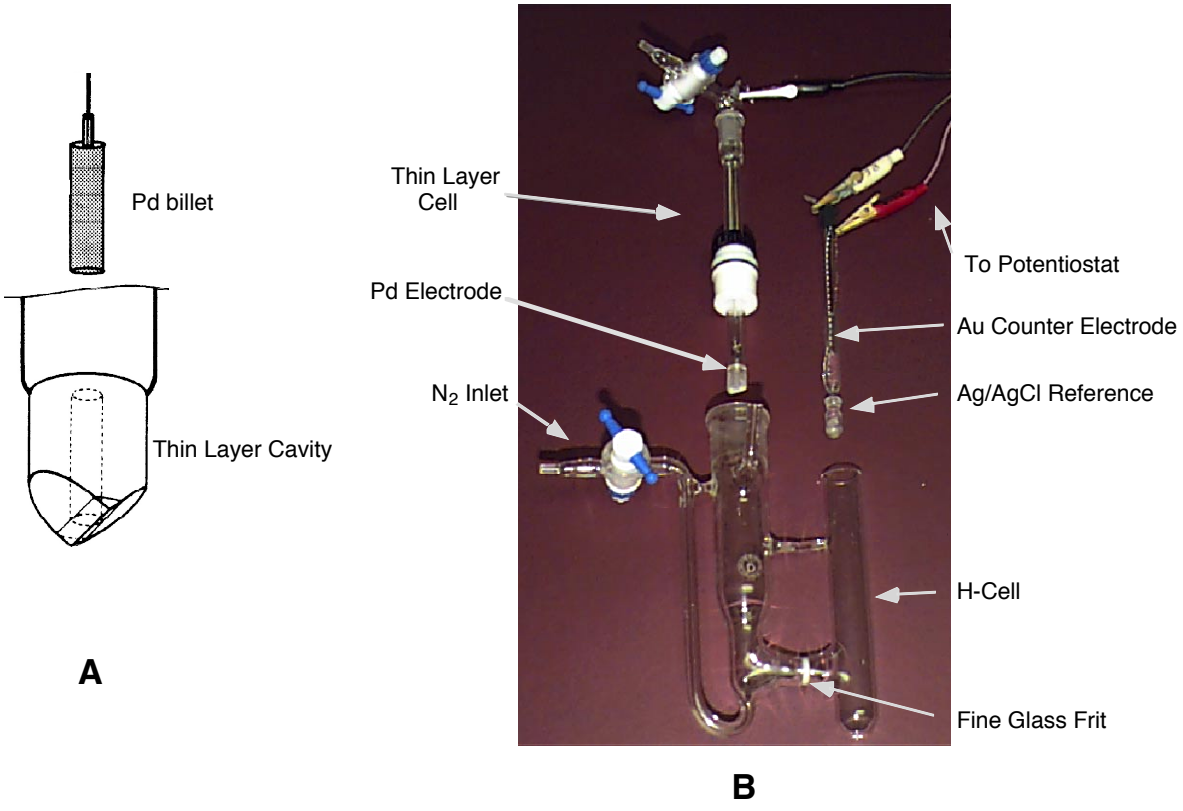

Figure 4. A: Magnified thin-layer cavity and the Pd billet; B: a thin-layer electrode and H-cell set-up.

When in use, a thin-layer cell is placed in the working-electrode compartment of an H-cell such that the pinholes are slightly below the meniscus of the electrolyte solution. The other compartment of the H-cell holds the reference electrode (Ag/AgCl, 1 *M* NaCl) and the auxiliary electrode (Pt wire), as shown in Figure 4-B. The experiments were performed using a conventional potentiostat (CV-27, Bioanalytical Systems Inc., West Lafayette, IN). The output was plotted on an X-Y recorder (Soltec, VP-6414S, Sun Valley).

The Pd electrode used in this study was fabricated from a pure Pd rod (99.99%, Wilkinson Co., Westlake Village, CA). The surface was metallographically polished with successive finer grades of diamond paste compounds (Beuhler Ltd., Evanston, IL) to a near mirror finish. The electrode billet was thermally annealed to redness in a hydrogen-oxygen flame, followed by quenching in Millipore water. This preparative procedure renders the surface to be near atomically smooth, with less than 5% surface roughness [21]. In this study, the surface area of the Pd electrode (1.26 cm^2) was calculated from its geometric area with an allowance for surface roughness factor of 1.05 [21]. Unlike Pt, there is no hydrogen chemisorption on Pd, and surface-area quantitation by adsorbed-iodine oxidation [21] results in the anodic dissolution of Pd [22, 23].

The volume of the thin-layer cavity (3.56 μL) was evaluated coulometrically based upon the Fe^{3+}/Fe^{2+} redox couple:

$$Fe^{3+} + e \leftrightarrow Fe^{2+} \qquad (8)$$

The standard solution was consisted of 1 m*M* (known to four significant figures) Fe^{2+} in 1 *M* H_2SO_4. The volume of the thin-layer cell can be obtained according to Faraday's Law:

$$V = \frac{Q}{nFC} \tag{9}$$

where Q is the electrolytic charge required for oxidation of Fe^{2+} to Fe^{3+}, C the concentration of the solute, V the volume of the thin-layer cavity, F the Faradaic constant, and n the number of electrons transferred during the oxidation. Two typical electrochemical experiments (voltammetry and potential-step coulommetry) are conducted using the system described above.

Voltammetry is generally a convenient starting electrochemical technique for a new system. In this technique, the potential applied to the working electrode is changed at a constant rate, and the current produced by the system is monitored as a function of the applied potential. The most popular type of voltammetry is cyclic voltammetry (CV). In CV, the applied potential is scanned linearly from an initial value, E_1, to a second value, E_2, then the scan direction is reversed and the potential is scanned back to E_1 (or some other potential).

Potential-step coulometry is employed to measure the charge transferred during anodic oxidation of electroactive species adsorbed on the electrode surface. Electrolytic charge is measured when the applied potential is stepped from an initial value, where no faradaic reaction occurs, to a final potential, where certain amount of faradaic current flows. According to Faraday's law, the electrolytic charge is related to the surface concentration of the adsorbate, Γ:

$$Q - Q_b = nFA\Gamma \qquad (10)$$

where Q is the total charge measured with the adsorbed species present on the surface only, and Q_b is the background charge (obtained in the same manner but I the absence of the adsorbed species), n the number of electrons transferred, F the Faraday's constant, and A the electrode surface area.

Measurement of Surface Coverage

Measurement of absolute surface concentrations was based on the removal of hydroquinone (H_2Q) or benzoquinone (BQ) sample from the solution phase when chemisorbed onto the Pd electrode. Since only unadsorbed H_2Q (or BQ) exhibits reversible quinone-diphenol redox reaction, the amount of unadsorbed molecules can be calculated from the difference between the H_2Q (or BQ) concentration in the bulk and inside the thin-layer cell (after chemisorption).

A single filling of TLE introduces a precise amount of solute into the thin-layer cavity. If the bulk concentration (C^o) were relatively low (less than 1 mM), the majority of the solute would be chemisorbed onto the clean surface; as a result, there is a significant decrease in the solute concentration (C) inside the thin-layer cavity:

$$VC = VC^0 - A\Gamma \qquad (11)$$

where Γ (mol/cm^2) is the absolute surface concentration (packing density) of the chemisorbed organic, A (cm^2) is the surface area of the electrode, and V is the volume of the thin layer cavity. Based on Faraday's law, the single-filling electrolytic charge (Q_1-Q_{1b}, where Q_{1b} is the background charge obtained in an otherwise identical experiment

in which the dissolved reactant has been rinsed from the cell) required for the reversible quinone/diphenol reaction of the unadsorbed material equals:

$$Q_1 - Q_{1b} = nFVC = nFVC^0 - nFA\Gamma \qquad (12)$$

If the thin-layer cavity is then flushed and refilled with the reactant solution multiple times so that the electrode surface is saturated with adsorbed species and the reactant concentration equals that in the bulk solution, C^0, the electrolytic charge, Q, is given by:

$$Q - Q_b = nFVC^0 \qquad (13)$$

An expression for the surface coverage is derived when Equation (12) is subtracted from Equation (13):

$$\Gamma = \frac{(Q - Q_b) - (Q_1 - Q_{1b})}{nFA} \qquad (14)$$

In general, the charge due to the background current remains the same from one filling to another. Equation (14) can be further simplified to:

$$\Gamma = \frac{Q - Q_1}{nFA} \qquad (15)$$

Equation (15) gives only the amount of molecules adsorbed onto the substrate in a single filling. In most cases, the substrate will not be saturated after only one filling. To calculate the total amount of adsorbed molecules on the surface, i.e., the surface concentration, the amounts of adsorbed molecules from all the fillings, ranging from the very first filling (when the substrate is clean) up to the last filling (when the substrate is saturated with the adsorbate), have to be summed. This gives us:

$$\Gamma = \sum_{t=1}^{x} \Gamma_t = \sum_{t=1}^{x} \frac{(Q - Q_t)}{nFA} \qquad (16)$$

where t denotes the number of fillings.

Measurement of n_{ox}

n_{ox} is the number of electrons transferred during the oxidation of one chemisorbed molecule, and it reflects the stoichiometry of the following oxidation process:

$$\text{Aromatic}_{(ads)} + O_2 \rightarrow \text{Oxidation Products} + n_{ox}\, e^- + H_2O$$

The greater n_{ox} is, the more complete the electrochemical oxidation reaction is. It is also obvious that changes in n_{ox} are indicative of changes in the oxidation product distribution.

Based on Faraday's law, determination of n_{ox} requires precise measurements of the surface concentration (Γ) and the electrolytic charge (Q_{ox}) for oxidation of the chemisorbed species.

$$n_{ox} = \frac{Q_{ox} - Q_{ox,b}}{FA\Gamma} \qquad (17)$$

Q_{ox} can be determined by potential-step coulometry. A background charge $Q_{ox,b}$ due to oxidation of the substrate is determined coulometrically in the same manner as Q_{ox}, but in the absence of chemisorbed species.

Ultrahigh Vacuum Electrochemistry (UHV-EC)

The information derived from traditional electrochemistry methods, such as TLE, represents only the macroscopic properties of the electrode-electrolyte interface. In order to obtain an atomic-level perspective of the electrochemical interface, ultra-high vacuum electrochemistry (UHV-EC) approaches were employed. To avoid any ambiguities that

might be derived from the experimental process, the following measures have been taken: (*i*) surfaces with uniformed composition and well-characterized structure, Pd(100) single crystal electrode surface in this case, are utilized as the working electrode in the UHV-EC studies; (*ii*) highly purified chemical reagents and gases are employed to avoid contaminations from any trace-level impurities; and (*iii*) highly sensitive surface analysis techniques are used to extract detailed structural and compositional information about important surface intermediates formed on the surface before and after the electrochemical reactions.

Most surface sensitive techniques take advantage of the low kinetic energy properties of low-energy electrons (usually with a kinetic energy ranging from 10 to 500 eV). Because the low kinetic energy that these electrons bear renders them a minimum mean free path (4 - 20 Å) through a solid, the employment of low-energy electrons in these techniques ensures that the information obtained belongs to the topmost surface layers, not from the bulk [24,25,26,27,28,29]. On the other hand, standard structure characterizing techniques such as X-ray diffraction (XRD) provide information characteristic of the bulk rather than the surface because of the deep penetration of X-rays into the bulk material.

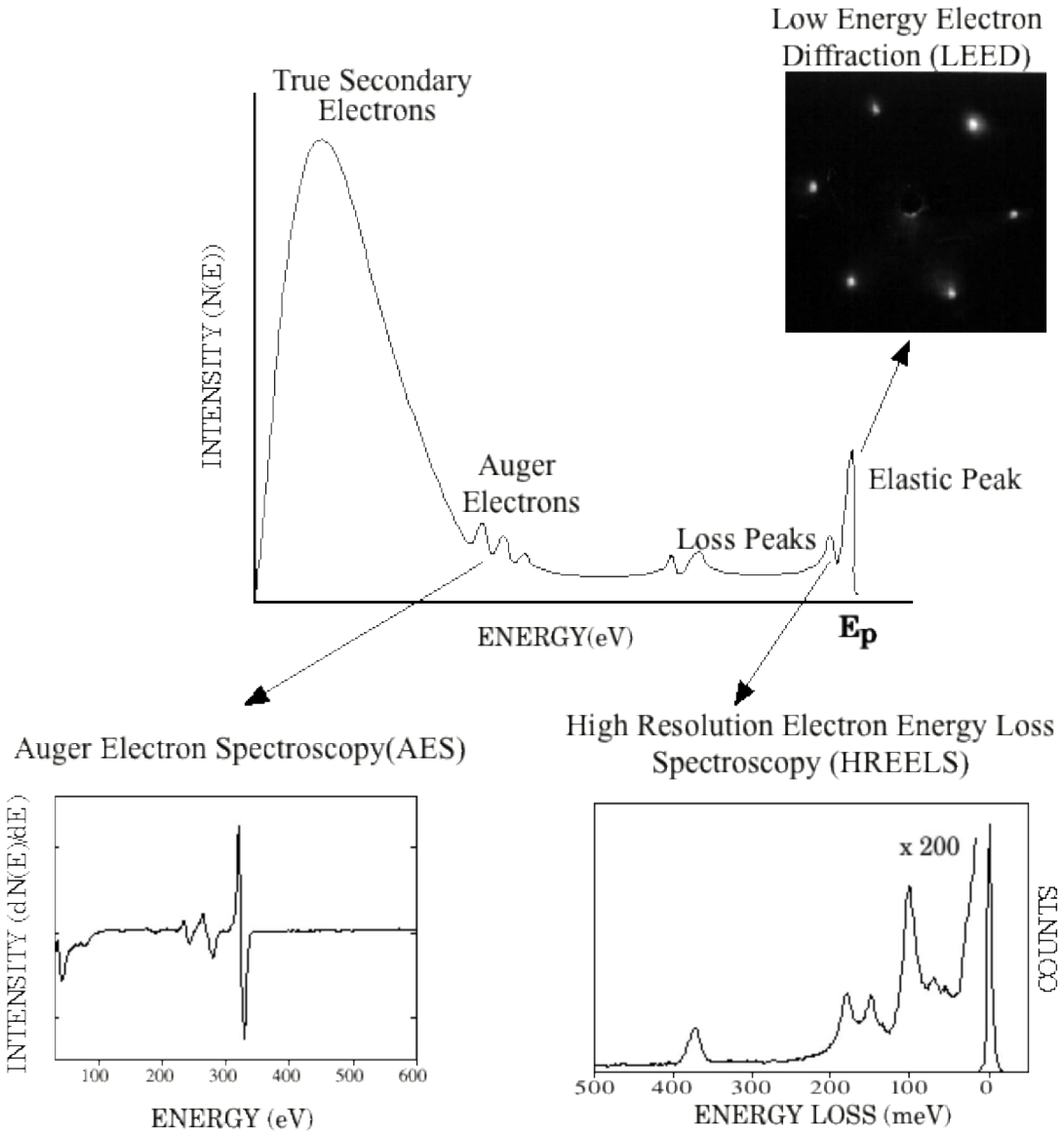

Figure 5. Energy distribution of scattered electrons.

When a solid surface is subjected to a beam of electrons of incident energy E_P, it backscatters and emits electrons with an energy distribution depicted in Figure 5, which is a plot of the number of electrons N(E) as a function of the electron energy E. Backscattered and emitted electrons are also called primary and secondary electrons, respectively. The energy distribution plot can be divided into four regions. (*i*) The elastic peak at E_P is a result of primary electrons that are scattered elastically (these electrons comprise only a few percent of the total incident electrons). (*ii*) The energy loss peaks appearing on the lower energy side of the elastic peak are caused by inelastically scattered primary electrons upon interactions with surface adsorbed species. (*iii*) The small peaks residing in the medium-energy range of the spectrum are attributed to Auger electrons and primary electrons that are inelastically scattered upon interactions with the electronic states in the solid. (*iv*) The broad peak at the lower end of the spectrum is created by true secondary electrons, a result of multiple inelastic interactions between the incident and bound electrons.

Surface analysis techniques employed in this study make use of the low-energy electrons in regions (*ii*) and (*iii*) of the energy distribution spectrum. They are high-resolution electron energy loss spectroscopy (HREELS) and Auger electron spectroscopy (AES). The general principles of these techniques will be briefly discussed.

Auger Electron Spectroscopy (AES)

AES is one of most popular techniques for surface elemental analysis [30]. The formation of Auger electrons is depicted in Figure 6-A. When a beam of electrons of energies typically between 2 to 10 KeV strikes a solid sample surface, a core (in Figure 6, K) level electron is emitted. An electron in an upper (L_1) level fills into the vacancy in the core level immediately, releasing its energy (E_K-E_1), which is transferred to another electron in a different upper level such as L_3, resulting in its ejection. The second emitted electron (from L_3) is the Auger electron, and is labeled as KL_1L_3 to indicate the energy levels involved. The kinetic energy (E_A) of this Auger electron is given by:

$$E_A = E_K - E_{L_1} - E_{L_3} - e\varphi_{SP} \qquad (18)$$

where e is the electronic charge and φ_{SP} is the spectrometer work function. E_A is characteristic of a given atom which affords AES the element-specificity. Since there are a total three electrons involved in the overall Auger process, it is obvious that AES is not applicable for the analysis of elements H and He. Even though the incident electrons are of high energies, the emitted Auger electrons are normally of much lower energies. Therefore, AES is still a surface sensitive technique.

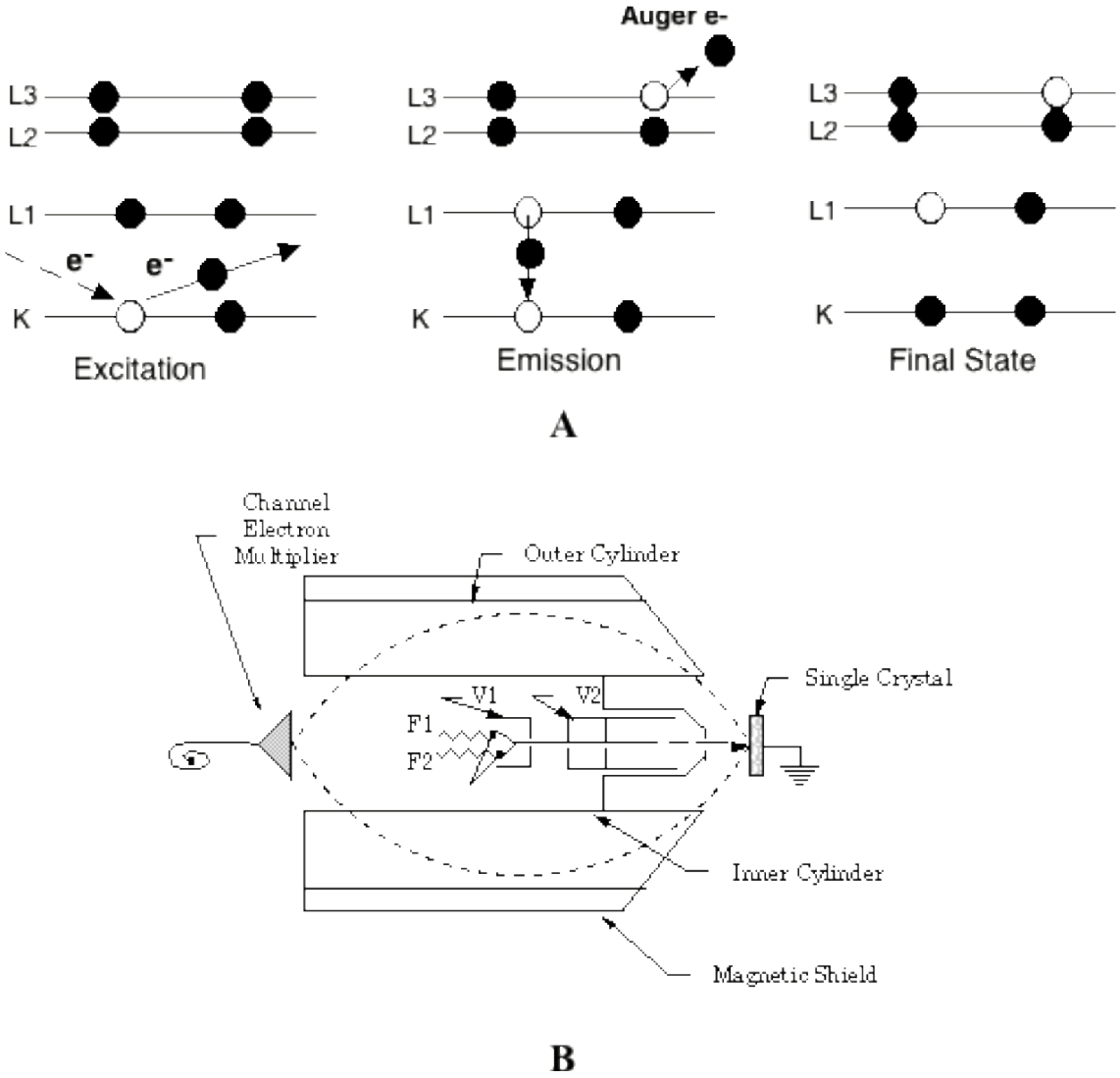

Figure 6. A: The Auger emission process. B: Schematic diagram of the cylindrical mirror analyzer.

The energy analyzer employed in our AES system is a PE 10-155 cylindrical mirror analyzer (CMA, Perkin Elmer, Eden Praire, MN), depicted in Figure 6-B. The analyzer consists of two coaxial cylinders. In the center of the inner cylinder is located an electrostatic electron gun, from which the incident electron beam is generated. Energy analysis of the emitted Auger electrons is achieved by application of a negative ramp voltage to the outer cylinder while the inner cylinder is held at ground. The ramped potential applied to the outer cylinder is proportional to the kinetic energy of the selected Auger electrons. Only electrons with the appropriate energy will be deflected and pass between the two cylinders. A channel electron multiplier is positioned at the outlet of the cylinders, serving as the detector. In measurement, the CMA is scanned nominally at 5 eV/S. The electron gun beam current is adjusted 1 μA above background. Low incident beam currents are employed to minimize any electron-beam-induced damage on the surface.

AES is a powerful technique for qualitative surface elemental analysis. For a surface with a certain elemental composition, AES renders a unique derivative (dN(E)/dE) spectrum. Identification of each element present on the surface is achieved by measuring the kinetic energy of its Auger electrons, which give characteristic peaks in the obtained AES spectrum. AES spectra of most elements have been documented for routine identification purposes [31]. Figure 7 shows an AES spectrum of a clean and ordered Pd(100) surface. In this study, surface cleanness is ascertained by the presence of only Pd peaks in AES spectrum.

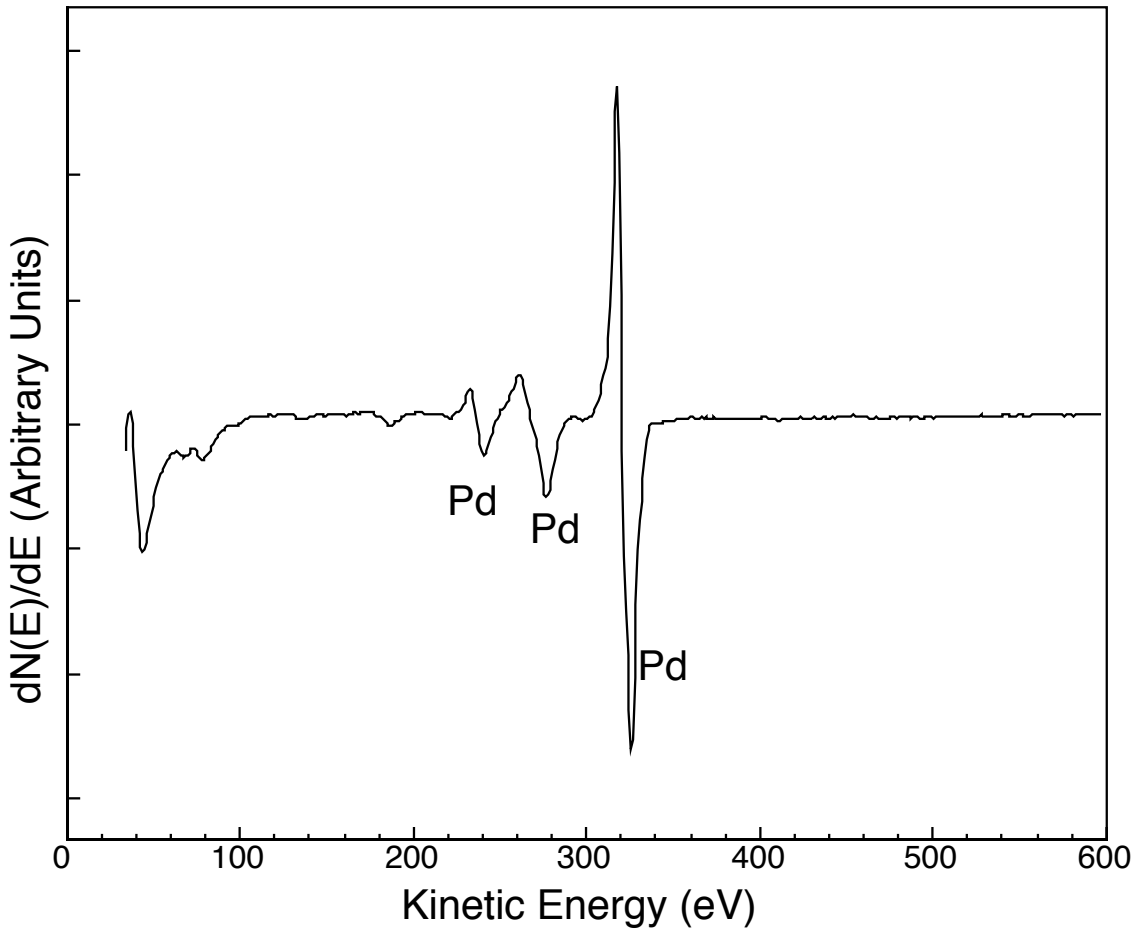

Figure 7. AES spectrum of a clean Pd(100) surface. Experimental conditions: beam energy = 2 KeV; beam current = 1.6 μA.

Quantification of AES signal of the adsorbate is made by measuring the Auger current of the adsorbate, I_a, calculated by double integration of the adsorbate Auger derivative signal A corrected for the clean surface signal A_c [32]:

$$I_a = \frac{4}{k^2}\int_0^{E_P}\int_0^{E}(A - \phi_b A_c)dE'\,dE \qquad (19)$$

where ϕ_b is the observed attenuation of the substrate signal by the adsorbate, and k is the modulation amplitude. The Auger current of the adsorbate is then normalized by I_{Pd}, the Auger current of the substrate Pd, from the same spectrum. This normalization process is employed in this study because the normalized value (I_a/I_{Pd}) is not a function of k, the modulation amplitude, and any changes in the beam current and sample positioning from different runs can be compensated in the normalization process.

High-Resolution Electron Energy Loss Spectroscopy (HREELS)

HREELS has rapidly emerged as a very important tool for studying vibrational properties of clean and adsorbate-covered surfaces because of its high surface sensitivity and wide spectral range. HREELS provides information on the chemical structure of adsorbed species based on characteristic vibrational frequencies. When a beam of monoenergetic low-energy electrons strikes on a surface, individual electrons of the beam lose a discrete amount of energy upon interaction with a certain vibrational mode of surface atoms and adsorbed molecules. An analysis of these electrons with discrete energy loss provides direct information on vibrational frequencies of species adsorbed at the surface.

Two major mechanisms are involved in the electron energy loss process: dipole scattering and impact scattering. Dipole scattering describes the long-range interaction of incident electrons with the induced dipole at the surfaces. At metal surfaces, the dipole moment induced by vibrations of adsorbed species on the surface generates a virtual image dipole of opposite sign. For dipoles oriented parallel to the surface, the total dipole moment is zero since the real dipoles are cancelled out by their images. On the other hand, dipoles that are perpendicular to the surface are increased by a factor of two because of their image dipoles (Figure 8-A). Thus, dipole scattering is subjected to a very important surface dipole selection rule: only those vibrational modes that produce dynamic dipole moments perpendicular to the surface can be observed in the HREELS spectra. Also, dipole scattering theory dictates that the loss peaks due to this mechanism is strongly peaked in the direction of specular reflection, where the angle of incidence equals the angle of reflection. In other words, if the backscattered electrons are collected at a different angle from that of the specularly reflected beam, the loss features due to dipole scattering disappear. Impact scattering, on the other hand, is the result of short-range electrostatic interaction between the incident electrons and the oscillating dipoles at the surface. Therefore, impact scattering is not limited by the surface dipole selection rule. All the vibrational modes, parallel or perpendicular, are active and can contribute to the HREELS spectra. Also, loss peaks due to impact scattering can be observed at any angle, including specular direction, theoretically. However, since dipole scattering is the dominant mechanism at specular angle, the signal due to impact scattering would "drown" in that of dipole scattering. Therefore, the best position to observe impact

scattering is at an off-specular angle. The combination of dipole and impact scattering allows, in principle, all the vibrational modes of the adsorbate/substrate complex to be identified. Also, the surface dipole selection rule in dipole scattering is useful to determination of the molecular orientation of the adsorbed species. These great features have made HREELS a powerful technique in surface vibrational spectroscopy.

Figure 8-B shows a schematic diagram of the LK 2000 HREELS spectrometer (L.K. Technologies Inc., Bloomington, IN). The spectrometer is composed of an electron gun, a two-stage monochromator, a single-stage energy analyzer, and a channeltron detector. Both energy monochromation and energy analysis are conducted by 127° cylindrical deflection analyzers (CDA). The two-stage monochromator is used to narrow the energy spread of the incident electrons, which originates from the electron gun with an initial energy spread of 0.3 eV, to 1 or 2 meV. An intermediate lens system is used between these two stages to focus and collimate the beam from stage 1 to stage 2. With a zoom lens system, the highly monoenergetic beam of low-energy electrons (1-10 eV typically) is focused and accelerated onto the sample. The inelastically scattered electrons are then focused and decelerated through another zoom lens system before they are detected by the channel electron multiplier. The signal is fed to a preamplifier as pulses for further processing by counting electronics.

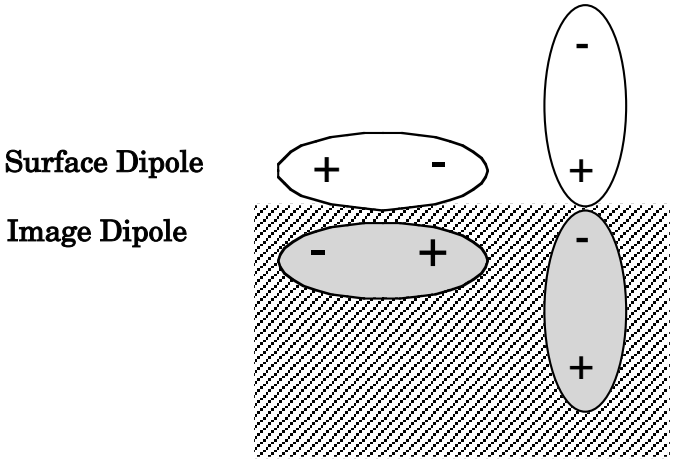

A

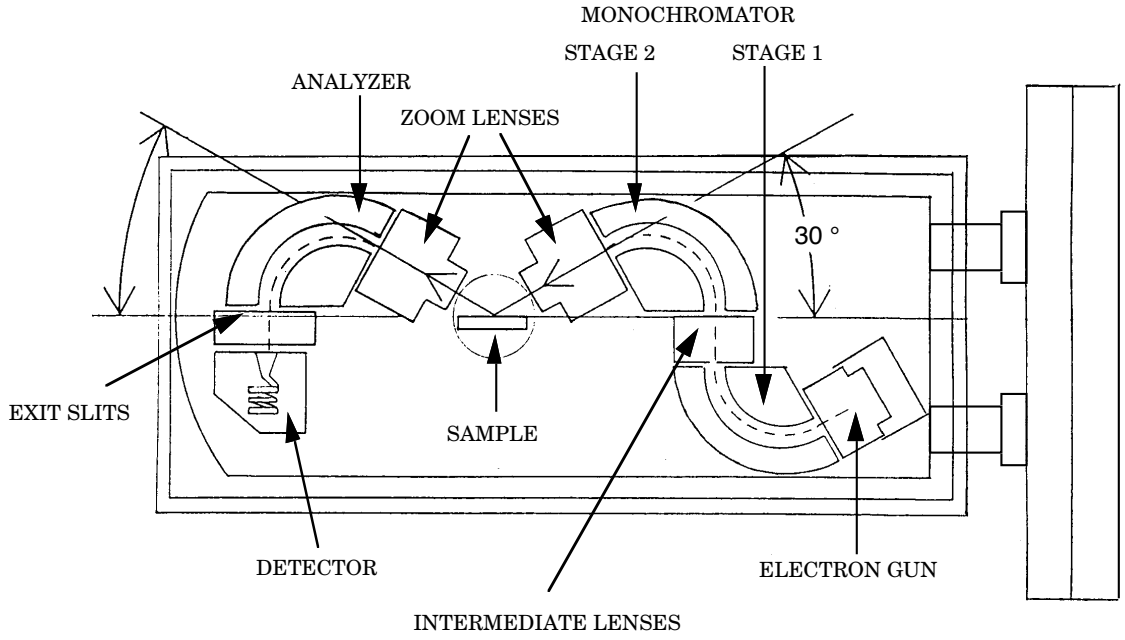

B

Figure 8. A: Depiction of surface and image dipoles. B: Schematic diagram of an HREEL spectrometer.

The specular angle in this system is 62º from the surface normal. When off-specular measurements are needed, either the sample or the analyzer is rotated so the detection can be made at an off-specular angle. The analyzer in this LK 2000 system can not be rotated, so the sample is rotated instead to get the off-specular measurements. In this study, all HREELS spectra are recorded at a specular direction.

Assignments of HREELS loss peaks were made by comparing the frequencies in HREELS spectra with characteristics IR group frequencies of molecules in the liquid, solid, and gaseous states [33]. However, since the frequencies of a molecule tend to shift when the molecule is chemisorbed due to its chemical bonding to the surface and lateral interactions from neighboring molecules, it is also very important to consider the interaction of the molecules with metal surfaces as in organomtallic complexes [34].

HREELS spectra are usually normalized based on matching the intensities of elastic peaks of different spectra. This normalization method is appropriate for HREELS studies on smooth surfaces where most electrons are scattered elastically. It is, however, not applicable to studies conducted on relatively rough surfaces. A chemisorbed adlayer usually introduces a degree of roughness to the surface, and electrochemical oxidation causes additional roughness. As a result, more electrons are inelastically scattered, which in turn causes the elastic peak intensity to decrease dramatically. Therefore, a different normalization method, based on matching the intensities of the background region in different spectra, was employed in our study [35]. The normalization procedure is as follows: (*i*) a clean Pd spectrum was obtained and its elastic peak count rate was set to 2.5×10^5 cps, the maximum counts obtained on a clean spectrum. (*ii*) Each spectrum for

adsorbed organic species was then multiplied by a constant to normalize the background of a spectrum (2100~2700 cm^{-1}) to that of the clean Pd spectrum. This method assumes that the background region of a spectra is mainly due to impact scattering mechanism. In other words, the intensity of the background spectrum has a direct relationship with the incident electron beam energy. This normalization method works well with the chemisorption and anodic oxidation of H_2Q on Pd.

HREELS offers extremely high sensitivity. For example, the detection limit for CO, a strong dipole scatter, can be as low as 0.0001 monolayer. This can be observed in the HREELS spectrum of a clean and ordered Pd(100) electrode surface shown in Figure 9. Even though the cleanness of the substrate has been ascertained by AES spectrum, there are still two peaks appearing at 368 cm^{-1} and 1908 cm^{-1}. They correspond to the ν(Pd-C) and ν(CO) stretch of background CO, respectively. The frequency indicates that CO is adsorbed in a bridging site [36].

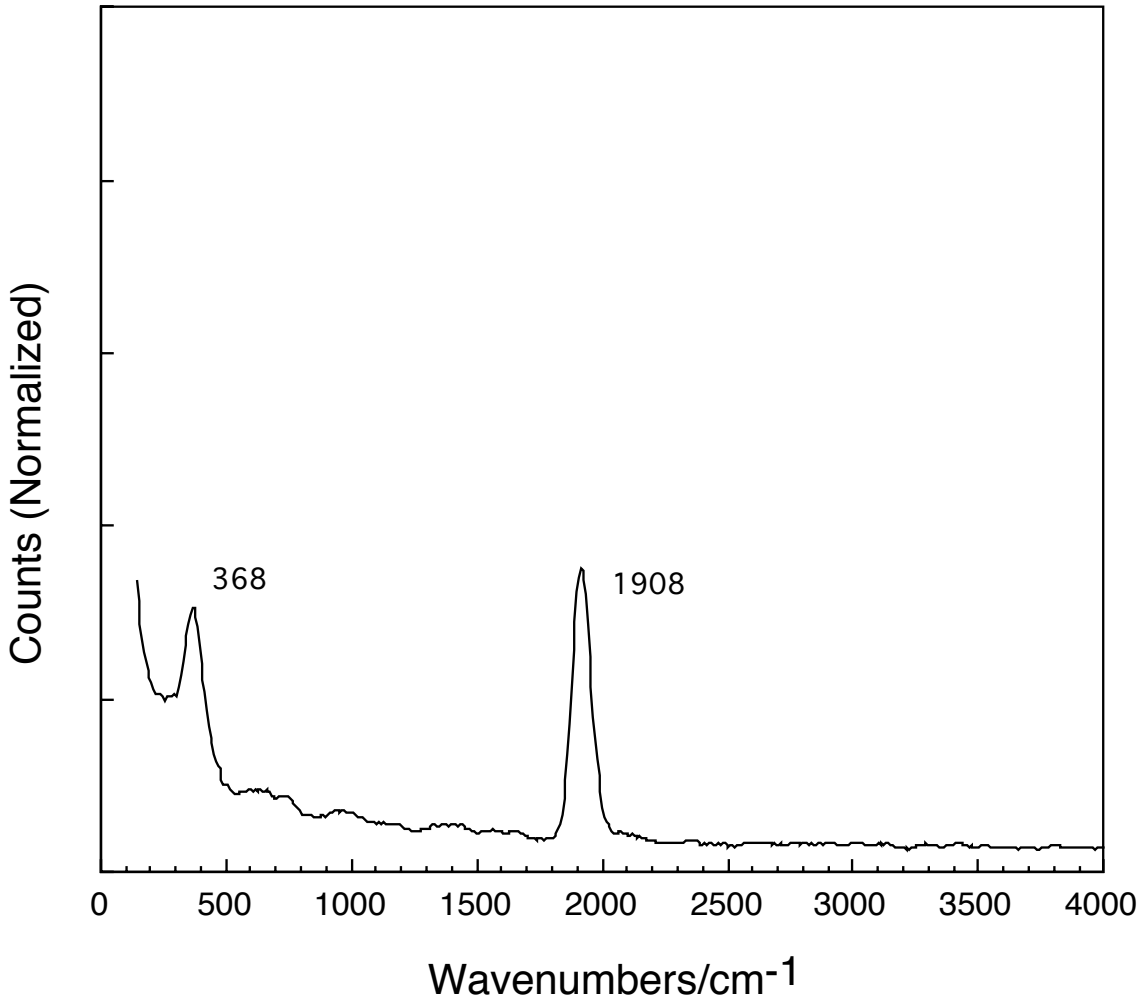

Figure 9. HREEL spectrum of a clean and ordered Pd(100) surface. Incidence and detection angles = 62° from surface normal. Resolution = 4 meV (32 cm^{-1})

Electrochemical experiments performed in the UHV-EC system were carried out using the same kind of potentiostat and X-Y recorder used in the TLE experiments. Figure 10 shows the electrochemical cell used in UHV-EC studies. The cell consists of two compartments. One of the compartments holds a Pt auxiliary electrode and a Ag/AgCl (1 m*M* NaCl) reference electrode, and the other one accommodates the Pd(100) working electrode. The two compartments are separated by a fine glass frit. A long tube connected to the working electrode compartment serves as the port where different solutions can be introduced in and out of that compartment. The Ag/AgCl (1 m*M* NaCl) reference electrode was calibrated using a Ag/AgCl (1 *M* NaCl) reference electrode. The potential of the Ag/AgCl (1 m*M* NaCl) versus the Ag/AgCl (1 *M* NaCl) was 0.20 V. The reason for using 1 m*M* NaCl Ag/AgCl reference for UHV-EC studies is to minimize possible Cl^- contamination brought in by the reference electrode.

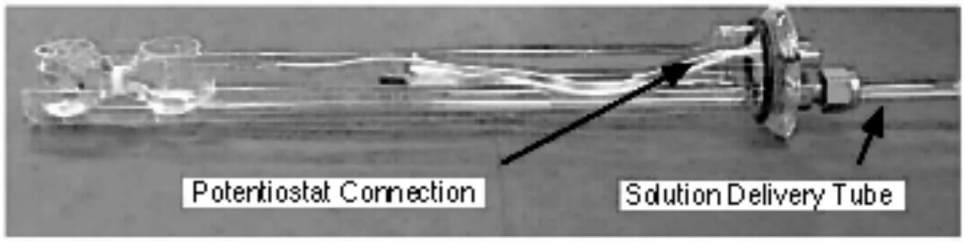

A

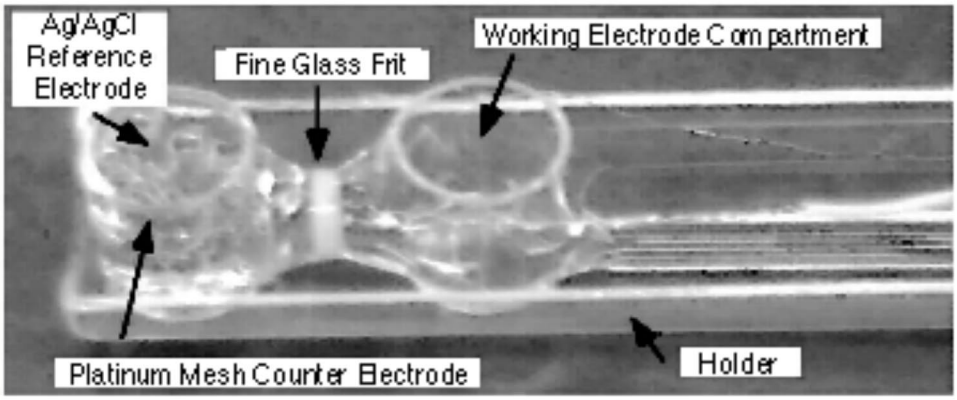

B

Figure 10. The electrochemical cell used in UHV-EC studies.

The UHV-EC apparatus used in this study is shown in Figure 11. This all-stainless-steel vacuum chamber was built upon a TNB-X series 500 vacuum pumping system (Perkin Elmer, Eden Prairie, MN). It consists of two compartments: the electrochemistry (EC) and surface analysis (SA) chambers. A gate-valve (MDC Vacuum Products, Hayward, CA) was installed between the two chambers so that the EC chamber can be isolated from the vacuum system when EC experiments are carried out at atmospheric pressure. The SA chamber is the main chamber and it is equipped with (i) a LEED optic (Perkin-Elmer, Eden Prairie, MN) for surface structure analysis, (ii) an AES optic (Perkin-Elmer, Eden Prairie, MN) for elemental analysis of the surface, (iii) a HREELS optic (LK Technologies, Bloominton, IN) for vibrational spectrosopic information from the surface, (iv) a quadrupole mass analyzer (UTI Instrument Company, Sunyvale, CA) for residual gas analysis, (v) a custom-built ion cage (LVC Engineering, Santa Barbara, CA) for sputter-cleaning, and (vi) two variable-leak valves (Varian, Lexington, MA) for gas dosing. The entire ensemble was baked to about 470 K for several days to attain a base pressure in the 10^{-10} Torr range. The Pd(100) single-crystal can be transferred between the EC chamber and SA chamber using an X-Y-Z-R manipulator (Huntington Laboratories, Mountain View, CA), which is installed on a twin-rail positioning table (Lintech, Mountain View, CA) so the crystal can be lowered or raised easily. This configuration allows the crystal to be easily transferred in a controlled and basically contaminant-free environment.

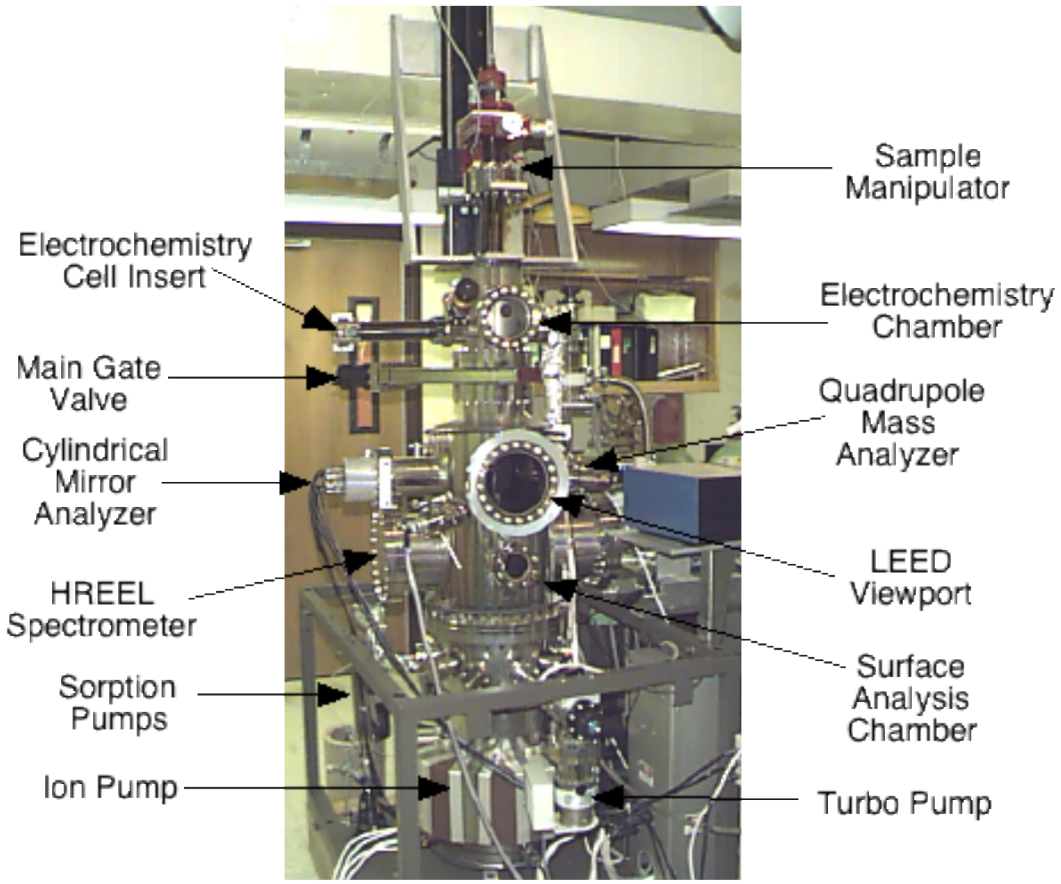

Figure 11. Picture of the UHV chamber used for the UHV-EC studies.

The Pd(100) single crystal electrode (99.999%), purchased from the Materials Research Center at Cornell University (Ithaca, NY), was a circular disk with a diameter of 0.9 cm and a thickness of 0.3 cm. Both faces of the disc were aligned within 0.5º of the (100) crystallographic plane and were metallographically polished to mirror finish. The edges were not oriented, but polished. Two 0.5 mm Pd wires (99.99%, Aldrich, Milwaukee, WI), were spot-welded to the side-edges of the crystal and attached to the sample holder. In addition to mechanical support, the wires provided electrical contact with the sample for control of potential and for resistive sample-heating. A Pt-10% Rh/Pt thermocouple wire (Omega Engineering, Stanford, CT) was spot-welded to the top-edge of the sample for temperature measurements and feedback-control for the crystal temperature controller (Omega Engineering).

In order to obtain a clean and well-ordered surface, the Pd(100) single-crystal electrode undergoes several cycles of thermal annealing at 1020 K in 10^{-6} Torr of O_2 (99.8%, Botco, Bryan, TX), Ar^+-ion sputtering at 10^{-5} Torr Ar, and thermal annealing at 1020 K in vacuum. Surface cleanness and ordering are then confirmed by AES and LEED, respectively.

A typical UHV-EC experiment follows sequentially these procedures: The Pd(100) is cleaned and characterized before it is transferred to the EC chamber. The gate valve between the two chambers is closed so that the EC chamber is isolated from vacuum. Ultra-high-purity argon (99.9999%, Botco, Bryan, TX) is introduced into the EC chamber, and once the pressure inside of the EC chamber reaches 1 psig, another gate valve is opened and the electrochemical cell is introduced into the EC chamber.

After the EC experiment, the cell is then removed from the EC chamber, the gate valve is closed, and the chamber is pumped down by a three-stage pumping system. Two liquid-nitrogen chilled sorption pumps are used to pump the pressure from atmosphere to about 5×10^{-4} Torr. A 56 L/s turbomolecular pump (Balzers, NH) is then employed to lower the pressure further down to 10^{-7} Torr. The pressure can be reduced to UHV levels ($\sim10^{-9}$ Torr) by a 300 L/s triode ionization pump and a liquid-nitrogen cooled titanium sublimation pump. After the three-stage pumping, the crystal is then transferred back to the SA chamber for further characterization.

Electrochemical Scanning-Tunneling Microscopy (EC-STM)

Scanning-tunneling microscopy (STM) was developed by Binning and Rohrer in 1981, and has been proven to be unique among imaging and surface analysis techniques because it provides three-dimensional real space images of surface and adsorbate layers with atomic resolution [37].

The imaging process is illustrated in Figure 12-A. When a sharp metal tip, usually of W or Pt, is positioned above a surface within a very short distance (typically 5~50 Å), the wave function of the tip and the substrate overlap. The electrons tend to tunnel across the barrier between the surfaces with the application of a low bias between the sample and the tip. The resulting tunneling current, I_t, is exponentially dependent on the the tip-sample distance d:

$$I_t = \Delta E_t \exp(-2\kappa d) \qquad (20)$$

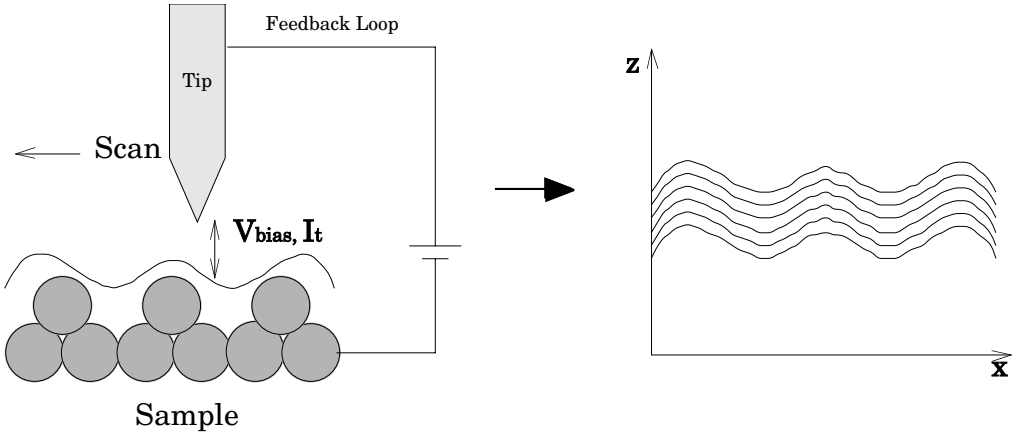

A

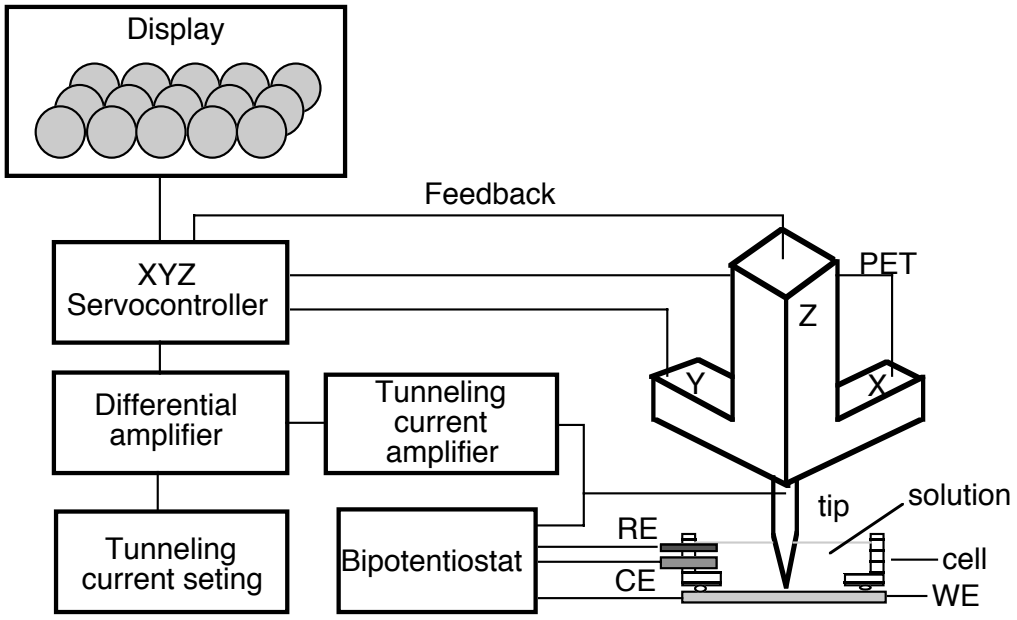

B

Figure 12. A. Imaging process of STM. B. Schematic diagram of EC-STM.

where ΔE_t is the tunneling bias, and κ is the decay constant of the wave function in the tunneling barrier (usually 1.0 $Å^{-1}$) [38].

The STM can be operated in two modes (constant current and constant height) to obtain images. In the constant current imaging mode a feedback mechanism is employed so that the applied bias and the tunneling current can be maintained constant as the tip scans the sample surface. This mode requires a constant tip-sample separation d based on equation 15, Therefore the vertical position (the height) of the tip is constantly changed in order to maintain this distance constant. The signal corresponding to the change in the height of the tip is recorded, producing a constant charge density contour of the surface. In constant height mode, the height and applied bias are maintained constant, and the variation in the tunneling current is related to the charge density and recorded instead.

Since STM was first applied for studies in electrolyte solutions in 1986 [39], it has become a popular *in situ* technique for studies of electrode-electrolyte interfaces. *In situ* STM is also called electrochemical STM (EC-STM). In EC-STM, a bipotentiostat has to be employed to independently control the electrode potentials of the substrate (which is also the working electrode, WE) and the tunneling tip with respect to a reference electrode (RE). The Faradaic current flowing through the substrate and the counter electrode (CE) is collected by a current follower, while the tunneling current is measured by a tunneling current amplifier. Employment of a bipotentiostat successfully prevents the interference of the faradaic current with the tunneling current, which was a problem in early EC-STM models. A simple schematic of EC-STM is illustrated in Figure 12-B.

A Nanoscope III scanning probe microscope (Digital Instrument, Santa Barbara, CA) was used for EC-STM measurements. The electrochemical experiments were carried out in a custom-built Kel-F electrochemical (EC) cell with a four-electrode configuration. The EC cell was equipped with a Pt quasi-reference electrode and a Pt auxiliary electrode. The working electrode, a Pd(111) single-crystal bead, was secured by a conductive plate and an O-ring seal.

The single crystal surfaces used for EC-STM studies were prepared using the Clavilier method [40, 41]. A single crystal bead (3 mm diameter) was made by melting a 0.8 mm Pd wire (99.995%, Aldrich, Milwaukee, WI) in an O_2/H_2 flame. This bead had several single crystal facets oriented in different planes. One of the (111) facets was carefully chosen and used directly as the working electrode for the EC-STM experiments. The single crystal surface was cleaned by flame annealing at about 1000 K for a period of 15-30 minutes, slow cooling in an Ar stream, and immersion in Milli-Q Plus water saturated with H_2. The electrode was then quickly transferred to the EC cell through air but with a droplet of water to protect the surface from contamination.

The preparation of the tunneling tips was carried out by electrochemical etching of a 0.25 mm W wire (99.995%, Aldrich, Milwaukee, WI) in 1 *M* KOH with 15 V AC. The tip was further coated with transparent nail polish (Nutra Nail) to minimize the Faradic current [23]. All EC-STM experiments were conducted by Dr. Y.-G. Kim.

Reagents

The supporting electrolyte 1.0 *M* H_2SO_4 used for TLE studies were prepared from fuming sulfuric acid (Aldrich Chemicals, Milwaukee, WI). The 10 m*M* H_2SO_4 used for UHV-EC studies were made from double distilled grade sulfuric acid (Aldrich Chemicals, Milwaukee, WI). Hydroquinone (H_2Q) and benzoquinone (BQ) were purchased from Aldrich and used as received. Milli-Q® Plus water was used to prepare all the aqueous solutions.

RESULTS AND DISCUSSION

Thin Layer Electrochemistry: Polycrystalline Pd

The chemisorption of hydroquinone (H_2Q) and benzoquinone (BQ), from aqueous solutions, onto a polycrystaline Pd thin-layer electrode surface was investigated by thin-layer electrochemistry (TLE). The chemisorption isotherm for H_2Q and BQ molecules was obtained. The elecrochemical oxidation of chemisorbed H_2Q was studied.

Figure 13 is a cyclic voltammogram of a clean Pd electrode in a 1 *M* H_2SO_4 supporting electrolyte. Surface oxidation starts as early as 0.47 V [42]. When the potential is switched negatively, a large cathodic peak due to the reduction of the surface oxide appears at 0.44 V. Below 0.10 V, the cathodic current is due to a combination of hydrogen adsorption, absorption and evolution; these processes are reversible as can be seen when the potential is switched back to the positive direction.

Chemisorption

Figure 14 shows the thin-layer current-potential curves of the same clean Pd electrode in a 0.10 m*M* H_2Q solution. The peak at 0.46 V is ascribed to the 2-electron/2-proton oxidation of the dissolved H_2Q species to BQ:

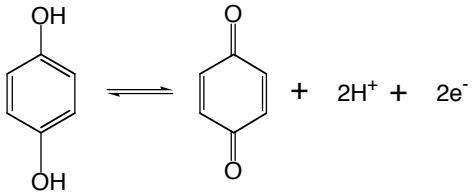

(21)

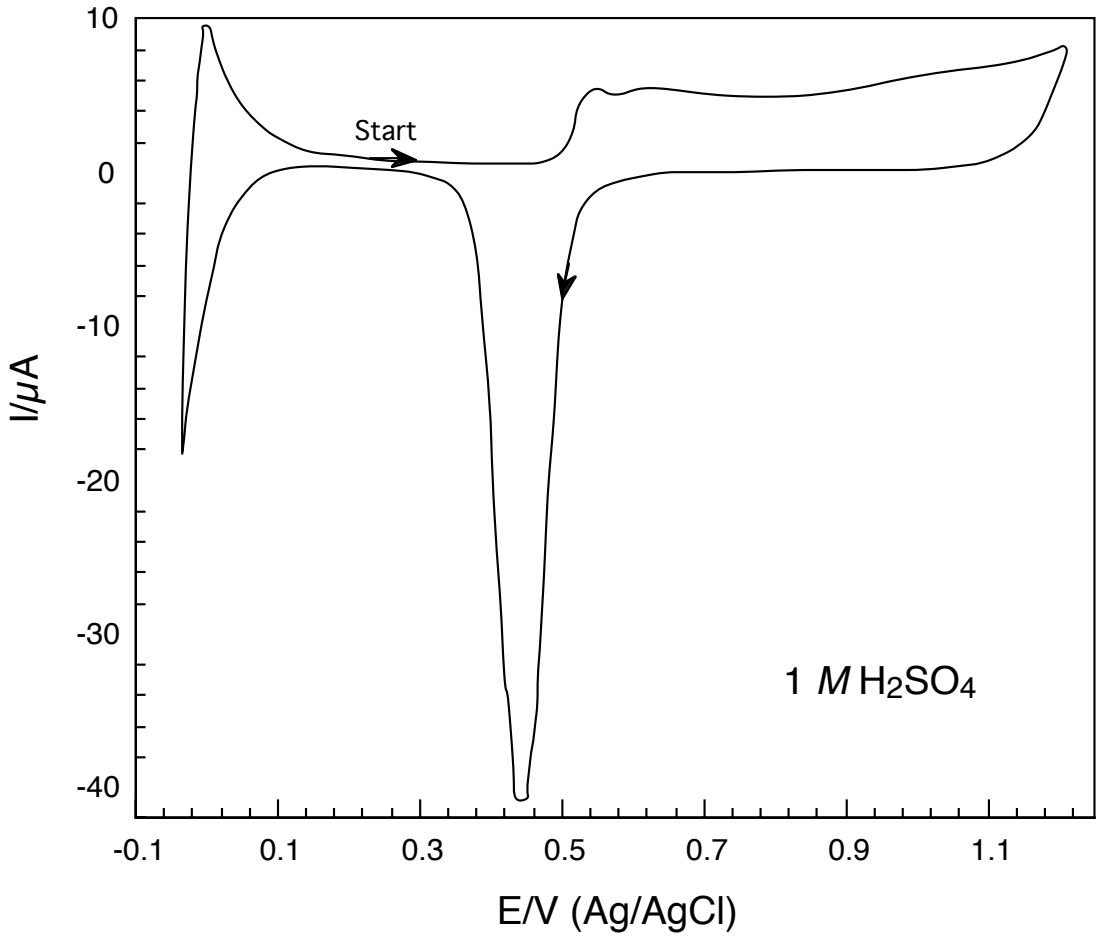

Figure 13. Thin-layer cyclic current-potential curve of a clean Pd electrode in a thin-layer cell in 1.0 *M* H_2SO_4. Scan rate: 2 mV/s.

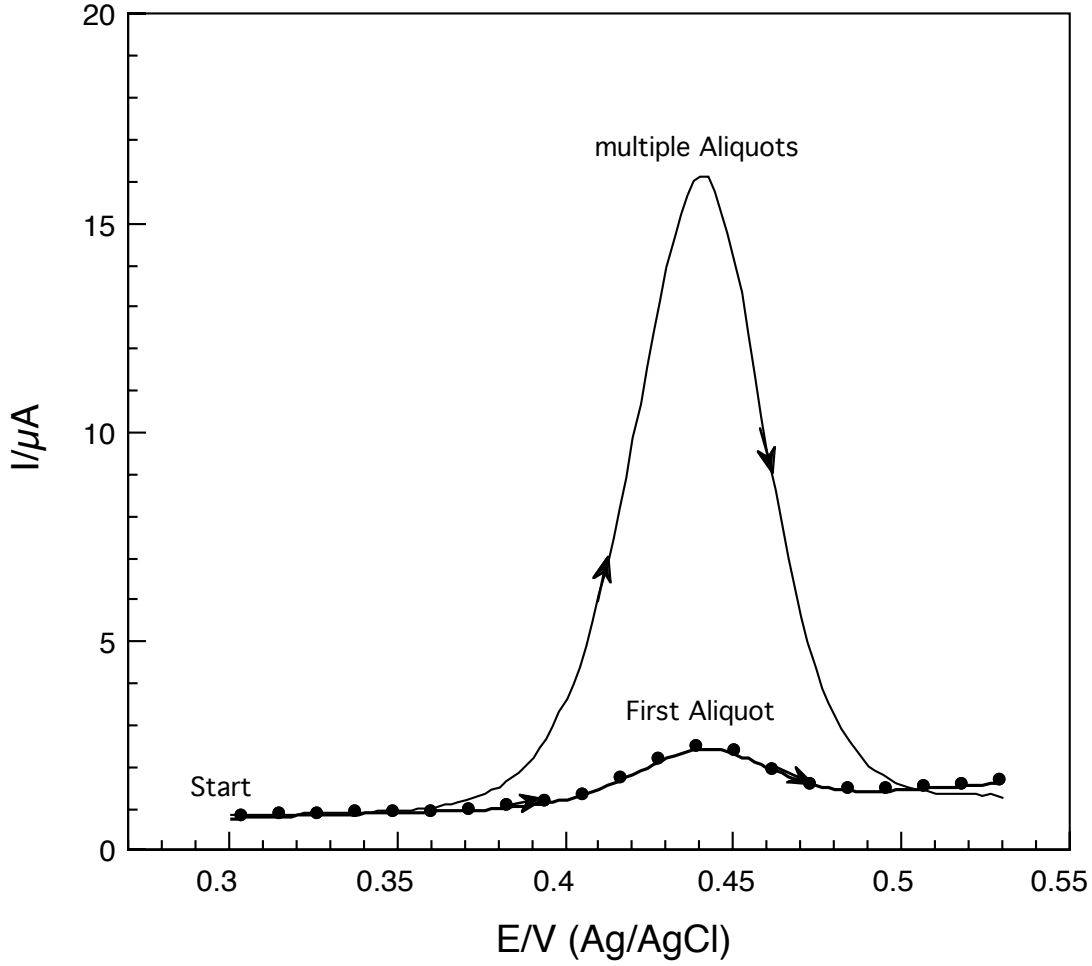

Figure 14 [43]. Thin-layer current potential curves for a Pd electrode after the thin layer cavity is filled only with a 1.0 m*M* H_2Q solution (A), and multiple times to insure that the surface is saturated with the organic compounds (B). Experimental conditions are the same as in Figure 13.

Noticeably, the oxidation peak obtained after only a single filling of H_2Q solution is smaller than that obtained when the electrode surface is saturated with multiple rinses of the organic compound. As indicated in the experimental section, the diminution of the peak after only the first exposure of the H_2Q solution to clean Pd is due to chemisorption of H_2Q, and the chemisorbed speices behave differently from the unadsorbed compound.

Measurements based upon the results in Figure 14 for Γ (mol/cm^2), the absolute surface concentration of the adsorbed molecules were then carried out at various solute concentrations. The results, in terms of a plot of Γ-vs.-log C for both H_2Q and BQ are shown in Figure 15. The near-identity of the plots for H_2Q and BQ is obvious. Although a similar result was obtained previously on polycrystalline Pt [44], the detailed shapes of the isotherms are different on Pt and on Pd. Specifically, in Figure 15, there is a hint of the existence of two plateaus, a lower one at $C^0 \leq 0.1$ m*M* and a higher one at $C^0 \geq 1$ m*M*; on Pt, these two plateaus are very sharply defined [44].

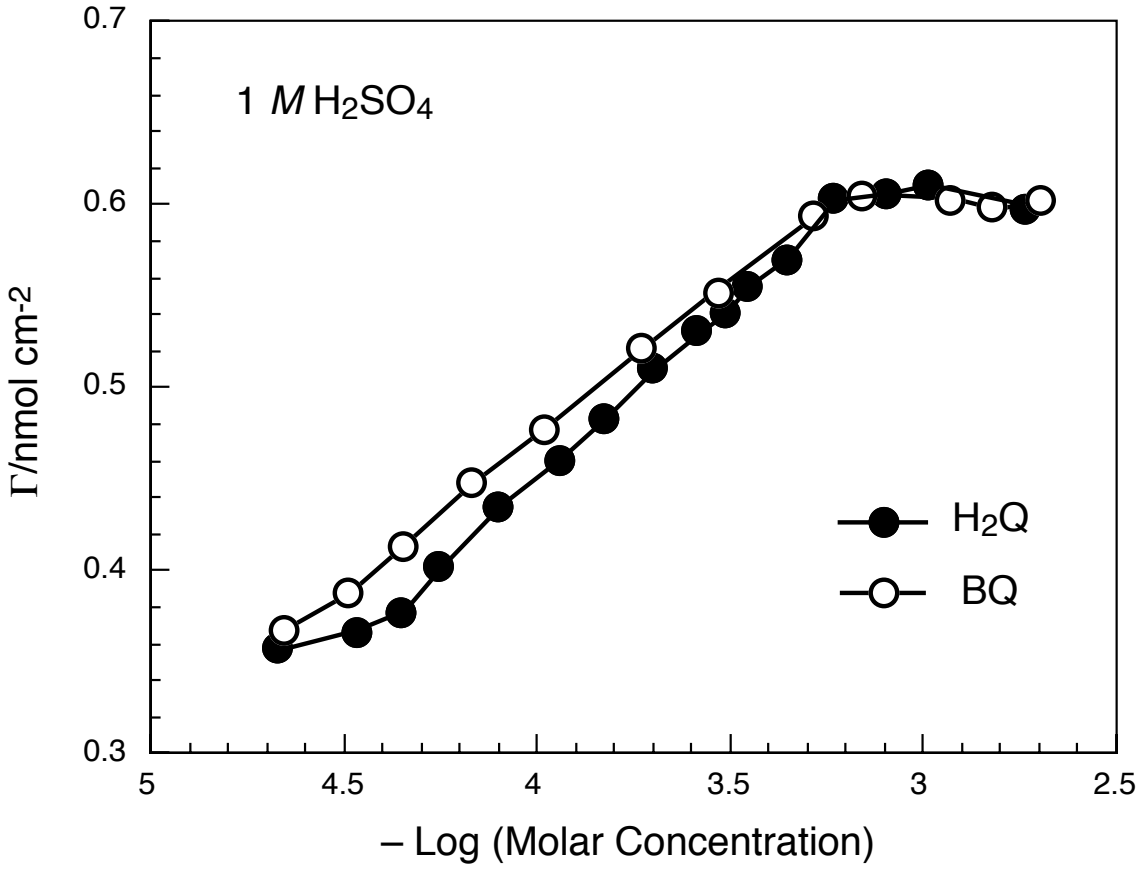

Figure 15. Chemisorption isotherms, Γ vs. -log C plots, from H_2Q and BQ solutions at a smooth polycrystalline Pd electrode. Experimental conditions were as described in the text and in Figure 13.

The plateau regions in the isotherm are related to the orientation of the molecules in the adsorbed layer. Earlier studies of H_2Q on Pt have shown that in the low concentration region the adsorbed molecules assumed a parallel (η^6) orientation, while those adsorbed in the high concentration region assumed an edge-vertical (η^2) orientation [44]. To extract information about orientation of the adsorbed molecules on Pd electrode, the surface area occupied by a single molecule in the adsorbed layer, σ_{expt}, was obtained from the plateau values of Γ according to the equation:

$$\sigma_{expt}\ (\text{Å}^2/\text{molecule}) = 10^{16}/(N_A\Gamma) \qquad (22)$$

where N_A is Avogadro's constant. A molecular model based on tabulated covalent and van der Waals radii was then used to relate the σ_{expt} values to certain molecular orientations. In this model, each molecule was considered to be packed in a rectangular unit cell. The area occupied by an adsorbed molecule was represented as the cross-sectional area (σ_{calcd}) of a rectangular solid unit cell in a plane parallel to the electrode surface [44]. The cross-sections for various adsorbed-molecule H_2Q orientations were then compared with σ_{expt}. The results are listed in Table 1.

Table 1. Experimental and calculated molecular cross-sections.

	σ_{expt} Pd ($Å^2$)	σ_{expt} Pt [44] ($Å^2$)	σ_{calcd} ($Å^2$)
Low-concentration plateau	46.5	52.7	53.8 (η^6)
High-concentration plateau	27.9	27.5	28.6 (2,3-η^2)

The cross-section obtained in the high-concentration plateau (σ_{expt} = 27.5 Å^2) suggests an edge-vertical (2,3-η^2) orientation (σ_{calcd} = 28.6 Å^2), a result that is in agreement with previous results on Pt. Since there is no well-defined lower-concentration plateau, the σ_{expt} was calculated from the lowest Γ value measured, 46.5 Å^2. This is smaller than that obtained for Pt (52.7 Å^2) as well as that calculated for a completely flat (η^6)-oriented species (53.8 Å^2). This result suggests that the chemisorbed species formed at low concentrations are not completely parallel to the surface but are slightly tilted. Support for this claim can be obtained from high-resolution electron energy loss spectroscopy (HREELS) studies of H_2Q and BQ chemisorbed on Pd(111) and Pd(100) single-crystal surfaces: the vibrational spectra obtained showed peaks that would not have been probed were the molecules oriented completely parallel to the surface [20]. The HREELS work also demonstrated that, in the flat orientation, the chemisorbed species is BQ and not H_2Q; that is, oxidative chemisorption of H_2Q occurs to yield chemisorbed BQ. A negative rest-potential shift observed upon the chemisorption of H_2Q suggested an oxidative-adsorption process. As expected, BQ itself undergoes direct surface-coordination to yield chemisorbed BQ.

Based on the above results, the concentration-dependent initial (unadsorbed)-state to final (adsorbed)-state reactions are summarized in Figure 16. These reactions are identical to those found previously for smooth polycrystalline Pt surfaces.

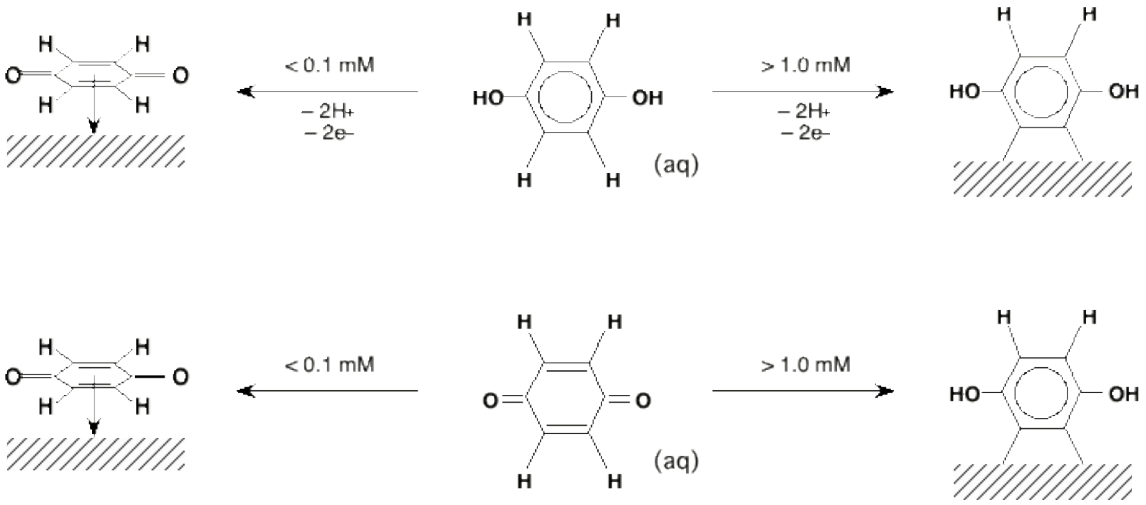

Figure 16. The effect of concentration on the adsorption of H_2Q and BQ onto polycrystalline Pd from 1 *M* H_2SO_4 solutions.

Anodic Oxidation

Earlier studies on polycrystalline Pt electrodes revealed that the anodic oxidation of chemisorbed species is strongly dependent upon the initial (pre-oxidation) molecular orientations [44]. We expected that such orientation-dependent electrocatalytic reactions would also transpire on Pd; hence, studies in this regard were undertaken.

Figure 17 shows current-potential curves for irreversible electrochemical oxidation of η^2-H_2Q and η^6-BQ at a Pd thin-layer electrode. The solid curve is for the electrode surface, pre-saturated with η^2-oriented species, in the presence of *unadsorbed* H_2Q; the curve with closed circles is for η^2-adsorbed material in the absence of unadsorbed organic. The large oxidation peak at 0.85 V is due to the oxidative desorption of the organic species and the concomitant oxidation of the Pd surface. The two curves are identical above 0.55 V, indicating that the anodic oxidation does not occur unless the organic compound is adsorbed onto the metal (non-oxided) surface. Hence, the presence of unadsorbed H_2Q (or BQ) does not affect the anodic oxidation of the chemisorbed species.

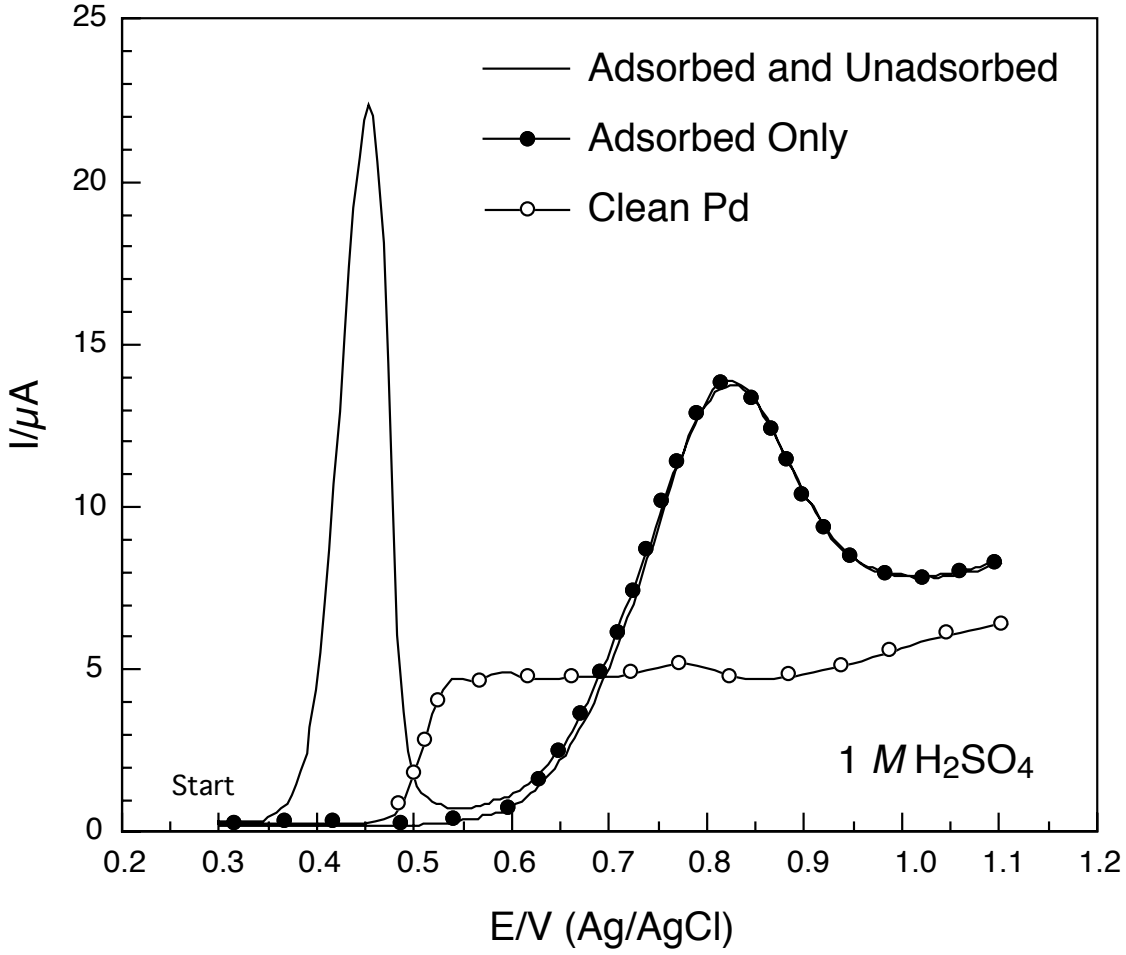

Figure 17 [43]. Thin-layer current-potential curves for anodic oxidation of H_2Q chemisorbed at a Pd thin-layer electrode in the presence and absence of dissolved H_2Q (1 m*M*). Scan rate: 2 mV/s. Other experimental conditions were as in Figure 13.

Current-potential curves for H_2Q adsorbed in flat and edgewise orientations are shown in Figure 18. It is noteworthy from the Figure that anodic oxidation, both in terms of peak potential and peak area, is identical for both surface species. This fact suggests that, since surface coverages for these two surface species are different, the extents of anodic oxidation are functions of adsorbate orientations.

The extent of anodic oxidation can be monitored by the number of electrons (n_{ox}) transferred during electrochemical oxidative-desorption of a chemisorbed molecule. Clearly, the higher the n_{ox} value, the greater the extent of anodic oxidation. The measurement of n_{ox} is based upon Faraday's Law, written in the form:

$$n_{ox} = \frac{Q_{ox} - Q_{ox,b}}{FA\Gamma} \qquad (23)$$

where Q_{ox} is the Faradaic charge for the anodic oxidation of the adsorbed organic and $Q_{ox,b}$ is the background charge due to electrode-surface oxidation in the absence of adsorbate.

In Figure 19, Γ and n_{ox} are plotted simultaneously as functions of the concentration at which chemisorption was carried out. As is obvious in the Figure, n_{ox} is closely correlated with Γ. The transitions in n_{ox} occur at the same concentrations where the transitions in Γ take place. This provides evidence for the suggestion made above that the anodic oxidation (i.e., the *magnitude* of n_{ox}) is strongly rooted to the initial adsorbed-molecule orientation. For η^6-BQ, n_{ox} was found to be 22.2 ± 0.3, a value not too different from 24, the expected number for complete oxidation of the η^6-BQ to CO_2.

$$\eta^6 - BQ + 10H_2O \rightarrow 6CO_2 + 24H^+ + 24e^- \qquad (24)$$

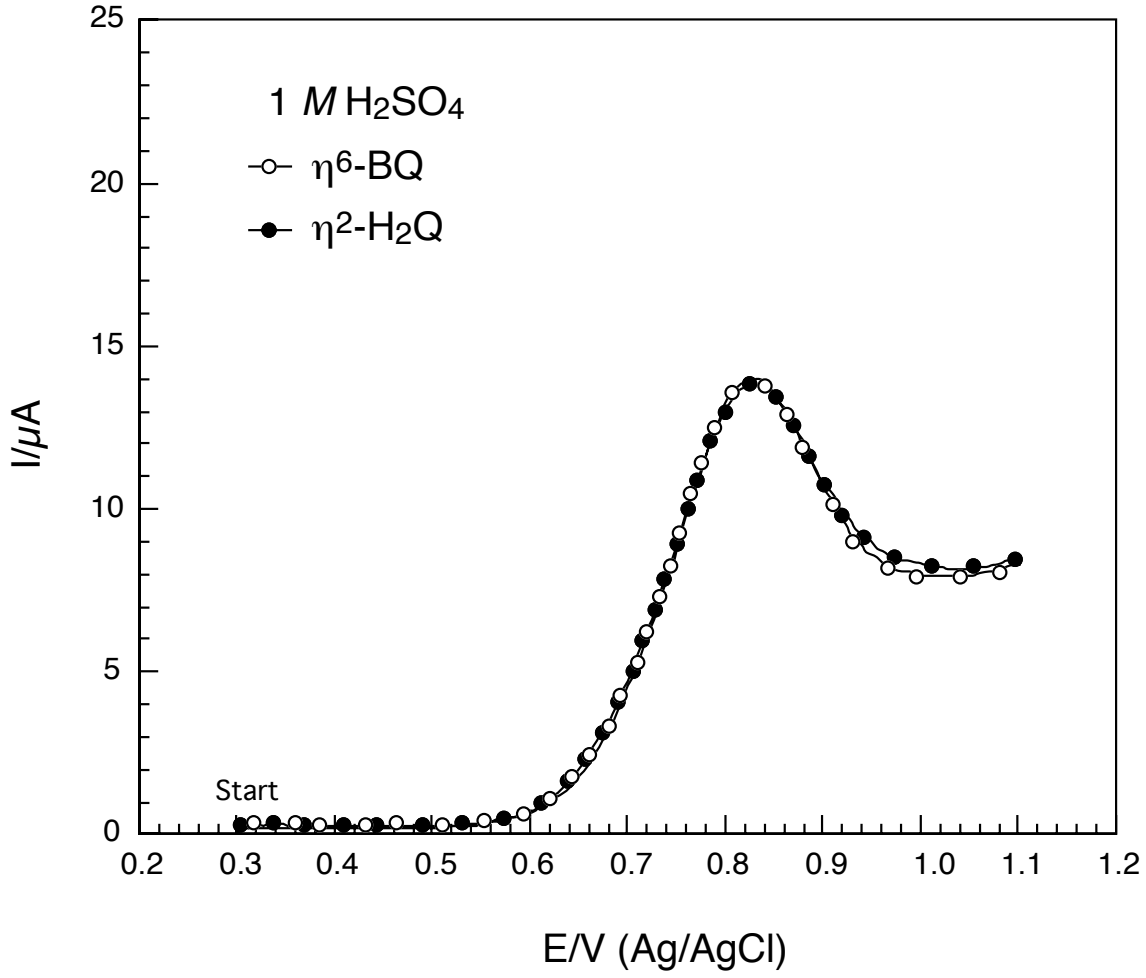

Figure 18. Thin-layer current-potential curves for anodic oxidation of H_2Q chemisorbed at a polycrystalline Pd electrode with different orientations. Scan rate: 2 mV/s. Other experimental conditions were as in Figure 13.

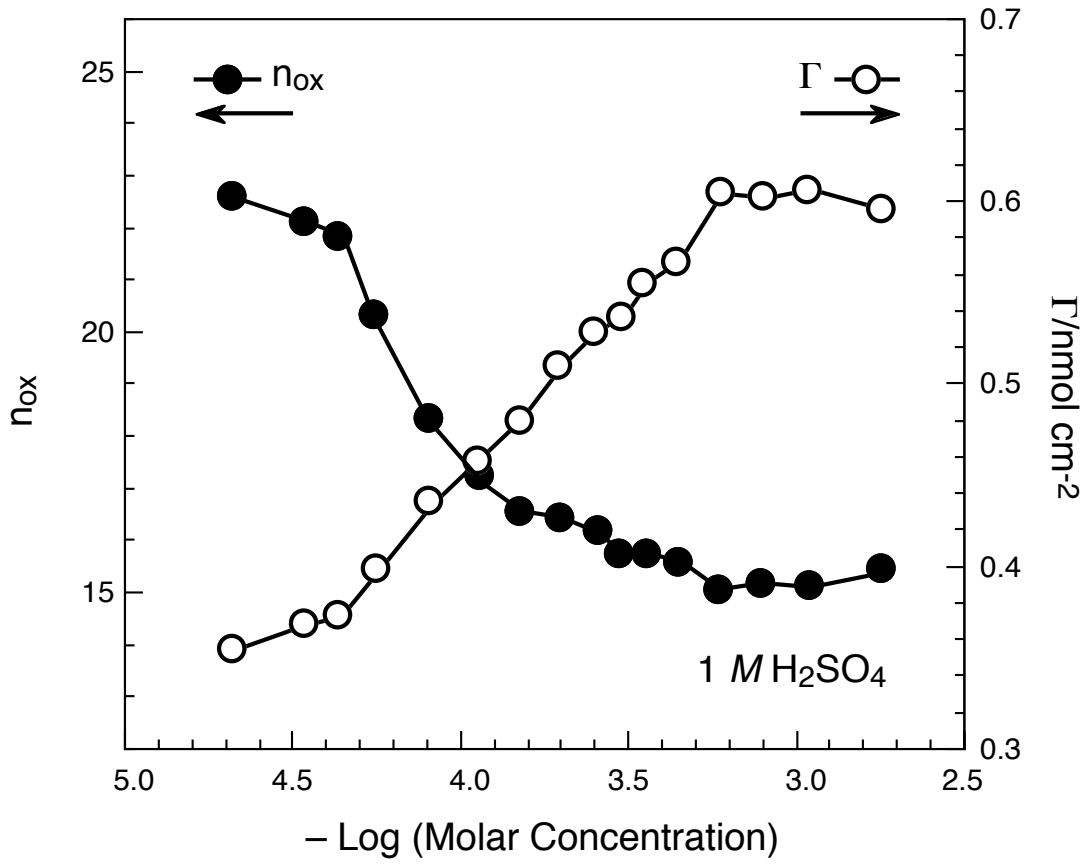

Figure 19. Simultaneous plots of the number of electrons for oxidative-desorption (n_{ox}) and the surface concentration (Γ) as a function of solute (H_2Q) concentration (-log C). Other experimental conditions were as in Figure 13.

For η^2-H_2Q, the measured n_{ox} was found to be 15.0 ± 0.2, nine electrons less than that required for complete conversion to CO_2. The lower n_{ox} value for η^2-H_2Q relative to η^6-BQ may be explained by the hypothesis, first reported in the studies with Pt [15], that only those carbons directly bonded to the electrode surface undergo complete conversion to CO_2. A n_{ox} value of 15 for 2,3-η^2-H_2Q is consistent with oxidation of the two adjacent (2,3) carbons that are directly attached to the surface to CO_2, and milder oxidation of the remaining (four-carbon) fragment to tartaric acid (n_{ox} = 14) or maleic acid (n_{ox} = 12) [15]. Chromatographic analysis of the product mixture from the anodic oxidation of η^2-H_2Q on Pt electrode verified the presence of maleic acid [45].

Two additional experiments were conducted with the η^2-adsorbed species. In one, the electrode was pre-saturated with η^2-H_2Q; the electrode was then rinsed with pure supporting electrolyte and subjected to selected anodic-oxidation potentials (0.30 V, 0.60 V, 0.70 V, 0.80V, 0.85 V, or 1.00 V) for 180 seconds. After oxidation, the thin-layer cavity was rinsed several times in the blank (organic-free) electrolyte while the potential was maintained at the anodic-oxidation potential. After multiple rinses, the potential was then switched to 0.30 V for 180 seconds, and a new current-potential curve was obtained. In these set of experiments, therefore, the products (at the pre-selected anodic-oxidation potential) are rinsed out of the cavity prior to re-equilibration at the double-layer region, 0.3 V. Hence, if any of the non-CO_2 products after the first oxidation cycle is surface-active, they will be removed and not available for re-adsorption at 0.3 V. The results are shown in Figure 20.

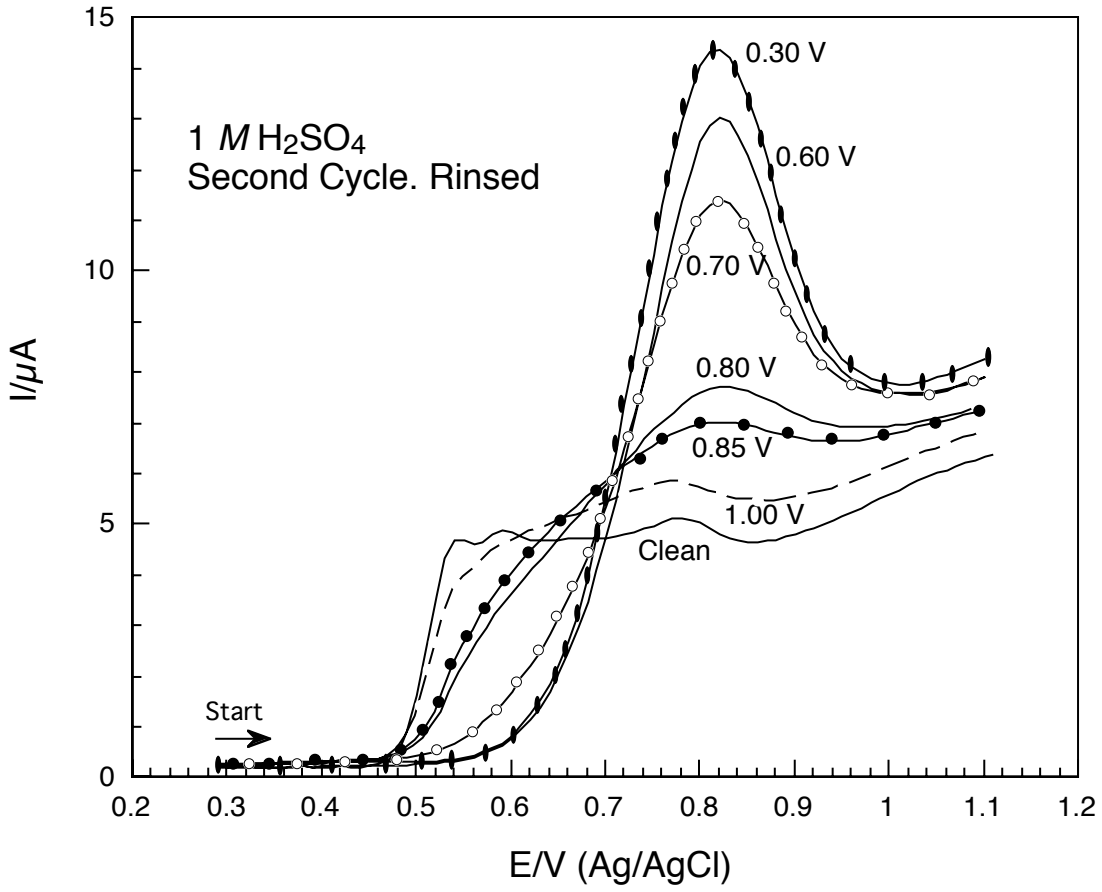

Figure 20 [43]. Second-cycle anodic-oxidation current-potential curves for η^2-H_2Q rinsed at pre-selected anodic-oxidation potentials. For one experiment, the anodic-oxidation potential was applied for 180 seconds and the thin-layer electrode was rinsed with pure supporting electrolyte, re-equlibrated at 0.3 V, and then re-oxidized at the same anodic-oxidation potential. Experimental conditions were as in Figure 13.

The data in Figure 20 are to be compared with the results in Figure 21 for the second set of experiments. Here, the thin-layer cell was not rinsed at the anodic-oxidation potential prior to re-equilibration at 0.3 V. In other words, non-CO_2 products after the first oxidation that are surface-active will be readsorbed upon re-equilibration at 0.3 V. In Figure 20, it is clear that the magnitude of the anodic-oxidation peak decreases as the anodic-oxidation potential was increased, provided the thin-layer cavity was rinsed *prior* to re-equilibration at a potential in the double-layer region at 0.3 V. The results in Figure 21, on the other hand, show that oxidation of η^2-H_2Q yields non-CO_2 products that are readsorbed on the oxide-free Pd surface. For example, the magnitude of the anodic-oxidation peak at 1.0 V in Figure 21 is much larger than that in Figure 20.

The following schematic reactions can thus be written to account for Figure 20 and 21:

$$\eta^2\text{-}H_2Q \xrightarrow[\text{Oxidation}]{\text{1st}} CO_2 + \underset{\text{Products}}{\text{Readsorbable}} \xrightarrow{0.3\ V} \underset{\text{Products}}{\text{Chemisorbed}} \xrightarrow[\text{Oxidation}]{\text{2nd}} CO_2$$

$$\eta^2\text{-}H_2Q \xrightarrow[\text{Oxidation}]{\text{1st}} CO_2 + \underset{\text{Products}}{\text{Readsorbable}} \xrightarrow{\text{Rinse}} \xrightarrow{0.3\ V} \underset{\text{Products}}{\text{No Readsorbable}} \xrightarrow[\text{Oxidation}]{\text{2nd}} \text{Pd Oxide}$$

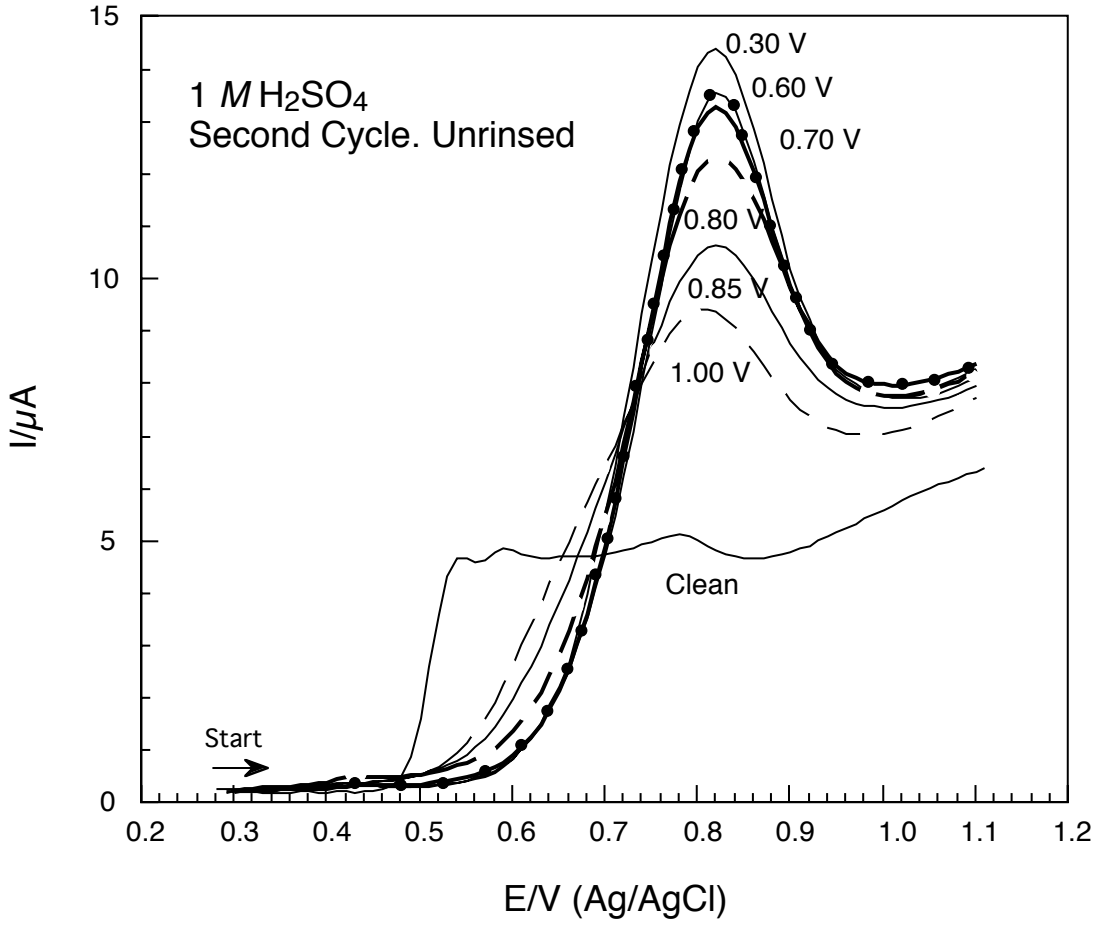

Figure 21 [43]. Second-cycle anodic-oxidation current-potential curves for η^2-H_2Q in which, in contrast to the experiments in Figure 20, the thin-layer electrode was *not* rinsed at the anodic-oxidation potential prior to re-equilibration at 0.3 V. Experimental conditions were as in Figure 13.

Electrochemical Scanning Tunneling Microscopy: Pd(111)

Figure 22 shows a high resolution electrochemical scanning tunneling microscopy (EC-STM) image of a clean Pd(111) single-crystal surface immersed in 0.05 *M* H_2SO_4 at a potential within the double layer region. The hexagonal array revealed in the image is as expected from a (1×1) structure of the Pd(111) surface.

The same Pd(111) single-crystal facet was then imaged while immersed in a 0.01 m*M* H_2Q + 0.05 *M* H_2SO_4 solution, and the result is shown in Figure 23. It can be seen clearly in this STM image that one of the para-oxygens is brighter than the other, which indicates that one of the oxygens is topographically higher than the other. This image supported the notion of a slightly tilted flat-oriented quinone that was raised in the above TLE studies. It is this tilted-flat orientation that renders one of the oxygen atoms in the molecule pointed slightly upwards while the other a little downwards.

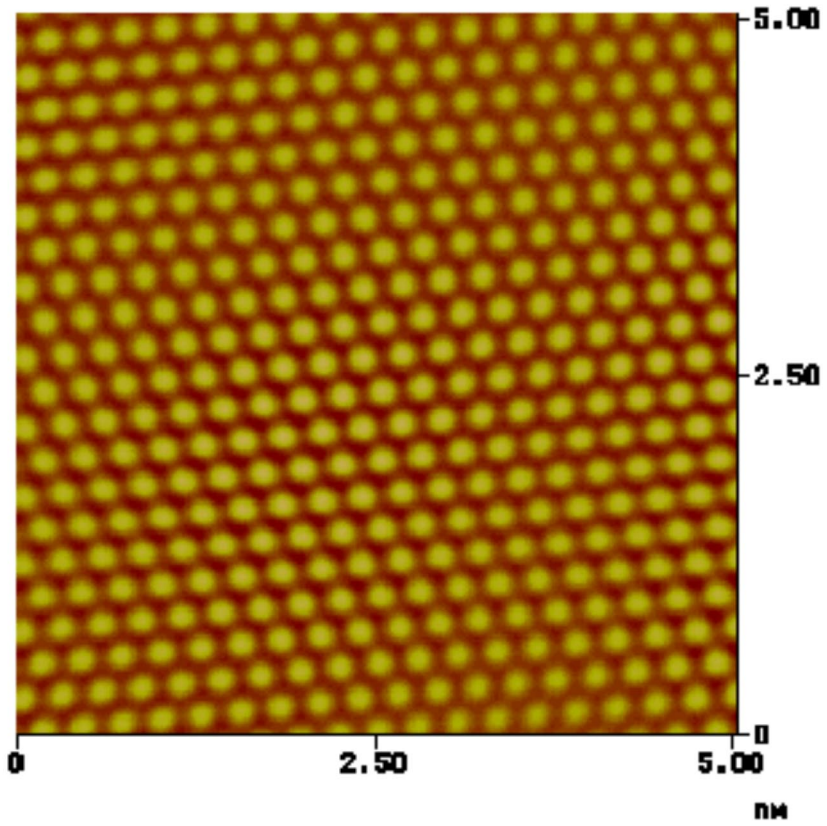

Figure 22. High-resolution STM image of a Pd(111) single-crystal facet immersed in an aqueous 0.05 *M* H_2SO_4 solution. The bias potential was 0.1 V; the tunneling current was 1 nA.

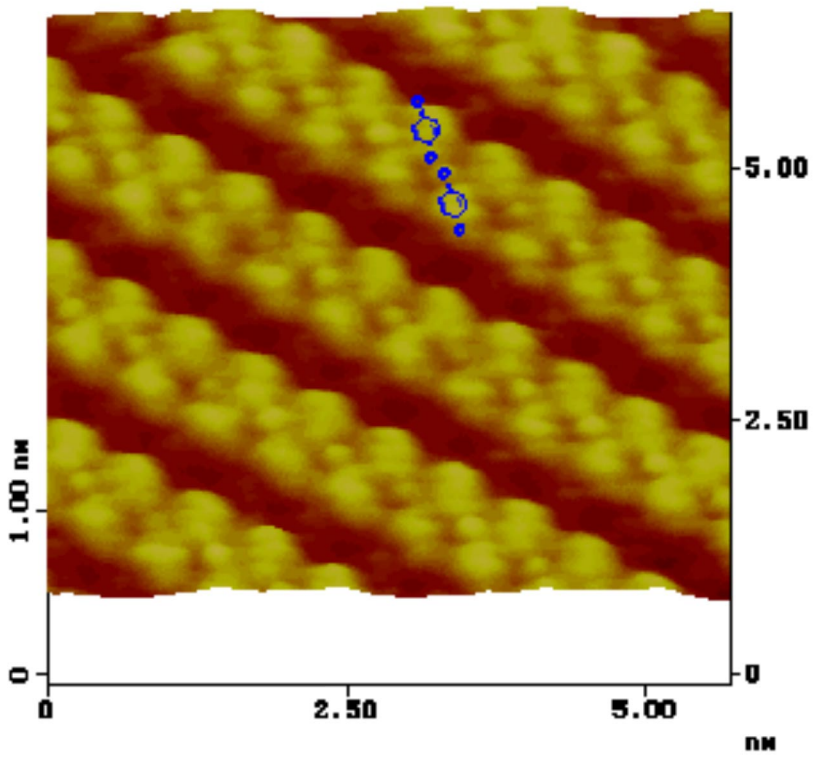

Figure 23. High-resolution STM image of a Pd(111) facet immersed in an aqueous 0.01 mM H_2Q + 0.05 M H_2SO_4 solution. The bias potential was 0.1 V; the tunneling current was 1 nA.

Ultra-High Vacuum-Electrochemistry: Pd(100)

To extend the TLE and EC-STM studies detailed above, similar experiments were performed on a Pd(100) single-crystal surface in an ultra-high vacuum-electrochemistry (UHV-EC) system. Chemisorption isotherms based on AES and HREELS measurements are discussed. Chemisorbed species with different molecular orientations were subjected to anodic oxidation at different oxidation potentials for various period of time. Results are discussed in terms of HREELS, AES and chronocoulometric measurements.

Supporting Electrolytes

UHV-EC necessitates the establishment of a suitable electrochemical environment that maintains the rigorously clean conditions demanded by ultra-high vacuum studies. Foremost, the electrochemical solution must be free from materials that interfere and/or alter the substrate-adsorbate chemistry. It is known that water is not chemisorbed on palladium and, hence, is readily displaced from the surface by the subject compounds; the use of Millipore®-grade water satisfies the solvent requirement. Selecting the appropriate supporting electrolyte is less straightforward since it may contain functional groups and/or impurities that are appreciably surface-active. The supporting electrolyte must be readily removed, under ultra-high vacuum, from the electrode during the surface analysis, and must have sufficient ionic conductivity to minimize ohmic (iR) drops during electrochemical (voltammetric and/or coulometric) experiments.

Trifluoroacetic acid (TFA), a relatively strong acid with a $K_a = 0.59$), had been used at low concentrations (1 m*M*) in earlier works that studied simple electrosorption in

the absence of voltammetric excursions [46]. TFA was found to be surface-inert and volatile. The HREELS of a Pd(100) electrode emersed from an aqueous 1 m*M* TFA solution resembled that of a UHV-prepared surface (Figure 24 A)[1]. Under such conditions, no TFA-derived species are found on the surface but there is insufficient ionic conductivity. At 10 m*M* concentrations, the HREEL spectrum in Figure 24 B shows two additional peaks at 3014 cm^{-1} (ν(C-H)) and at 1201 cm^{-1} (ν(C-F)) which are contributed by some unknown fluorine containing species. Such species, however, are displaced from the surface by H_2Q or BQ as evidenced by the absence of the above peaks. Nevertheless, since the identity of the species is unknown, TFA was not employed in this study.

Perchloric acid is another widely studied electrolyte. It is, however, prone to Cl^- contamination and the presence of chloride anions has been shown to influence the coverage and structure of chemisorbed organic compounds [47].

Sulfuric acid, which is widely used in a variety of electrochemical investigations, was also used in this study. Sulfuric acid electrolyte solutions can be prepared without much difficulty using double distilled grade sulfuric acid. The structure of H_2SO_4-derived ad-species on Pd(111) was recently studied in detail by EC-STM [48].

[1] It may be noted in Figure 24 A that, whereas AES shows that no other species existed on the UHV-prepared surface, the HREEL spectrum indicates the presence of CO (ν = 1910 cm^{-1} is due to the C≡O stretch and ν = 368 cm^{-1} to the Pd-C stretch). Traces of CO are ubiquitous in UHV systems and only small amounts ($\theta \leq 0.01$) are actually chemisorbed, but HREELS is ultra-sensitive to CO. Surface CO, however, is further minimized when the electrode is immersed in a dilute TFA and is completely absent when the electrode is exposed to aqueous solutions of H_2Q or BQ (*vide infra*) [20]. That is, the aromatic compounds displace adsorbed CO from the surface.

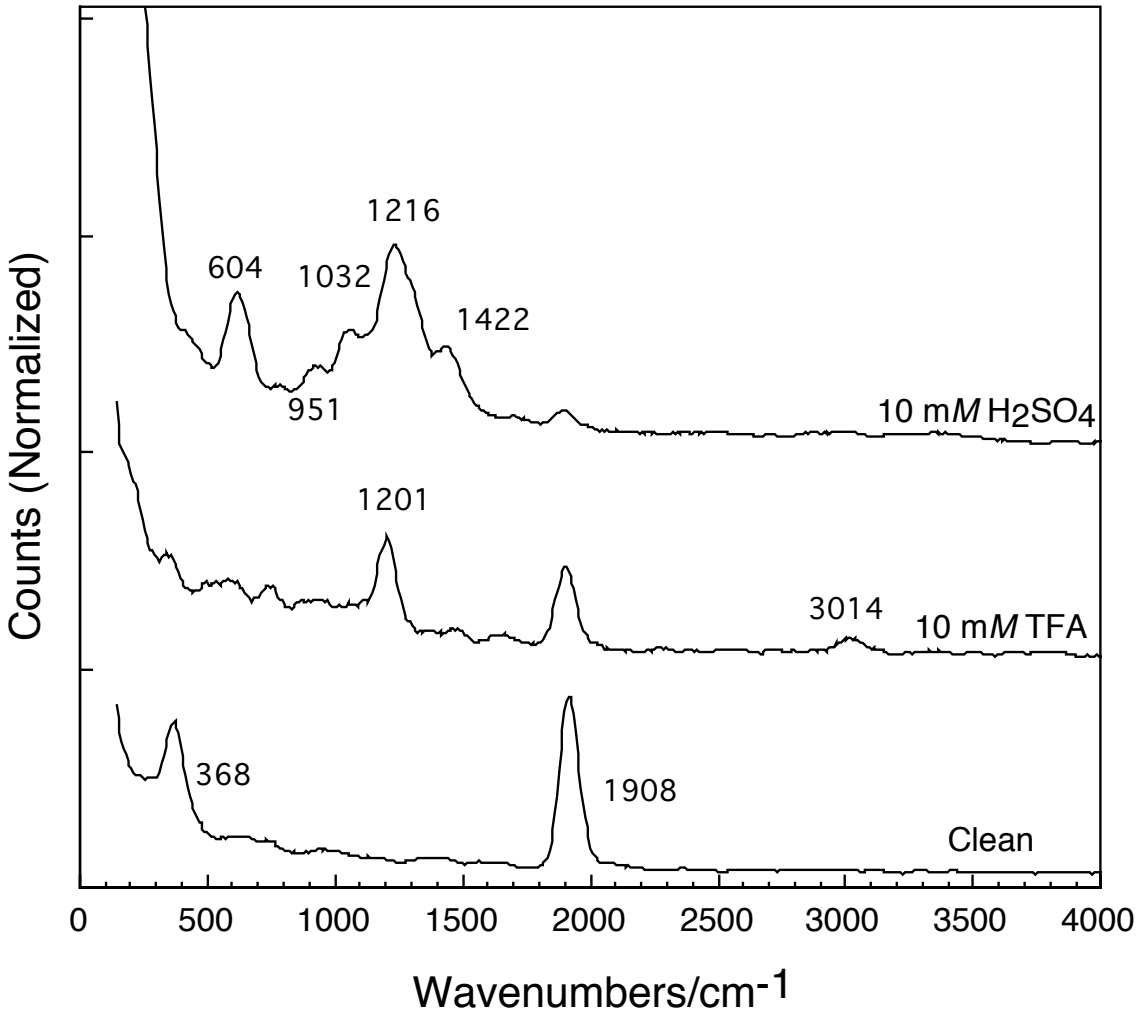

Figure 24. HREEL spectrum of a clean Pd(100) surface (A), Pd(100) after emersion from 10 mM TFA (B) and 10 m*M* H_2SO_4 (C), respectively. Experimental conditions: incidence and detection angles: 62° from surface normal; room temperature.

The HREEL spectrum of a Pd(100) surface emersed[2] from an aqueous 10 m*M* H_2SO_4 solution is shown in Figure 24 C. It is important to mention that the CO peak at 1908 cm^{-1} is barely observable, which indicates that sulfuric acid is sufficiently surface-active to displace CO from the surface. Further evidence of the surface-activity of H_2SO_4 is the fact that it survives ultra-high vacuum conditions and is present, albeit in submonolayer coverages, on the Pd(100) surface as revealed by both the HREEL and AES spectra (Figure 25). The peak assignments in the HREEL spectrum are given in Table 2; included in the Table are data from other published studies on polycrystalline and well-defined Pt [49,50,51,52] and Pd [53] surfaces, as well as from H_2SO_4 vapor [54,55,56]. It is noteworthy that the current work is the only one that shows all the peaks observed for vapor-phase H_2SO_4, although, except for the ν_s(SO) peak, the peak frequencies are not identical; this may be due to adorption-induced vibrational-frequency shifts [57].

[2] Emersion is a term coined to indicate that the electrode was removed from the electrolytic solution under potential control. It has been shown that, unless the electrode is overly polarized, the compact (inner) layer that consists of chemisorbed materials remains intact upon emersion [18]. That is, the coverage and structure of a chemisorbed layer is the same in solution and in ultra-high vacuum.

Table 2. IRAS frequencies for sulfate adsorbed on Pt and Pd single crystals and IR frequencies of sulfuric acid vapor compared to HREELS vibrational frequencies of H_2SO_4 on Pd(100) (cm^{-1}).

Peak Assignment	SO_2 bend	$\nu_s(SO)^*$	$\nu_{as}(SO)^*$	$\nu_s(SO)$	$\nu_{as}(SO)$
Polycrystalline Pt [49]		1030	1120	1200	
Pt(111) [50]				1200	
Pt(100), Pt(110) [51,52]			1100	1200	
Pd(111), Pd(100), Pd(110) [53]				1200	
Sulfuric acid vapor [54]	550.5	891.4	1157.1	1220.1	1464.7
HREELS (this work)	604	951	1032	1216	1422

ν_s, symmetric stretching vibration; ν_{as}, asymmetric stretching vibration; SO, S-O bond uncoordinated to metal; SO^*, S-O bond coordinated to metal.

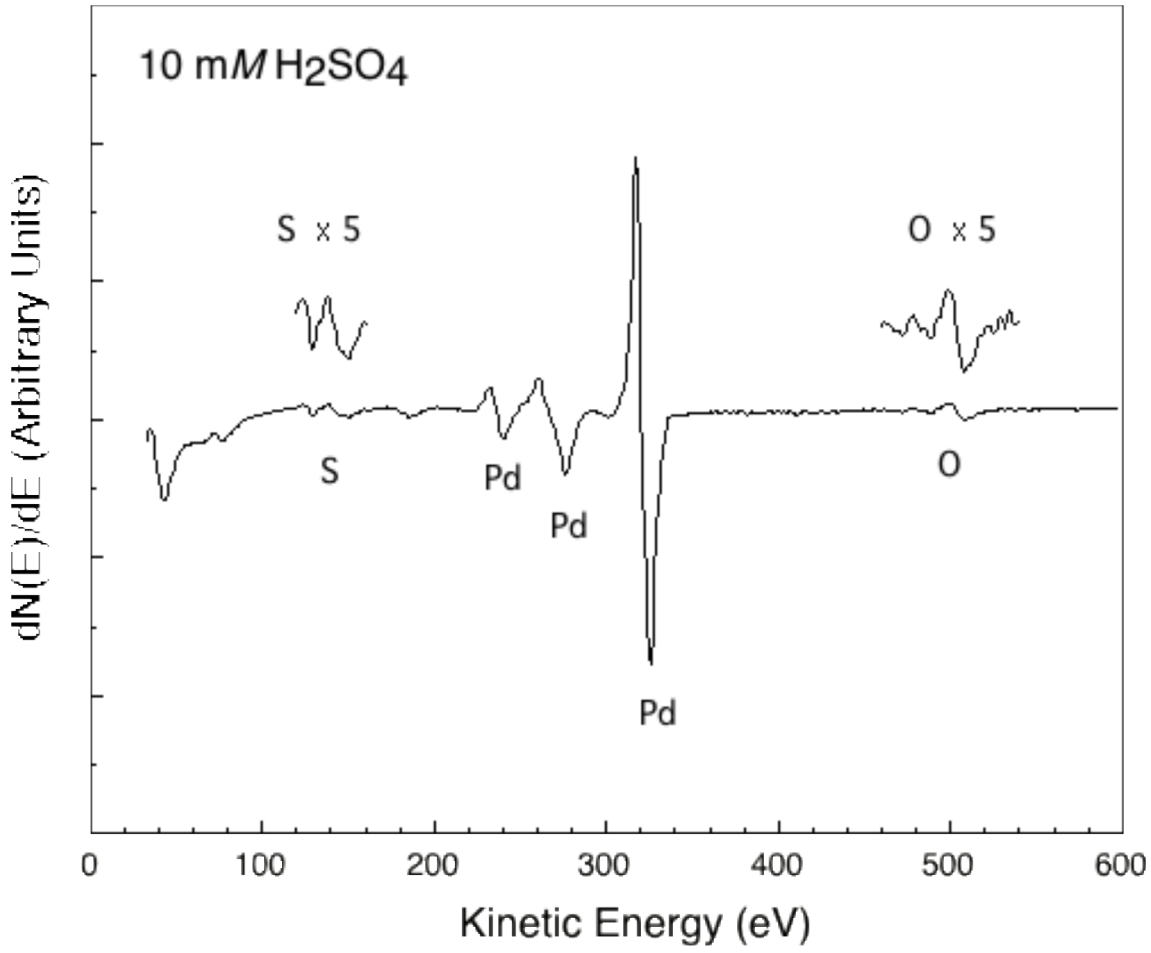

Figure 25. AES spectrum of a Pd(100) surface after emersion from an aqueous 10 m*M* H_2SO_4 solution. Experimental conditions: beam energy, 2 KeV; beam current, 1.6 μA.

Chemisorption

Figure 26 shows a series of HREEL spectra of a Pd(100) surface emersed from a 1 m*M* H_2Q + 10 m*M* H_2SO_4 solution for 180 seconds at potentials within the double-layer region. The electrode was then rinsed with either 1 m*M* H_2SO_4 or pure water following the emersion. The spectrum obtained after acid rinse (A) reveals two peaks at 604 and 1201 cm^{-1} which are more intense and broader than those obtained from the pure water rinse (B and C). The most probable scenario regarding the appearance of sulfate anions in the HREEL spectrum is the coadsorption of sulfate anions along with the organic molecules. Figure 27 shows the real space structure of a bigger aromatic compound, hydroquinone sulfonate (H_2QS) (A), and sulfate anions (B), adsorbed on Pd(111). The chemisorption of a sulfate anion occurs only at a three-fold site. The void space between H_2QS molecules is large enough to accommodate at least one sulfate anion. The coadsorption of the sulfate anions is not strong; as evidenced in Figure 26, the peak intensities (at 604 and 1201 cm^{-1}) diminishes with increasing number of rinses.

Additional experiment was conducted to ascertain the number of rinses that can eliminate essentially all the sulfate anions coadsorbed in the organic adlayer. Based on the previously documented inertness of TFA towards chemisorption on Pd surfaces [20,46], the HREEL spectrum of a Pd(100) surface rinsed three times with 1 m*M* TFA after emersion in 1 m*M* H_2Q + 1 m*M* TFA solution was used as reference for a sulfate-free Pd surface. Results in Figure 28 reveal that, after five water rinses, the amount of sulfate anions is virtually nil.

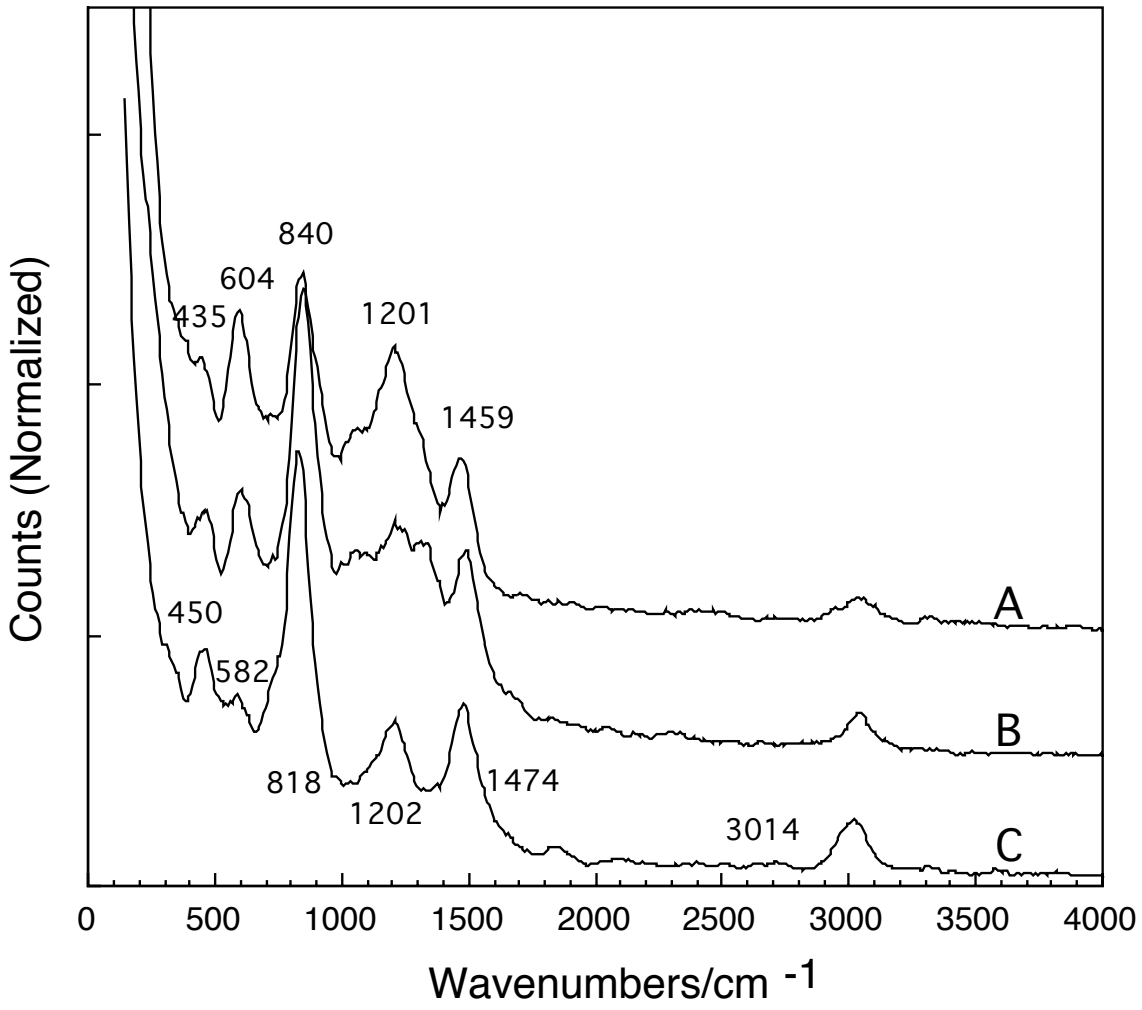

Figure 26. HREEL spectra of a Pd(100) surface emersed from a 1.0 m*M* H_2Q + 10 m*M* H_2SO_4 solution at 0.1 V vs. Ag/AgCl (1 m*M* Cl^-). The surface was then rinsed with (A) 1 m*M* H_2SO_4 solution 3 times; (B) pure water 3 times; and (C) pure water 5 times, respectively. Other experimental conditions were as in Figure 24.

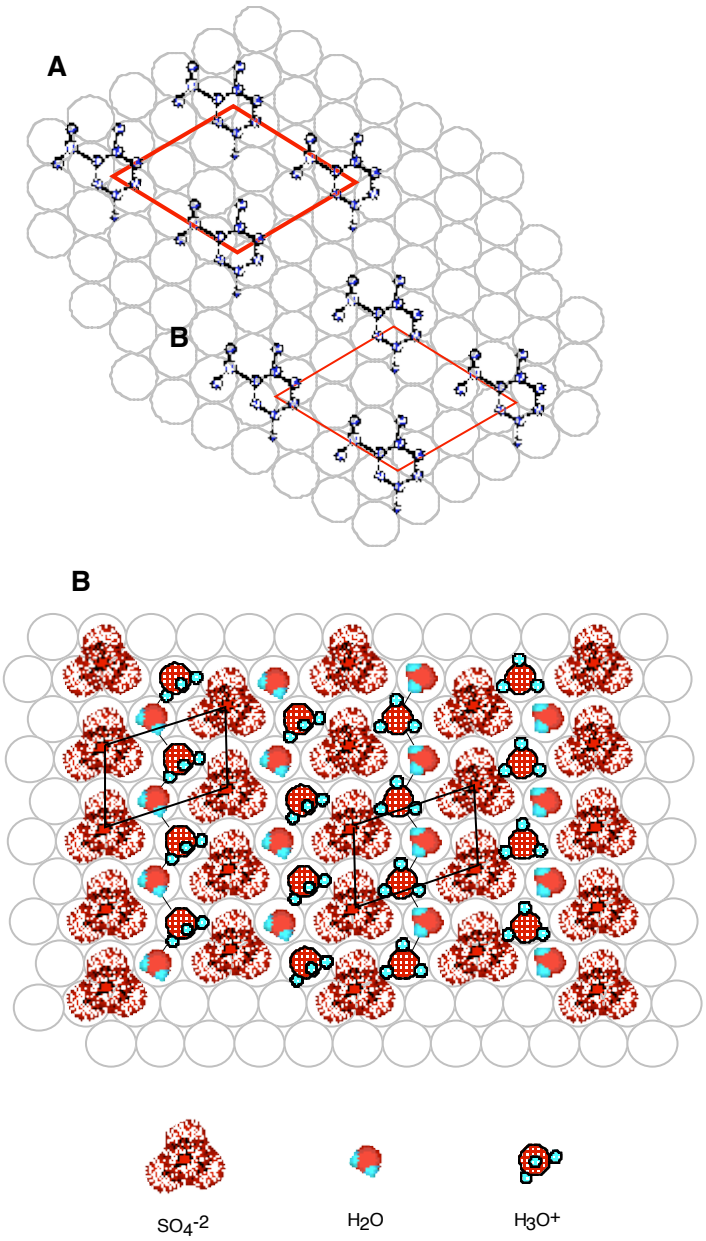

Figure 27. Schematic illustration of the adlayer structure of (A) (3×3)-H_2QS on Pd(111). (B) (√3×√7)-sulfate on Pd(111).

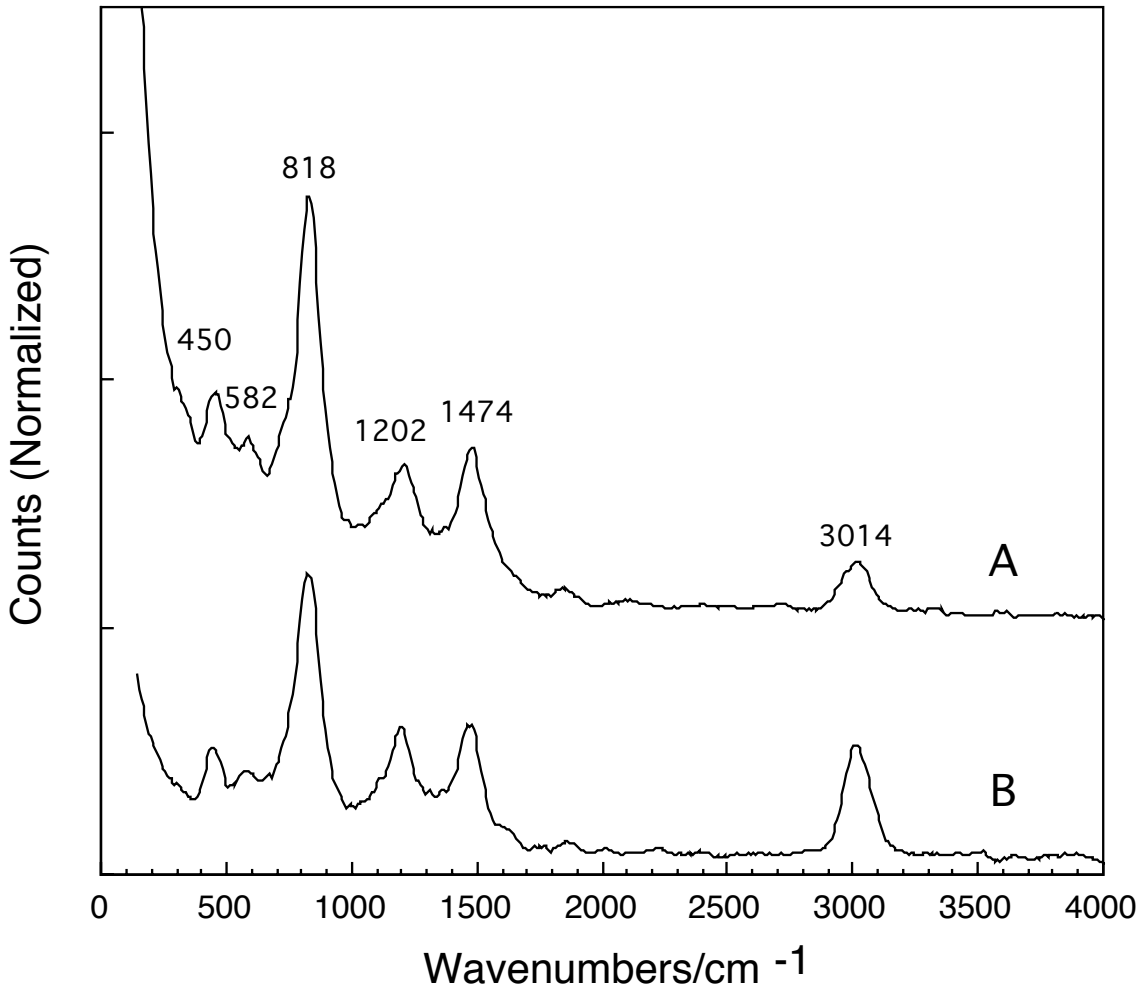

Figure 28. HREEL spectrum of a Pd(100) surface after emersion at 0.1 V vs. Ag/AgCl (1 mM Cl^-) from (A) a 1.0 m*M* H_2Q + 10 m*M* H_2SO_4 solution, then rinsed with pure water five times; and (B) a 1.0 m*M* H_2Q + 1.0 m*M* TFA solution, then rinsed with 1.0 m*M* TFA 3 times. Other experimental conditions were as in Figure 24.

Further evidence is provided by AES (Figure 29). The sulfur peak (152 eV) is very small and negligible[3]. Unless otherwise stated, this five-rinsing procedure is performed in all the experiments after the final emersion from a H_2SO_4 solution.

The peak assignments for the HREEL spectrum of species chemisorbed onto Pd(100) from a 1 m*M* H_2Q + 10 m*M* H_2SO_4 solutions (Figure 28) were based on previous similar work on a Pd(111) surface [20], as shown in Table 3.

An important feature of this HREEL spectrum is the loss peak at 818 cm^{-1} which corresponds to an out-of-plane CH bending mode, γ(CH). The fact that such peak is more intense than the one at 3014 cm^{-1}, an in-plane CH stretch mode ν(CH), implies that the chemisorbed organic molecule adopts a flat (η^6) orientation on the surface. Based on the metal-surface dipole selection rule of HREELS, the presence of in-plane modes, ν(CC), δ(CH), ν(C=O) and ν(CH), suggests that the surface species are not completely parallel to the surface, but are slightly tilted.

[3] The oxygen peak at 510 eV is believed to originate primarily from chemisorbed organic species, not from sulfate anions.

Table 3. Peak assignment of HREEL spectrum in Figure 28.

Wavenumbers/cm^{-1}	450, 582	818	1202	1474	3014
assignment	δ(CC)	γ(CH)	ν(CC) and/or δ(CH)	ν(C=O)	ν(CH)

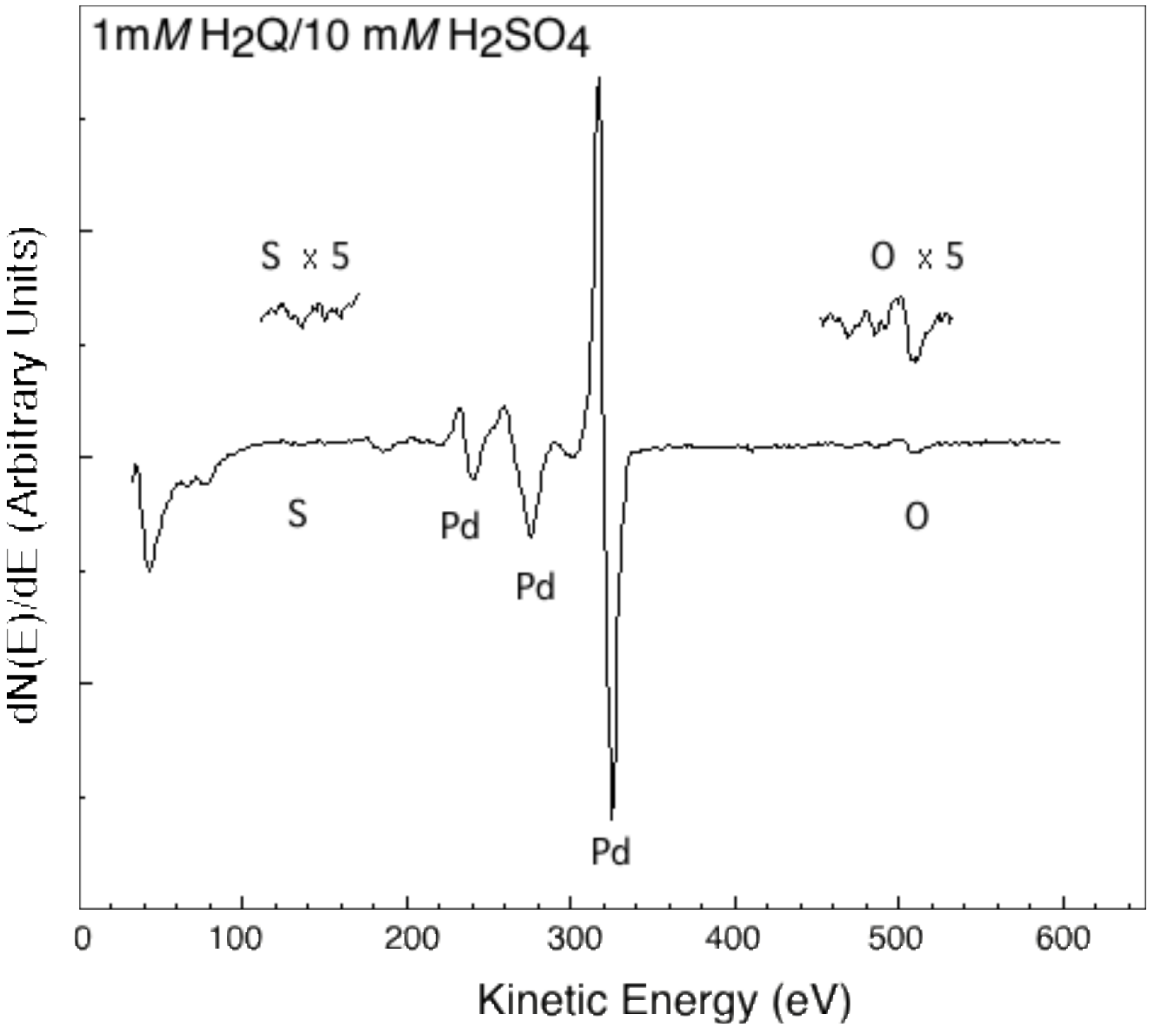

Figure 29. AES spectrum of a Pd(100) surface after emersion from an aqueous 1.0 m*M* H_2Q + 10 m*M* H_2SO_4 solution, followed by water rinse five times. Experimental conditions were as in Figure 25.

The appearance of the ν(CH) peak, as suggested in the literature studies of benzene, may be also due to impact scattering [58]. In HREELS, interaction of low energy electrons with the matter can be described using two mechanisms, the dipole scattering and impact scattering. Dipole scattering can be detected only at the specular position (mirror reflection), while impact scattering can be seen at all angles but is minimum at the specular angle. One way to distinguish if a vibrational mode is contributed by impact or dipole mechanism is by: (i) taking a pure impact HREEL spectrum at an off-specular direction; (ii) subtracting the pure impact spectrum from a specular HREEL spectrum, to obtain a pure dipole spectrum [59]. Since the HREEL spectrometer employed in this study is not equipped with a rotatable analyzer, a pure impact measurement is difficult to collect due to the limited rotation of the sample holder. A different diagnostic method was used to probe the mechanisms involved in the vibrational modes in the HREEL spectra.

According to the dielectric theory [60], the excitation probability (or normalized peak area) of impact scattering on a metallic substrate will increase as the primary energy of the incident electrons is increased; on the other hand, for dipole scattering, the excitation probability decreases with the primary energy of incident electrons. In other words, the peak-area dependence of the applied beam energy can provide information about the mechanism contributing to the vibrational modes of interest. A series of specular HREEL spectra obtained on Pd(100) electrode emersed from a 1 m*M* H_2Q + 1 m*M* TFA solution, with beam energies ranging from –2.01 eV to –8.85 eV, is shown in Figure 30. Normalized peak areas of the out-of-plane mode, γ(CH) band, and the in-plane mode, ν(CH) band, were plotted as a function of beam energy, shown in Figure 31. Evidently, peak areas of the γ(CH) band decreased as energy of the incident electrons was increased; this result is a strong indication that the γ(CH) band has a pure dipole character. Peak areas for the ν(CH) band, however, initially increased and then tapered off towards the end; this trend is not characteristic of either impact or dipole interaction. It is possible that the ν(CH) band is contributed by a composite of both dipole and impact interactions. The fact that the ν(CH) band partly exhibits a dipole character supports the notion that the chemisorbed species adopts a parallel with a slight tilt.

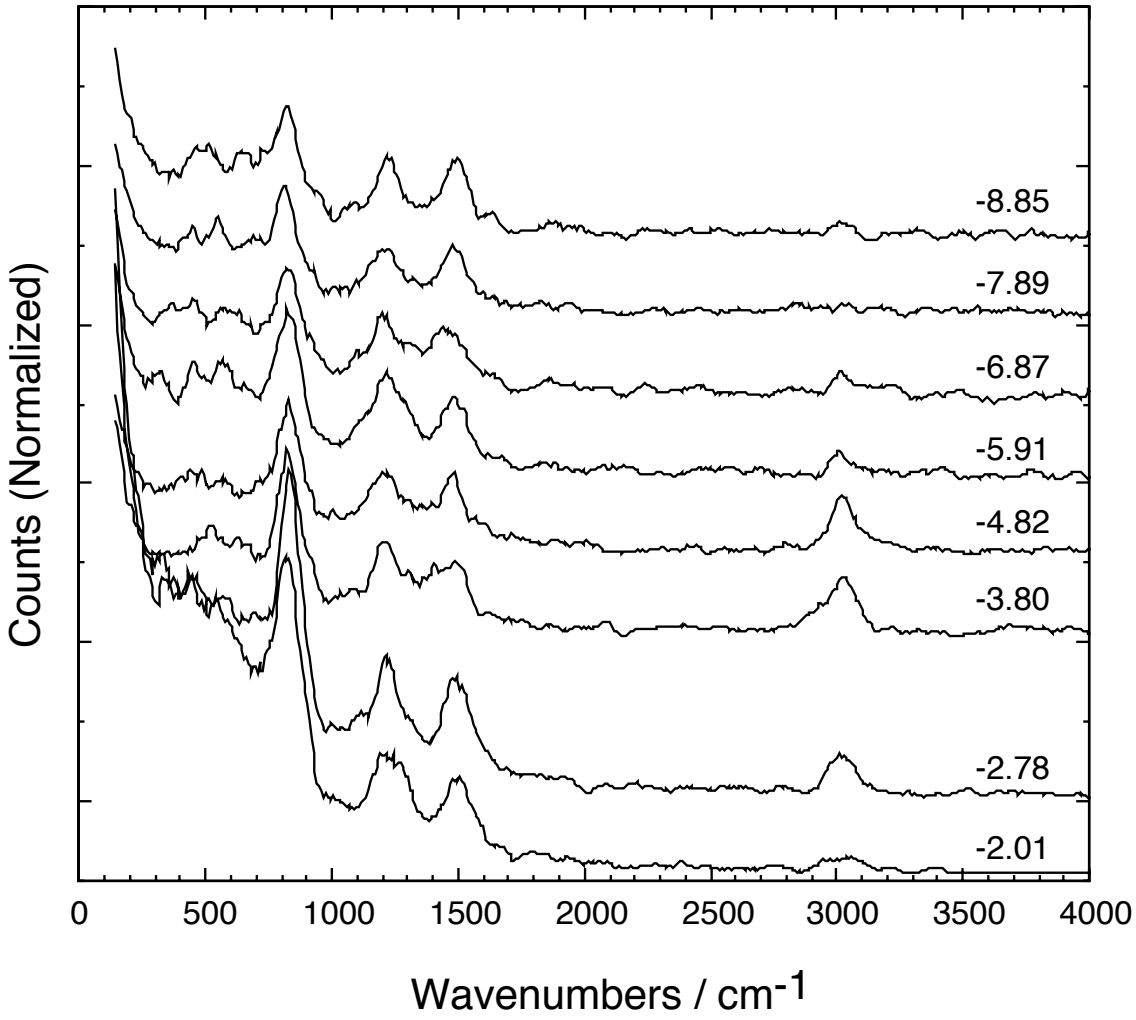

Figure 30. HREEL spectra obtained at different beam energies (eV) on a Pd(100) surface emersed from a 1 m*M* H_2Q + 1 m*M* TFA solution. Other experimental conditions were as in Figure 24.

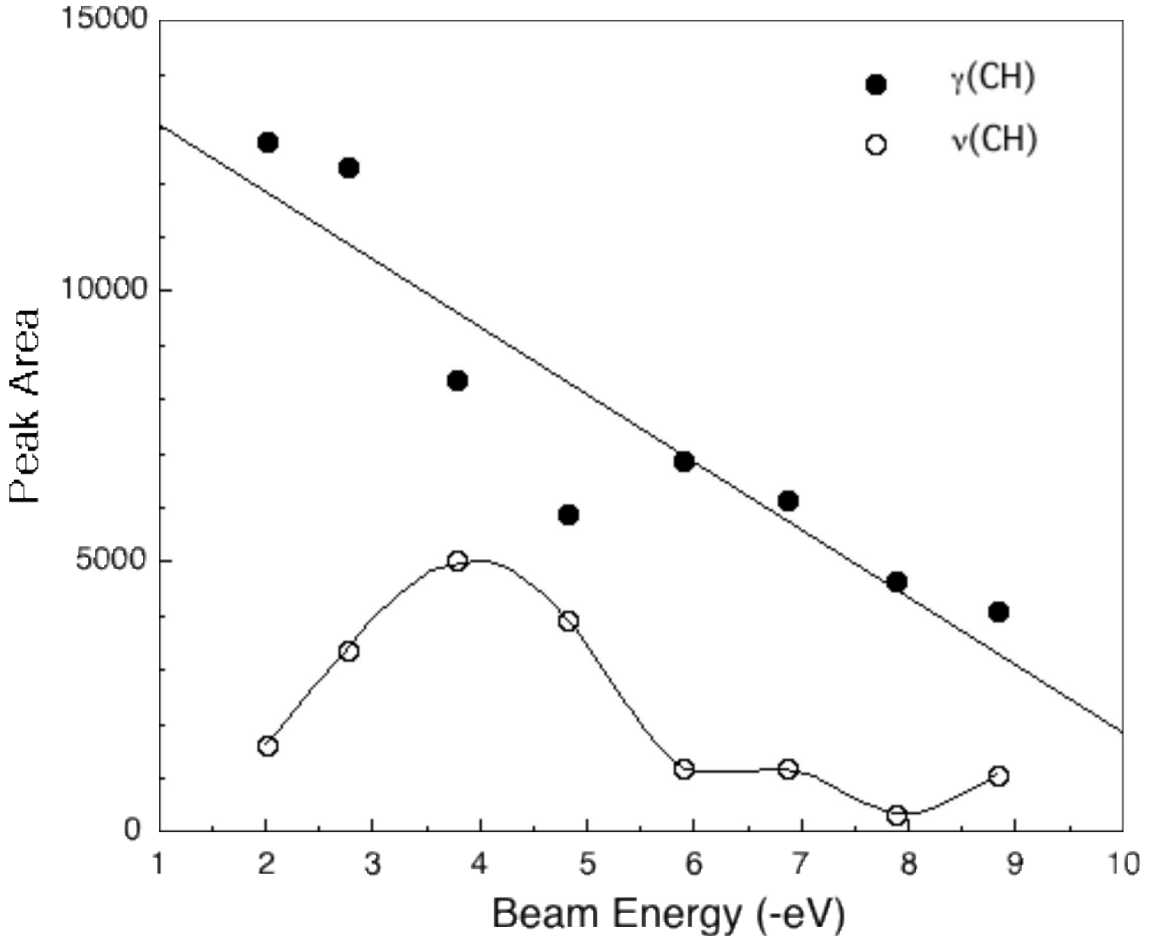

Figure 31. Peak areas of the normalized HREELS ν(CH) and γ(CH) bands as a function of the beam energy. The solid line interconnect the filled circles is a linear fit of the data points, the line interconnect the open circles does not represent any theoretical fit.

It is now confidently established that the chemisorbed species are not completely parallel to the surface but are slighted tilted, and this small tilt activated the in-plane modes appearing the specular HREEL spectrum.

While the HREEL spectrum of gas-phase H_2Q exhibits an in-plane ν(OH) stretch at ~3600 cm^{-1} [61], no such peak was observed in Figure 28. The absence of ν(OH) in the HREEL spectrum suggests the absence of a phenolic OH functional group in the adsorbed molecule. It can be inferred that H_2Q was oxidized to benzoquinone (BQ) upon chemisorption on Pd(100) surfaces.

Additional support for the (H_2Q_{aq}-to-BQ_{ads}) chemisorption process was provided by the HREEL spectrum obtained on Pd(100) surface after emersion from an aqueous 1 m*M* BQ + 10 m*M* H_2SO_4 solution, shown in Figure 32. It is clear that this spectrum is essentially identical to that obtained from a H_2Q solution. In other words, regardless of the starting material (H_2Q or BQ), the same adsorbed species is generated upon chemisorption. The surface reactions that accompany H_2Q and BQ chemisorption at Pd(100) can be written as follows:

$$Pd + H_2Q_{aq} \rightarrow Pd\text{-}\eta^6\text{-}BQ_{ads} + H_2 \quad (25)$$

$$Pd + BQ_{aq} \rightarrow Pd\text{-}\eta^6\text{-}BQ_{ads} \quad (26)$$

Both H_2Q and BQ are chemisorbed onto Pd(100) surfaces as Pd-η^6-BQ_{ads} in a slightly tilted η^6-orientation. These results agree well with the reported chemisorption of H_2Q and BQ on Pt electrodes [62,63].

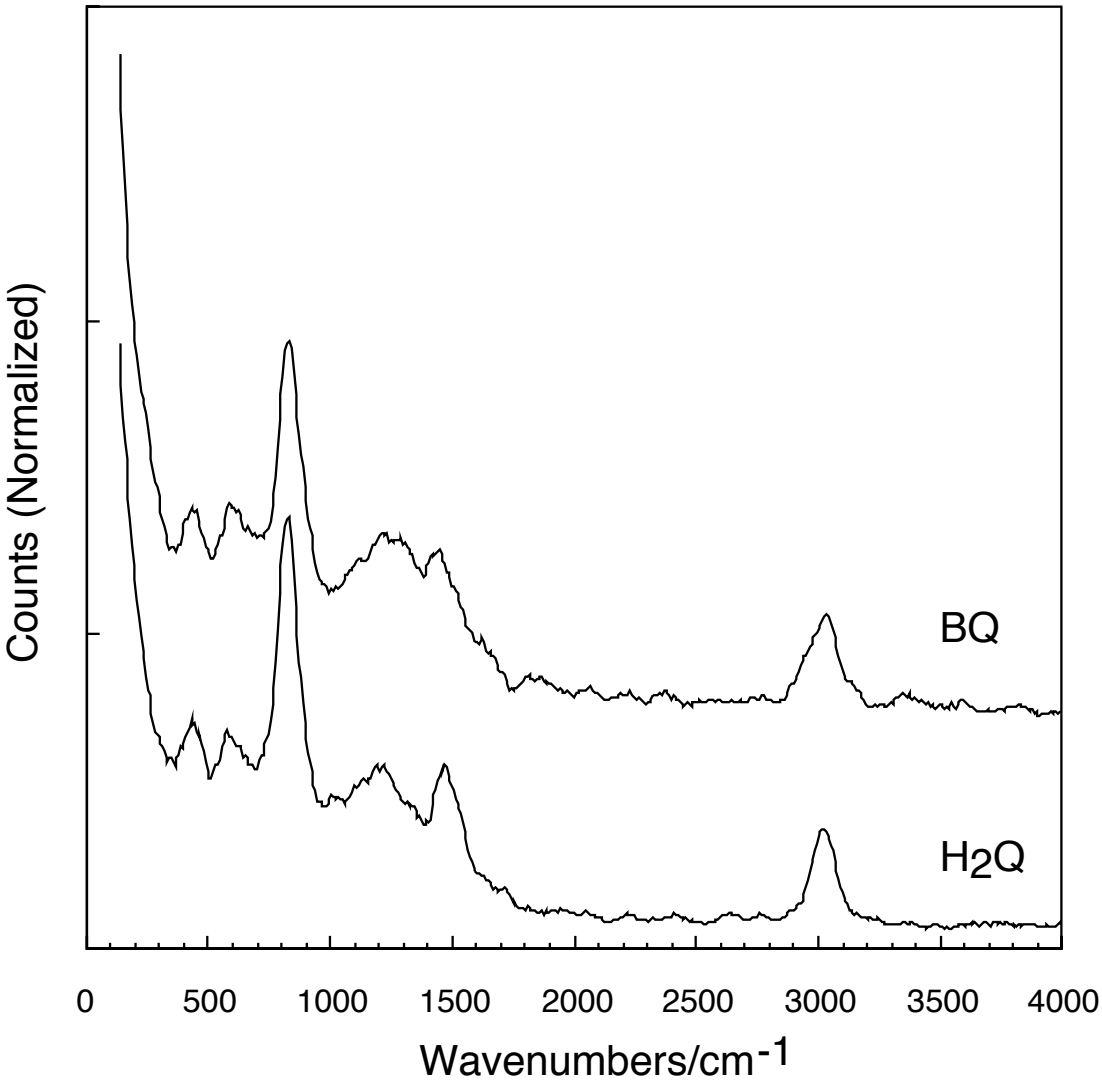

Figure 32. HREEL spectra of a Pd(100) surface after emersion from a 1 m*M* BQ + 10 m*M* H_2SO_4 solution and a 1 m*M* H_2Q + 10 m*M* H_2SO_4 solution, respectively. Other experimental conditions were as in Figure 24.

Chemisorption Isotherms

TLE experiments showed a significant effect of concentration on the mode of chemisorption of H_2Q. A similar isotherm was constructed by plotting AES and HREELS signals as a function of the adsorbate concentration.

Figure 33 shows a set of HREEL spectra obtained on the Pd(100) surface after exposure to H_2Q solutions of concentrations ranging from 0.02 m*M* to 1 m*M*. By dictates of the HREELS surface selection rule, a transition from parallel to edge-vertical orientation of surface species "turns on" some in-plane vibrational modes while deactivating out-of-plane modes. As can been seen from the spectra in Figure 33, no significant intensity changes were observed. This fact suggests that, under the condition of the present experiments, the orientation of chemisorbed species on Pd(100) surfaces seems to be concentration independent.

Corresponding AES spectra are shown in Figure 34. By visual comparison of the AES spectra, it appears that the oxygen signal showed no evident increase as the adsorbate concentration was increased. However, when the AES O/Pd ratios were plotted as a function of H_2Q concentration, a distinct growth can be observed (open squares in Figure 35). The increase in the AES O/Pd ratios indicates an increase in the surface concentration of the chemisorbed species; this relationship can also be evidenced by the H_2Q concentration-dependent increase in HREELS peak intensities. The integrated areas of the normalized[4] γ(CH) (filled circles) and ν(CH) (open circles) HREEL loss peaks were also plotted as a function of H_2Q concentration, as shown in

[4] The normalization procedure for all the HREELS spectra is described in the experimental section (page 26)

Figure 35. The AES O/Pd ratio registered only about 10% growth (from 0.029 to 0.032) as the H_2Q concentration was increased from 0.02 m*M* to 1 m*M*, while the HREELS γ(CH) peak area was nearly doubled (from 5051 to 8161). The high-energy electron beam (~2 KeV) employed in AES could result in electron-induced desorption (EID) of the surface species and even moderate damage to the substrate [64]; this phenomenon may be responsible for the non-dramatic increase in the AES O/Pd ratios. The HREELS ν(CH) peak area, on the other hand, kept an almost constant value at 4000. In view of the fact that ν(CH) mode is complicated by impact scattering mechanisms, the peak areas of normalized HREELS γ(CH) band are more precisely related to the surface coverages of the chemisorbed species. The significant growth in HREELS γ(CH) signal represented a substantial increase in the surface coverage of the chemisorbed species, which is possible only if the chemisorbed species reorient (from η^6 to η^2) and form more dense packing afforded by η^2 orientation.

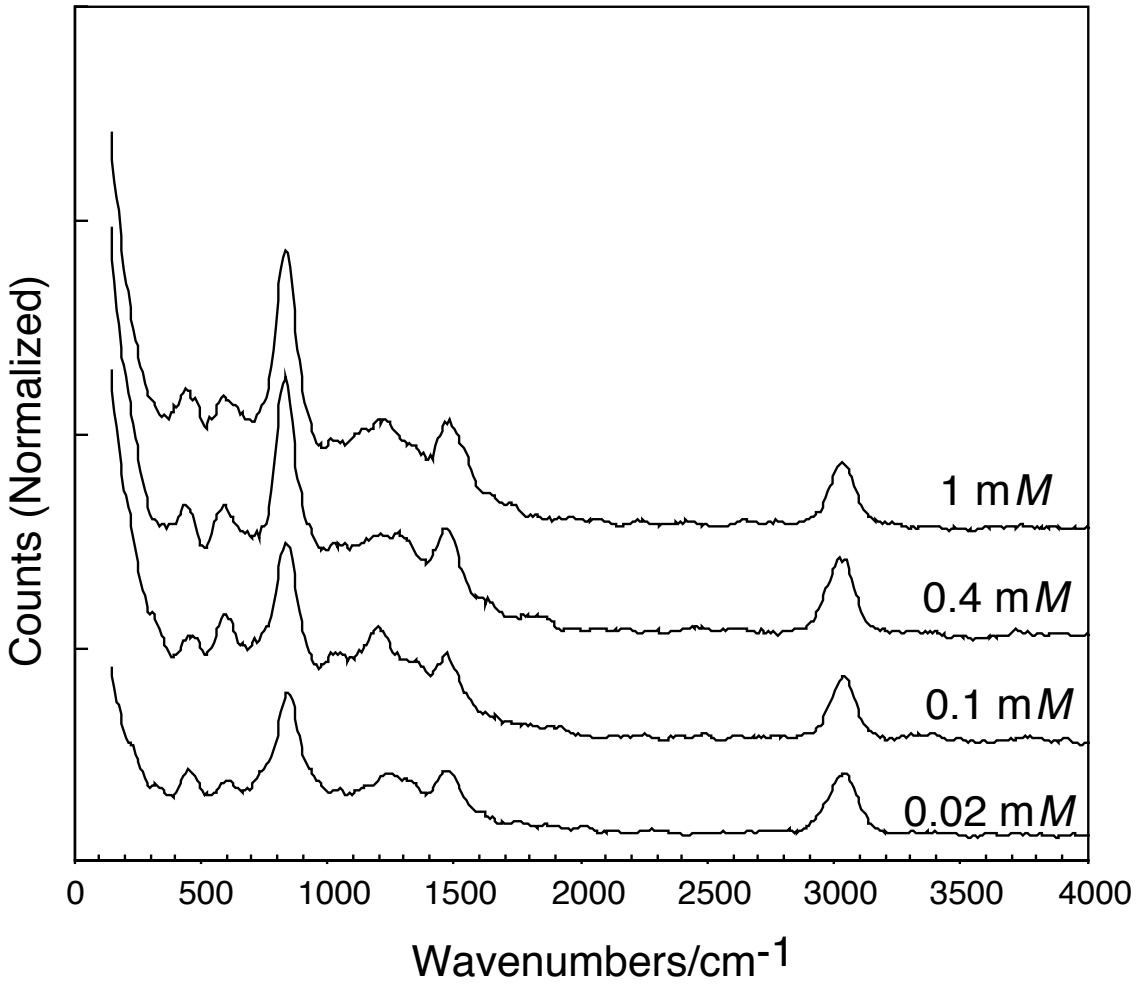

Figure 33. HREEL spectra of Pd(100) surface with surface complexes chemisorbed from H_2Q solutions of varied concentrations.

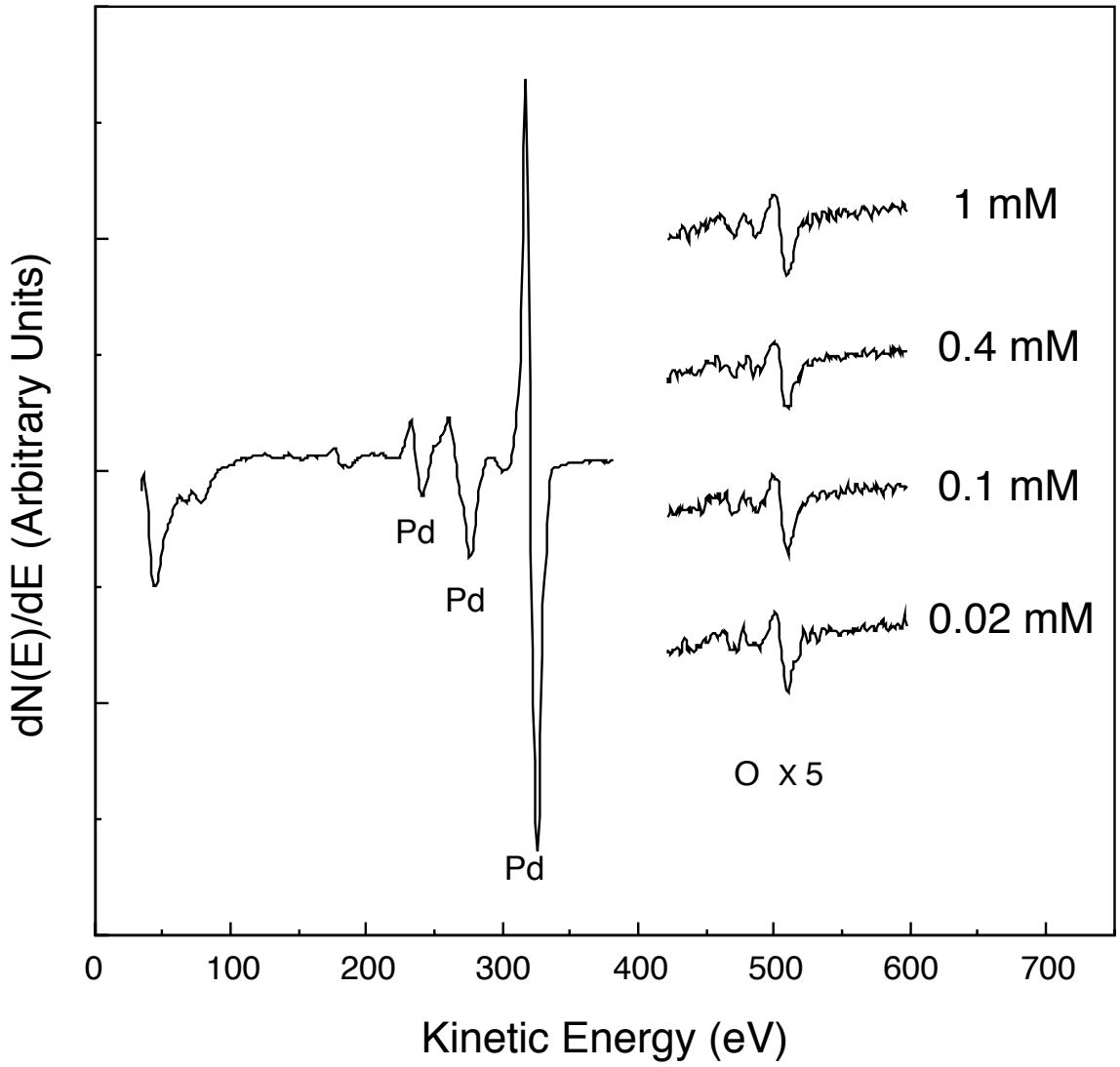

Figure 34. AES spectra of a Pd(100) surface with surface complexes chemisorbed from H_2Q solutions of varied concentrations.

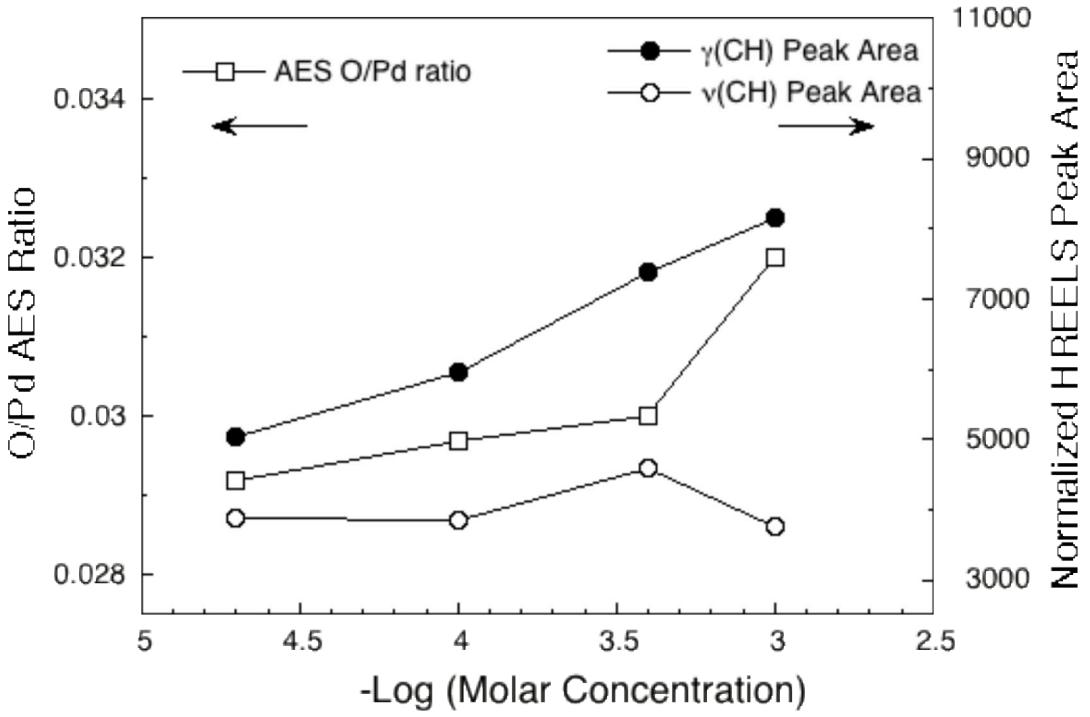

Figure 35. Plots of the O/Pd AES ratio, normalized γ(CH) and ν(CH) HREELS peak areas as a function of H_2Q concentration. The solid lines interconnect data points and do not represent any theoretical fit.

It is believed that, at high concentrations, the Pd surface was initially covered with edge-vertical species but, because of the ultra-high vacuum employed, only the well-anchored parallel Pd-η^6-BQ_{ads} species were observed in vacuum. The chemisorption of H_2Q onto Pd(100) can thus be surmised as:

$$Pd-\eta^6-BQ_{ads}+H_2 \xleftarrow{C<0.1mM} Pd+H_2Q \xrightarrow{C>1mM} Pd-\eta^2-H_2Q_{ads}+H_2$$

$$Pd-\eta^6-BQ_{ads} \xleftarrow{C<0.1mM} Pd+BQ \xrightarrow{C>1mM} Pd-\eta^2-H_2Q_{ads}$$

It might be worthwhile to mention that: (*i*) previous studies in chemisorption of H_2Q or BQ on Pt single crystals neither revealed η^2-oriented species even at high adsorbate concentrations (≥1m*M*) [46, 65]. (*ii*) IRAS spectra for the η^2-oriented species on Pt is diphenolic with the 2,3-carbons bound to the surface [14], and (*iii*) the similarity of Pt and Pd in terms of chemisorption-induced rest-potential shifts implies that the same oxidative chemisorption also takes place on Pd as well, i.e., 2,3-η^2-H_2Q are formed at higher concentration on either Pd or Pt. It is possible that the η^2-oriented surface complex is not stable under the UHV environment. When the Pd(100) electrode is brought into the surface analysis chamber for characterization, part of the η^2 species might be pumped away instantly.

Electrochemical Oxidation

The cyclic voltammogram of a clean and ordered Pd(100) electrode in 10 m*M* H_2SO_4 is given in Figure 36. Two features characteristic of an ordered Pd(100) single crystal surface are noticeable: (*i*) An oxidation-reduction (redox) peak at -0.25 V, typically absent in the TLE studies, is ascribed in literature to adsorption and desorption of sulfuric acid-derived anions on the ordered Pd(100) surfaces [53]; and (*ii*) the small oxidation peak at 0.40 V is due to oxidation of the ordered Pd(100) surface. Although the given voltammogram is diagnostic of a clean and ordered electrode surface, the surface becomes disordered even after one oxidation cycle. Therefore, in the succeeding experiments, no oxidation cycle was performed prior to chemisorption of organic compounds.

A clean Pd(100) electrode was emersed from a 0.02 m*M* H_2Q and a 1 m*M* H_2Q solution, respectively. The electrode was then submerged in a solution of blank electrolyte and linear sweep voltammetry was performed. Resulting current-potential curves are displayed in Figure 37. The large oxidation peak at 0.65 V is due to anodic oxidation of both the chemisorbed species and the surface. It has been previously established that, at the low concentrations, the chemisorbed adlayer consists of η^6-BQ while at high concentration η^2-H_2Q predominates (c.f. Figure 35).

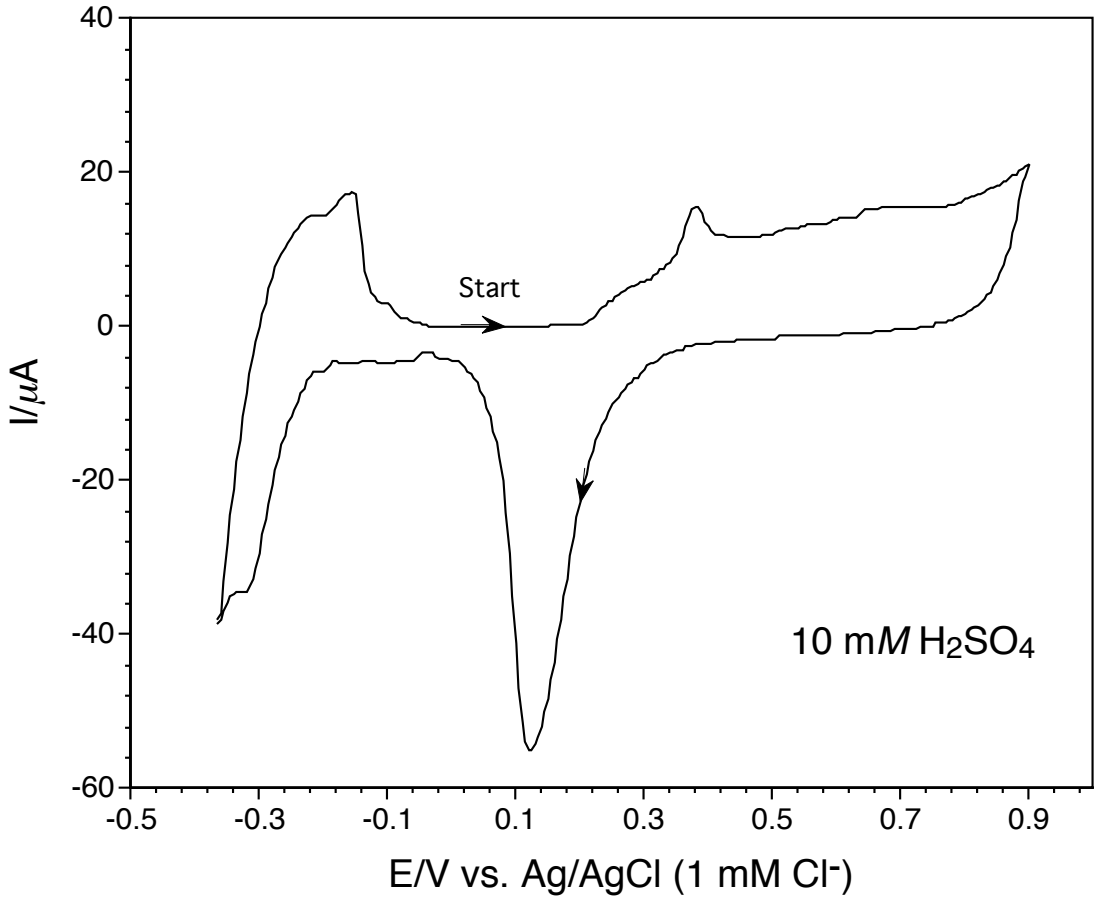

Figure 36. Cyclic voltammogram of a clean and ordered Pd(100) single crystal electrode in 10 m*M* H_2SO_4 solution. Scan rate: 5 mV/s. Note a different reference electrode (Ag/AgCl, 1 m*M* Cl^-) was used for UHV-EC experiments to minimize Cl^- contamination from the regular Ag/AgCl (1 *M* Cl^-) reference electrode used for TLE studies. A potential shift (~0.20 V) is expected compared to the CVs in TLE studies.

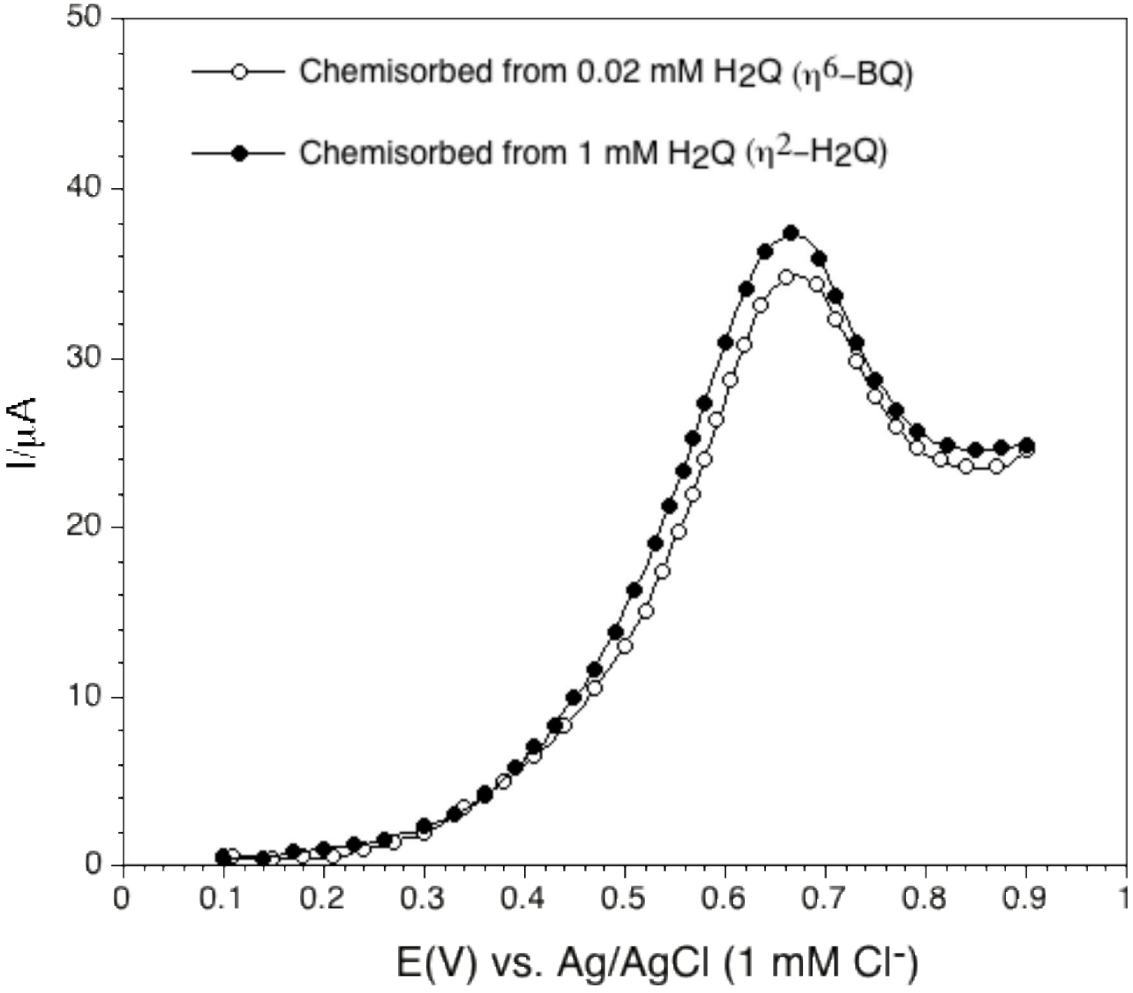

Figure 37. Current-potential curves for anodic oxidation of H_2Q chemisorbed at a Pd(100) electrode with different orientations. Scan rate: 5 mV/s. Other experimental conditions were as in Figure 36.

As shown in Figure 37, although the surface coverage of η^2-H_2Q is almost twice as much as that of η^6-BQ, the anodic oxidation peak for the η^2-species is *only slightly higher* than that of the η^6-species. This observation concurs with TLE results, strongly suggesting that the extent of oxidation is different for these two surface species.

The anodic oxidation reaction was further investigated by correlating HREELS, AES, and coulometric measurements with anodic-oxidation potential and electrolysis time. Specifically, two potential-step experiments were performed: (*i*) Anodic oxidation at different potentials with a fixed electrolysis time; (*ii*) Excursions to varying oxidation potentials with varied electrolysis time.

Anodic Oxidation at Different Potentials and Fixed Electrolysis Times

Before each anodic oxidation, the electrode was coated with η^2-H_2Q surface complexes chemisorbed from a 1 m*M* H_2Q solution. Figure 38 shows HREEL spectra obtained after a 3-minute anodic oxidation at pre-selected potentials varied from 0.1 V to 0.7 V, respectively. Not much difference can be observed in the HREEL spectra for η^6-BQ in Figure 39.

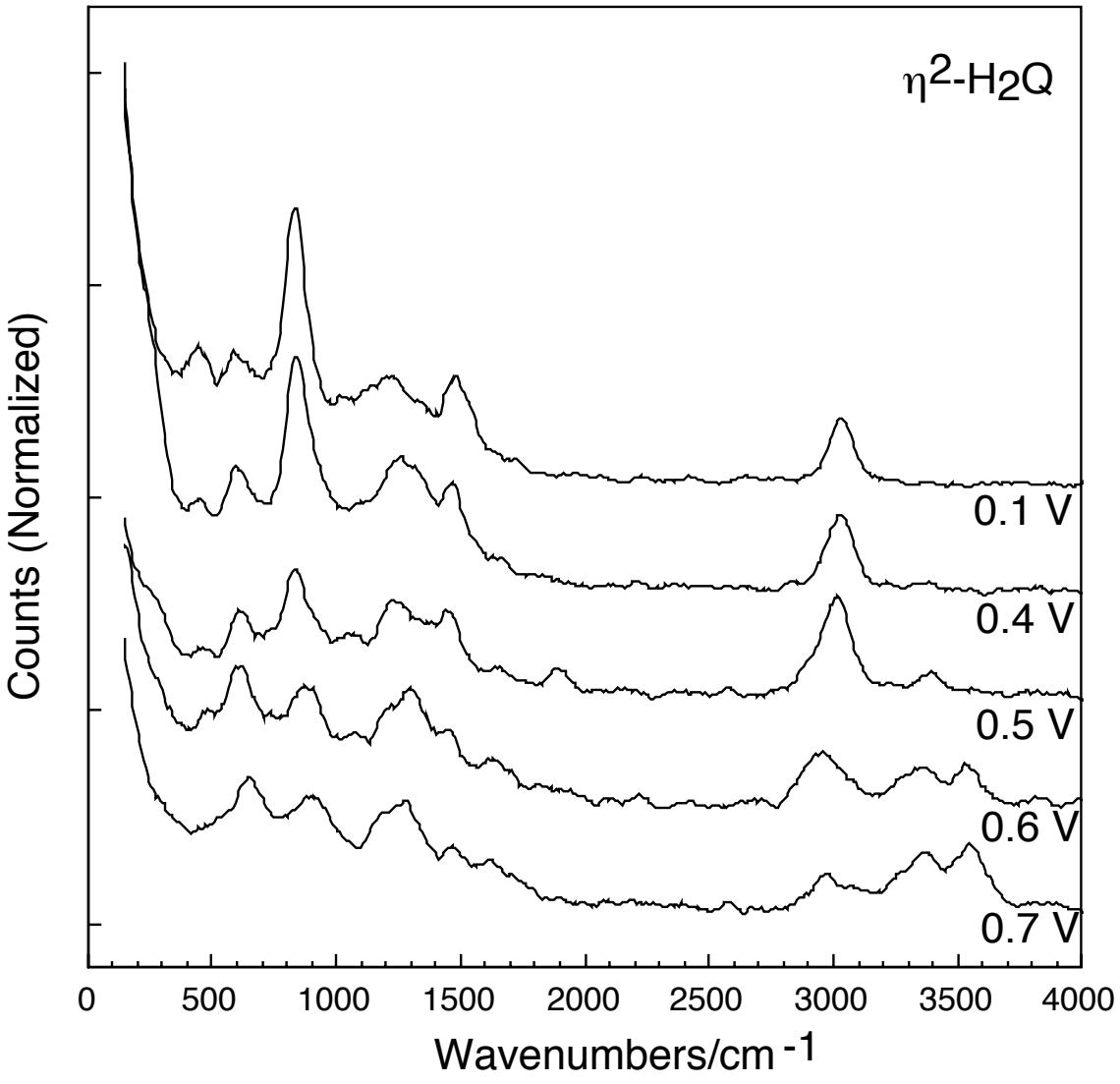

Figure 38. HREEL spectra of Pd(100) surfaces with η^2-H_2Q surface complexes subjected to different oxidation potentials (0.4 V, 0.5 V, 0.6 V, and 0.7 V) in 10 m*M* H_2SO_4 for 3 minutes.

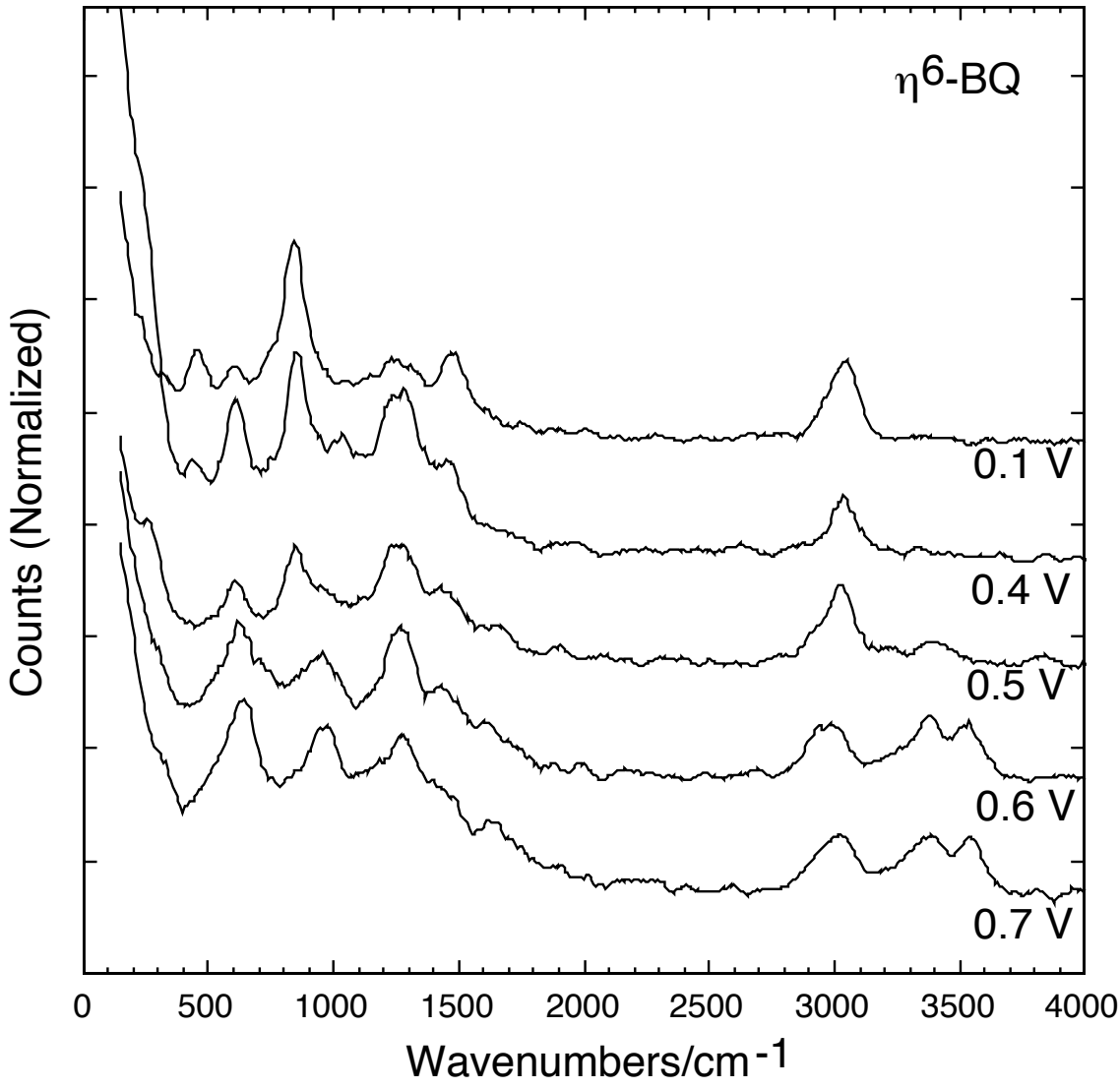

Figure 39. HREEL spectra of Pd(100) surfaces with η^6-BQ surface complexes subjected to different oxidation potentials (0.4 V, 0.5 V, 0.6 V, and 0.7 V) in 10 m*M* H_2SO_4 for 3 minutes.

The spectrum obtained at 0.4 V is similar to the one obtained at 0.1 V (open circuit potential), except for a slight increase in two loss peaks where the SO vibrations of the sulfate group (604 and 1216 cm^{-1}) overlap with the δ(CC) and ν(CC) (582 and 1202 cm^{-1}) of the organic species, and a small but noticeable decrease in the organic γ(CH) peak (818 cm^{-1}). The inception of anodic oxidation at 0.4 V is marked by the electrosorption of sulfate ions on the sites vacated by the oxidatively desorbed organic species. Substantiating this claim is the emergence of the characteristic sulfate loss peaks. As the potential increases, the surface coverage of chemisorbed species decreases while that of the sulfate anions increases. This trend, indicated by the gradual decrease in the γ(CH) peak and increase in the ν(SO) peaks, is possibly a result of the enhanced oxidation rate of the chemisorbed species at higher potentials. Oxidative removal of the organic species leaves the electrode surface susceptible towards oxidation. Surface hydroxyl groups are consequently formed; thereby OH stretching is detected at 3390 cm^{-1}. The higher the potential, the thicker the hydroxide layer becomes. A doublet can be observed in the hydroxide region (one at 3390 cm^{-1} and the other at 3544 cm^{-1}) in both 0.6-V and 0.7-V spectra. Peak splitting is thought to be a result of surface roughness introduced by surface oxidation. The one at lower frequency is assigned to hydroxide formed on (100) sites; the one at higher frequency, which appears later during the oxidation process, is probably due to hydroxide formation on roughened surface sites.

The origin of the peak 2962 cm^{-1}, present in both the 0.6-V and 0.7-V spectra, deserves further attention. Controlled experiments conducted in the absence of any chemisorbed organic species at 0.7 V revealed the same peak (Figure 40 C). Such result eliminates the possibility of assigning the peak to a ν(CH) mode. This peak most likely originates from hydrogen-bonded hydroxyl formed on the surface. Vibrations due to hydrogen-bonded hydroxyl groups are known to appear at the lower frequency side of the free (or isolated) hydroxyl group due to the hindrance brought by the hydrogen bonding [66]. A related case is the study by Henderson and Chambers who investigated the interaction of water with the α-Cr_2O_3(001) surfaces using HREELS [67]. Two loss peaks, appearing at 3600 and 2885 cm^{-1}, respectively, were observed in the HREEL data from the α-Cr_2O_3(001) surfaces exposed to H_2O at 300 K. The 3600 cm^{-1} peak was assigned to isolated surface hydroxyl group while the one at 2885 cm^{-1} was attributed to the hydrogen-bonded hydroxyl group.

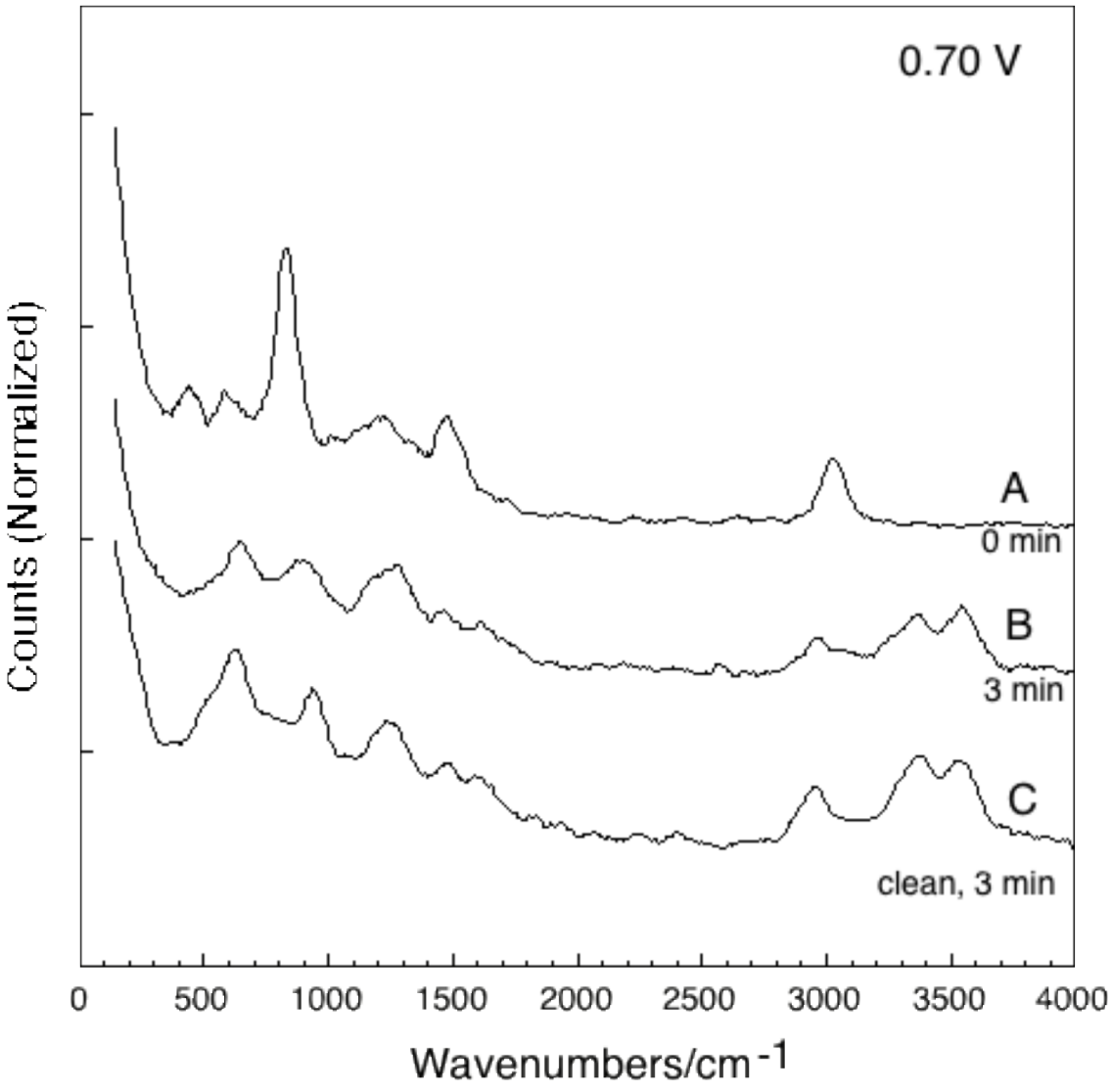

Figure 40. HREEL spectra of Pd(100) surfaces with η^2-H_2Q surface complexes (A) prior to oxidation; (B) after a 3-minute oxidation at 0.7 V; (C) after a 3-minute anodic oxidation at 0.7 V at a clean Pd(100).

As the applied potential is increased, the following subtle changes are observed in the HREEL spectrum: (*i*) Changes in the peak intensity and shape of the SO-stretch emanate from sulfate vibrational modes that are altered by hydroxide-laden rough surface. (*ii*) Extensive surface roughening induced by the imposition of high potentials gives rise to a small peak at ~1600 cm^{-1}, which is attributed to OH bending mode of the hydroxyl groups formed on the surface.

The roughness of the oxidized Pd(100) surface triggered a dramatic drop (about 20 times) in the counts of the HREELS elastic peak. The spectrum had to be scanned at least 40 times to achieve a reasonable S/N ratio. The roughened surface can be recovered after multiple cycles of thermal annealing in vacuum. In order to avoid possible damage to the crystallinity of the Pd(100) electrode, the applied potentials were limited to values below 0.8 V.

The progress of the reaction in terms of sulfate and hydroxide coverage is more dramatically depicted in the AES spectra (Figure 41). Clearly, as the potential increases, both oxygen and sulfur signals increased; this trend is consistent with HREELS results discussed above.

Coulometric data of the above potential-step experiments are shown in Figure 42. The background charge of a clean electrode was subtracted from the total charge arising from the organic-coated electrode. The plot reveals that, as the potential increases, the charge due to anodic oxidation of the organic surface complexes also increases; this implies that more surface speies are oxidized at higher potential. This behavior is also in good agreement with the HREELS data discussed above.

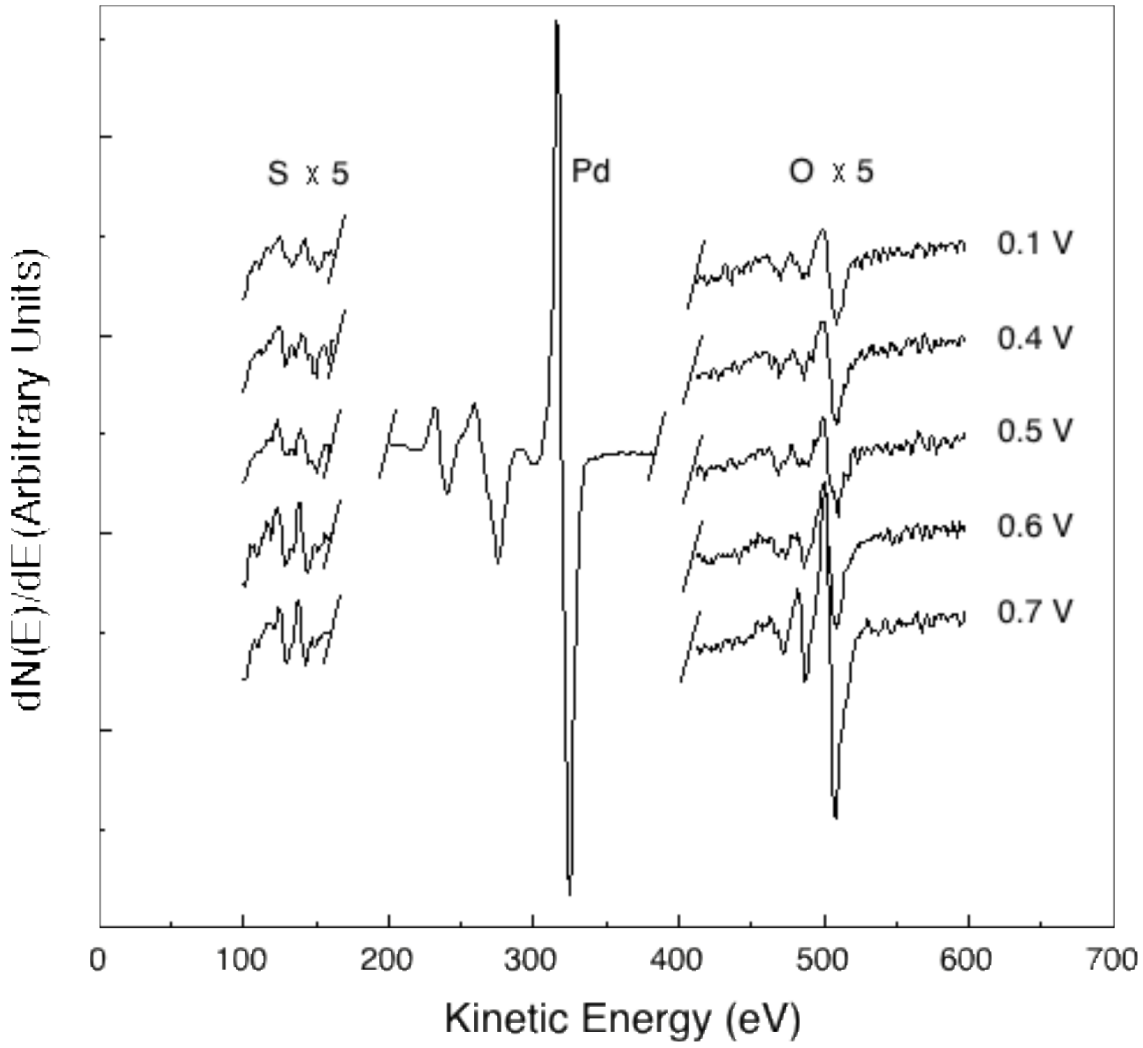

Figure 41. AES spectra of Pd(100) surfaces with η^2-H_2Q subjected to different oxidation potentials (0.4 V, 0.5 V, 0.6 V, and 0.7 V) in 10 m*M* H_2SO_4 for 3 minutes.

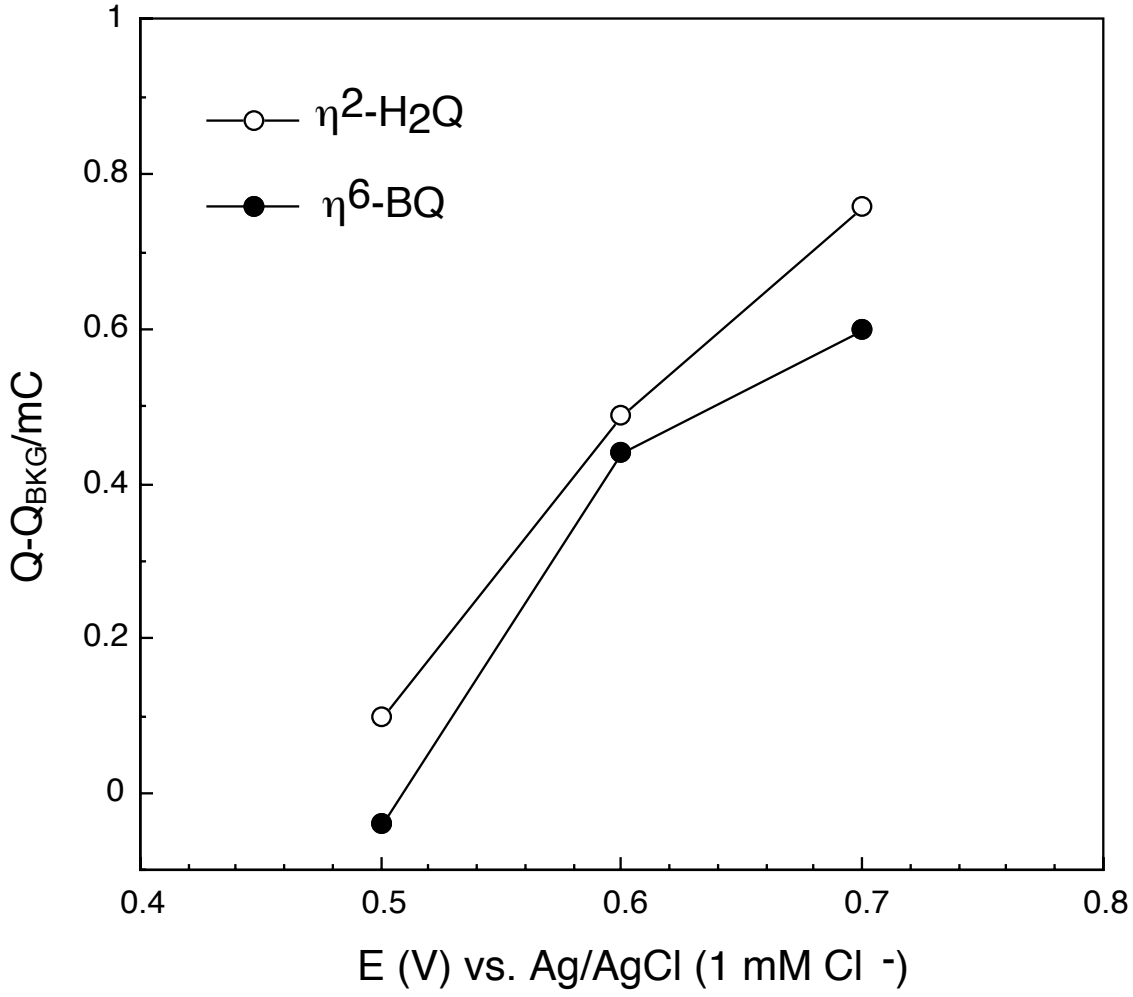

Figure 42. Coulometric charge transferred during 3-minute anodic oxidation at 0.5 V, 0.6 V and 0.7 V for chemisorbed species with different orientations. The background charge obtained on a clean Pd(100) surface was deducted.

Anodic Oxidation at Fixed Potentials and Varied Electrolysis Times

The influence of electrolysis time at a given anodic-oxidation potential was investigated. This kinetic experiment intended to measure the rate of decrease in the coverages in terms of the extinction of the integrated intensity of the γ(CH) peak. Unfortunately, a complete rate law could not be formulated, since although the surface coverage of the organic can be monitored in terms of the γ(CH) peak area, the coverages and/or solution concentrations of other reactants, e.g. the OH_{ads}, O_{ads}, and $O_{2(aq)}$, cannot be determined. These experiments are useful, nevertheless, to differentiate the anodic oxidation rates of η^2- and η^6-oriented species.

Figure 43 to Figure 45 give the time-dependent HREELS results for Pd-η^2-H_2Q complexes anodically oxidized at 0.4 V, 0.5 V, and 0.6 V. Data for only 3-minute oxidation at 0.7 V was shown in Figure 40. The chemisorbed organic species is only slowly oxidatively desorbed from the surface at 0.4 V, as evidenced by the gradual decrease in γ(CH) peak intensity as well as the moderate increase in the sulfate peak intensity (Figure 43). Note that the structural features for the chemisorbed organic species persist even after 12 minutes, which indicates that the extent of oxidation is limited at this potential. Unlike results obtained in the absence of chemisorbed organic complexes in a pure blank electrolyte, no surface hydroxyl peaks were observed on the electrode surface coated with the surface complexes at 0.4 V; that is, at 0.4 V, there is still a large fraction of chemisorbed species that prevent surface oxidation. Data obtained at 0.5 V (Figure 44) shows an increased oxidation extent compared to 0.4 V. The loss features due to Pd-η^6-BQ_{ads} surface complex decrease with time, but some surface

complexes still remain even after 8 minutes at 0.5 V, as evidenced from the presence of γ(CH) loss peak in the 8-minute spectrum. The surface showed signs of early oxidation in the growth of one loss peak in the 3300 cm^{-1} region. However, surface oxidation is insignificant if compared to the spectrum obtained on a clean electrode. The oxidation rate became prominent above 0.6 V, shown by the disappearance of the chemisorbed species even at 3 minute (Figure 40 and Figure 45). The 8-minute spectrum at 0.6 V and the 3-minute spectrum at 0.7 V appear essentially identical to their respective control clean Pd(100) data, implying that in both cases, the surface is oxidized to a similar extent with or without the involvement of chemisorbed organic species under these conditions. There were no other new features observed in HREELS data besides what have been described above, indicating the absence of partially oxidized intermediates on the surface. In other words, the chemisorbed species were desorbed from the surface upon either full or partial oxidation. It is worth to mention that the adsorbed organic complexes are oxidized one at a time, instead of being converted to the same partial oxidation products. The surface is left with the remaining intact organic species, not the oxidation intermediates.

At 0.4 V, the coulometric result of a clean surface is higher than that obtained on the electrode with η^2-H_2Q complexes (Figure 46). This is because at such low potential, the oxidation of both organic and surface does not proceed at an appreciable rate. At higher potentials, however, the charges obtained on surfaces with η^2-H_2Q complexes are higher than those of a clean surface.

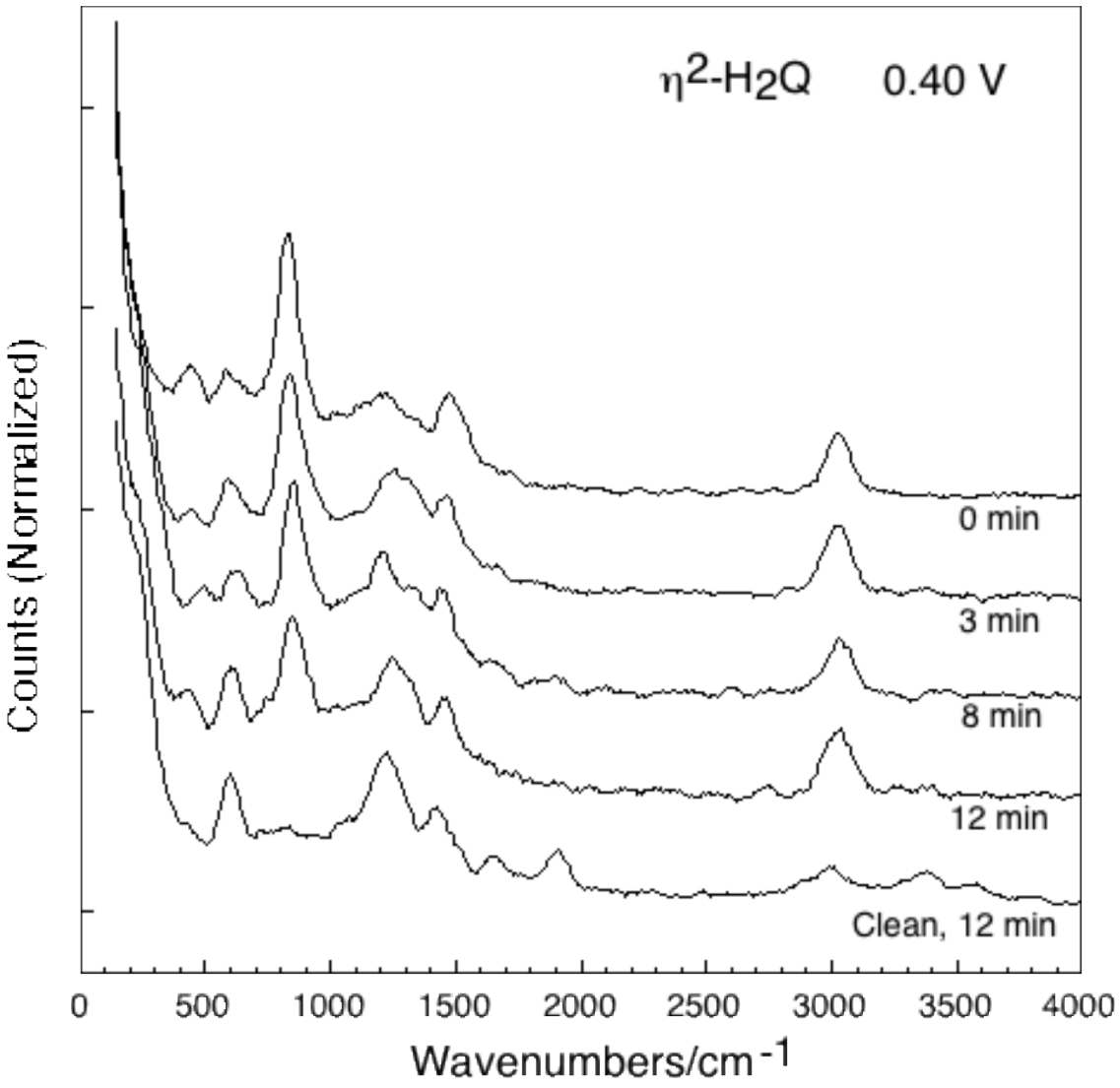

Figure 43. HREEL spectra of Pd(100) surfaces with η^2-H_2Q surface complexes subjected to anodic oxidation at 0.4 V in 10 m*M* H_2SO_4 for different electrolysis time: 3, 8, and 12 minutes, respectively.

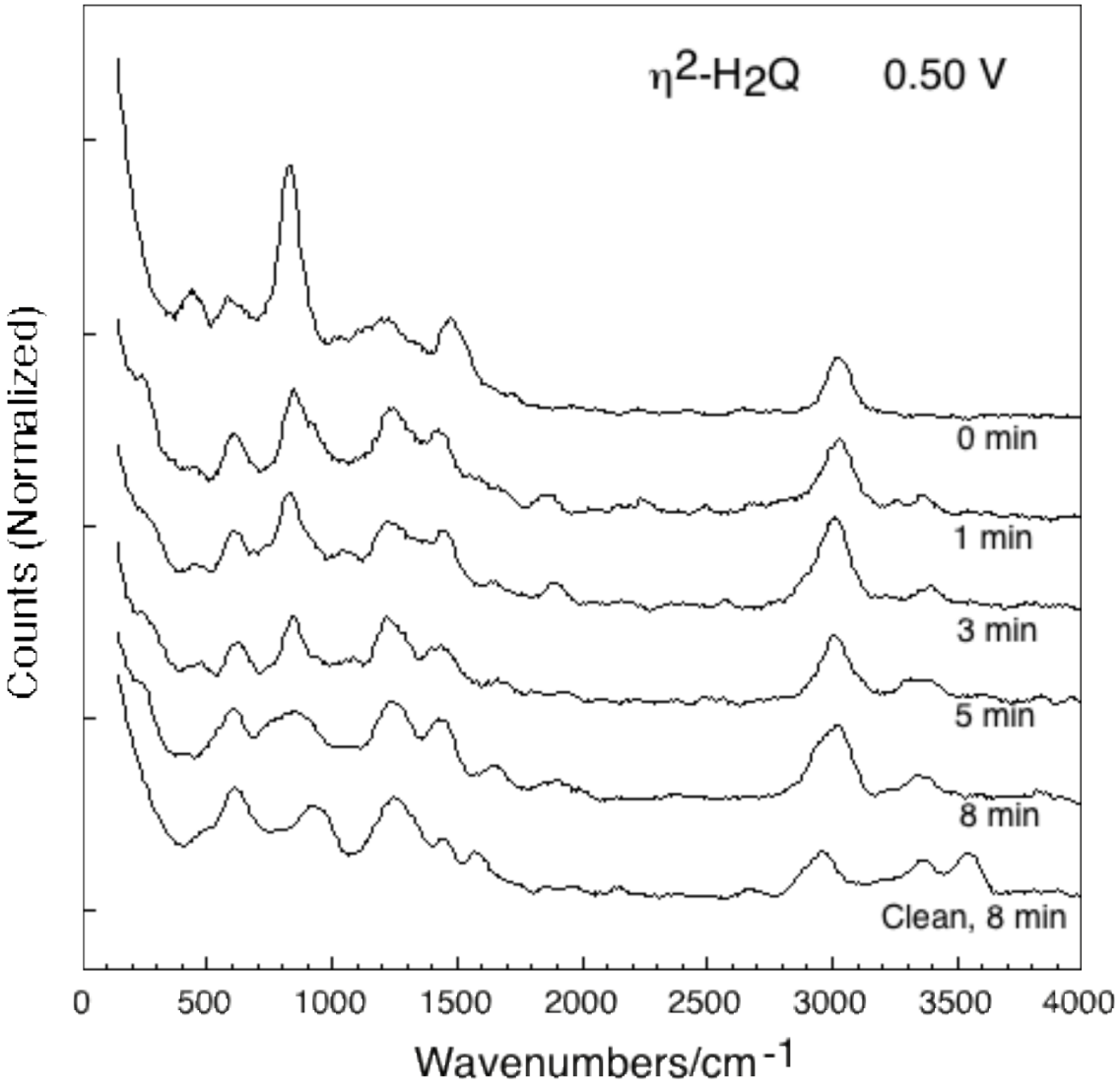

Figure 44. HREEL spectra of Pd(100) surfaces with η2-H2Q surface complexes subjected to anodic oxidation at 0.5 V in 10 mM H2SO4 for different electrolysis time: 1, 3, 5 and 8 minutes, respectively.

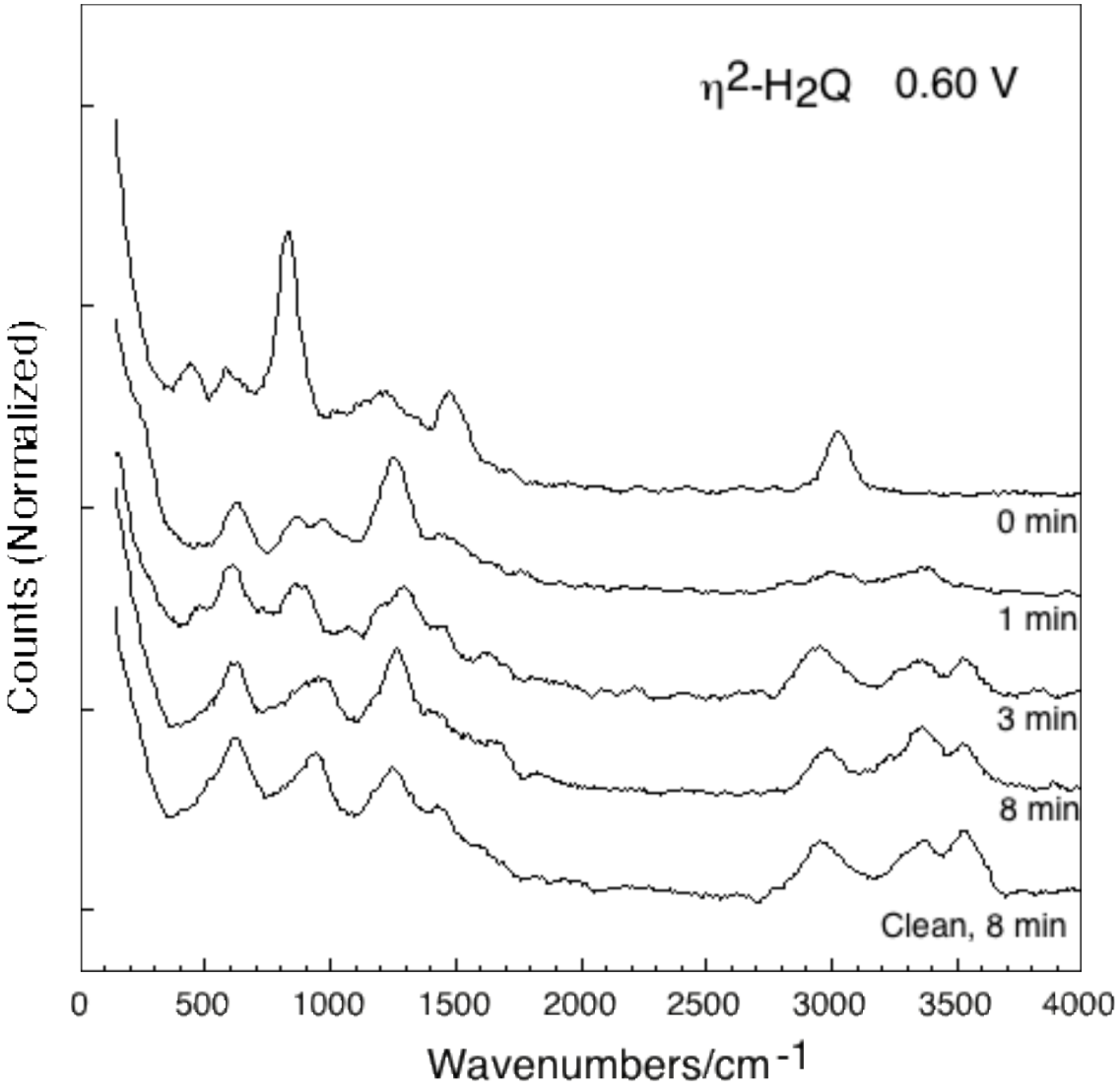

Figure 45. HREEL spectra of Pd(100) surfaces with η^2-H_2Q surface complexes subjected to anodic oxidation at 0.6 V in 10 m*M* H_2SO_4 for different electrolysis time: 1, 3, and 8 minutes, respectively.

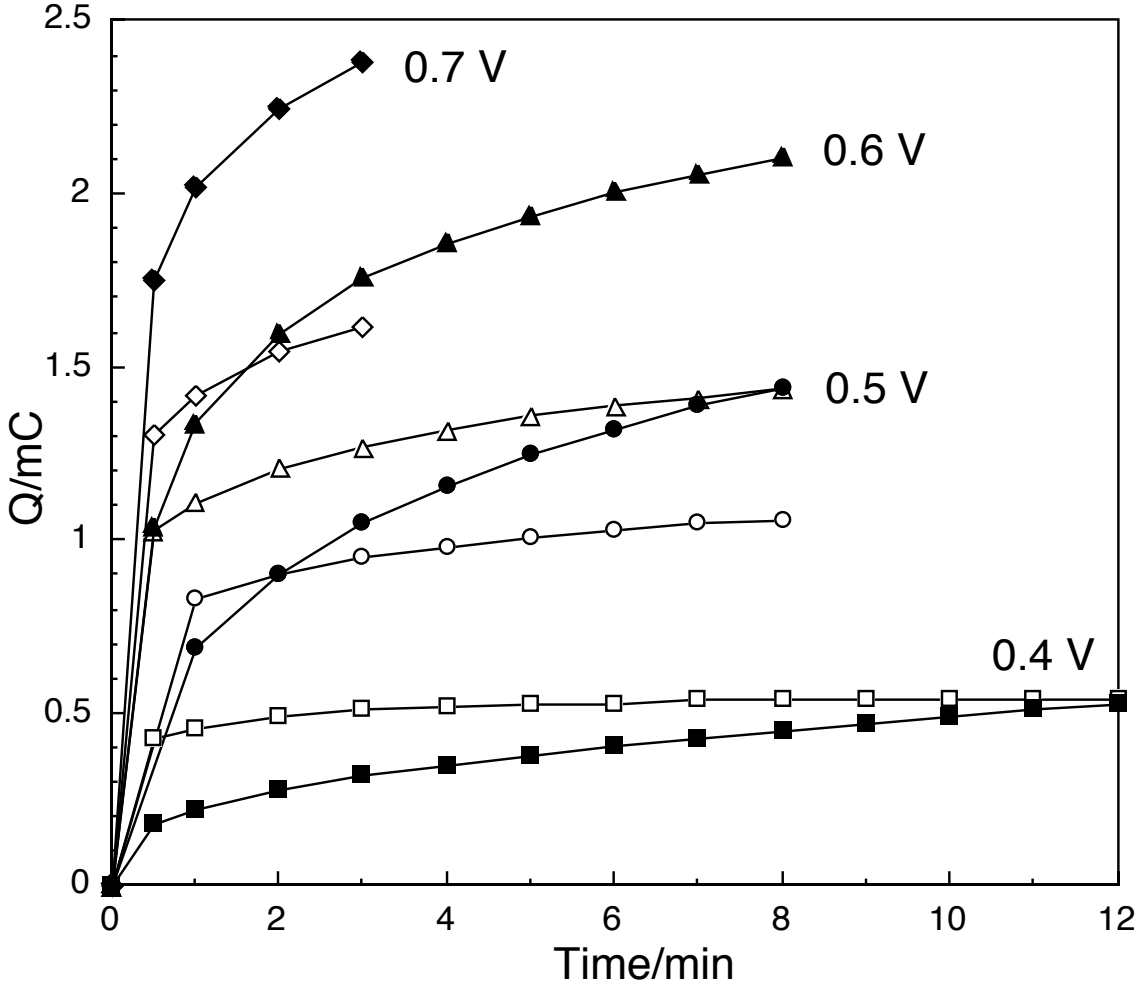

Figure 46. Chronocoulometric data of Pd(100) with η^2-H_2Q surface complexes oxidized in 10 m*M* H_2SO_4 at different potentials for different electrolysis time. The empty symbols are data collected on a clean Pd(100) electrode; the solid symbols are data obtained on a Pd(100) with η^2-H_2Q surface complexes.

Experiments identical to those described for η^2-H_2Q complexes were carried out also on η^6-BQ. The resulting chronocoulograms are given in Figure 51. Accompanying HREEL spectra are shown in Figure 47 to Figure 50. A cursory comparison of the η^2 and η^6 data suggest that there is little difference between them. On a closer analysis, however, the following significant differences are revealed.

(*i*) The surface coverage of η^6-BQ is almost half of that of η^2-H_2Q, but the anodic oxidation charge for both are not that different from one another (e.g. 2.22 mC for η^6 vs. 2.38 mC for η^2 after 3-minute anodic oxidation at 0.7 V); this result can only signify that the extent of oxidative desorption of η^2-H_2Q is much lower than that of η^6-BQ. That is, n_{ox} for η^6-BQ is much higher than n_{ox} of η^2-H_2Q, in agreement of what was described in TLE Studies.

(*ii*) Higher quantities of surface species are oxidatively desorbed from the surface during the electrochemical oxidation of η^2-H_2Q. This fact can be shown by measuring the area underneath the normalized HREELS γ(CH) peak: the decrease in the γ(CH) peak area is greater for η^2-H_2Q than η^6-BQ. Anodic oxidation reaction rates at different potentials for both species were determined based on the disappearance of the γ(CH) peak as follows:

$$\text{Rate}' \equiv \frac{\gamma(\text{CH})A_{(t_2)} - \gamma(\text{CH})A_{(t_1)}}{t_2 - t_1} \tag{27}$$

$$\text{Anodic Oxidation Rate} = -\text{Rate of disappearance of } \gamma(\text{CH}) \tag{28}$$

$$\text{Rate} \equiv -\frac{\gamma(\text{CH})A_{(t_2)} - \gamma(\text{CH})A_{(t_1)}}{t_2 - t_1} \tag{29}$$

The reaction rates shown in Table 4 demonstrate that the rate of anodic oxidation of η^2-H_2Q is more than twice than that of η^6-BQ. This difference in rate is most probably due to the higher adsorption strength of η^6-BQ and the greater number of electrons involved in the anodic oxidation of η^6-BQ compared to that of η^2-H_2Q.

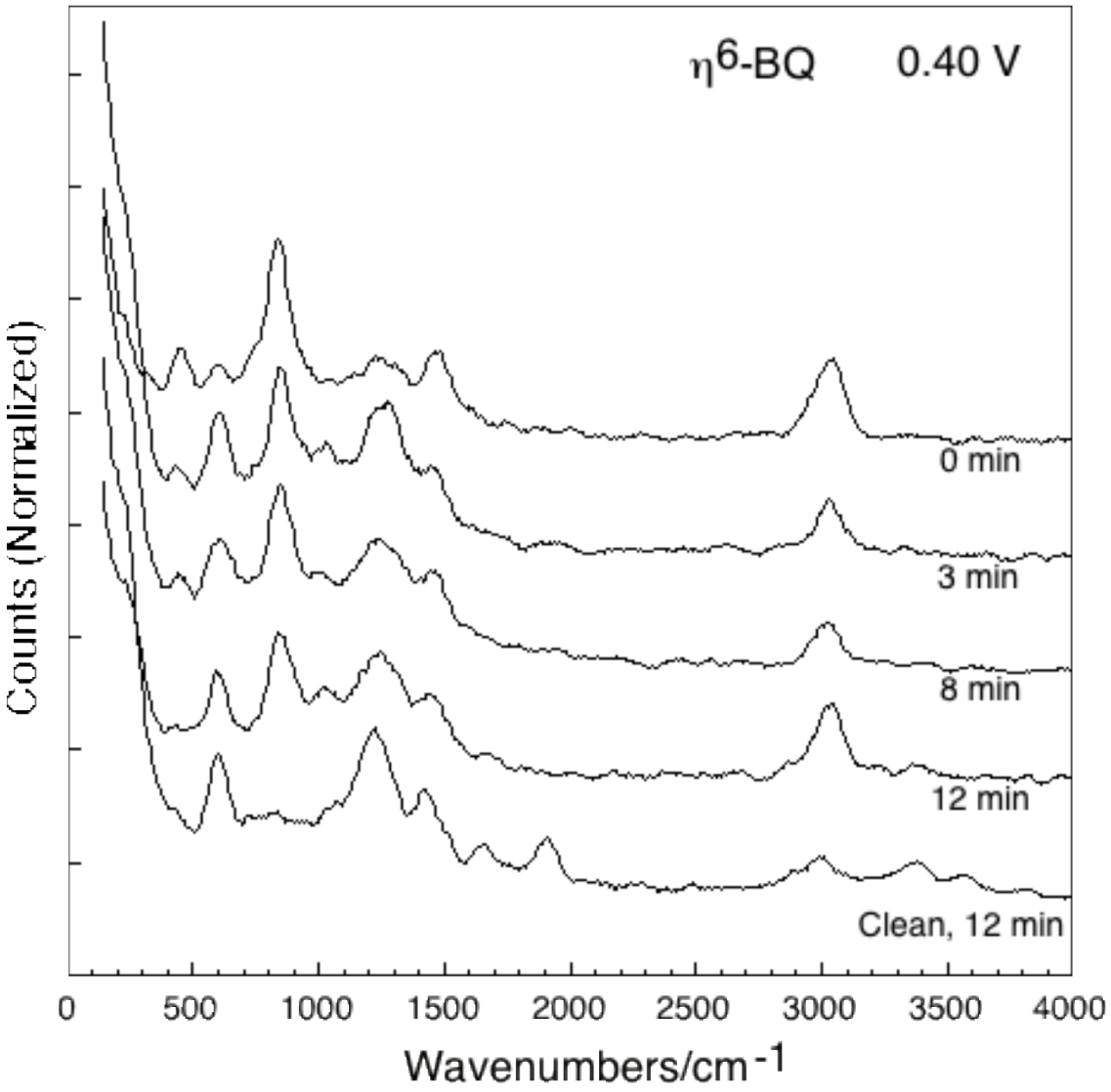

Figure 47. HREEL spectra of Pd(100) surfaces with η^6-BQ surface complexes subjected to anodic oxidation at 0.4 V in 10 m*M* H_2SO_4 for different electrolysis time: 3, 8, and 12 minutes, respectively.

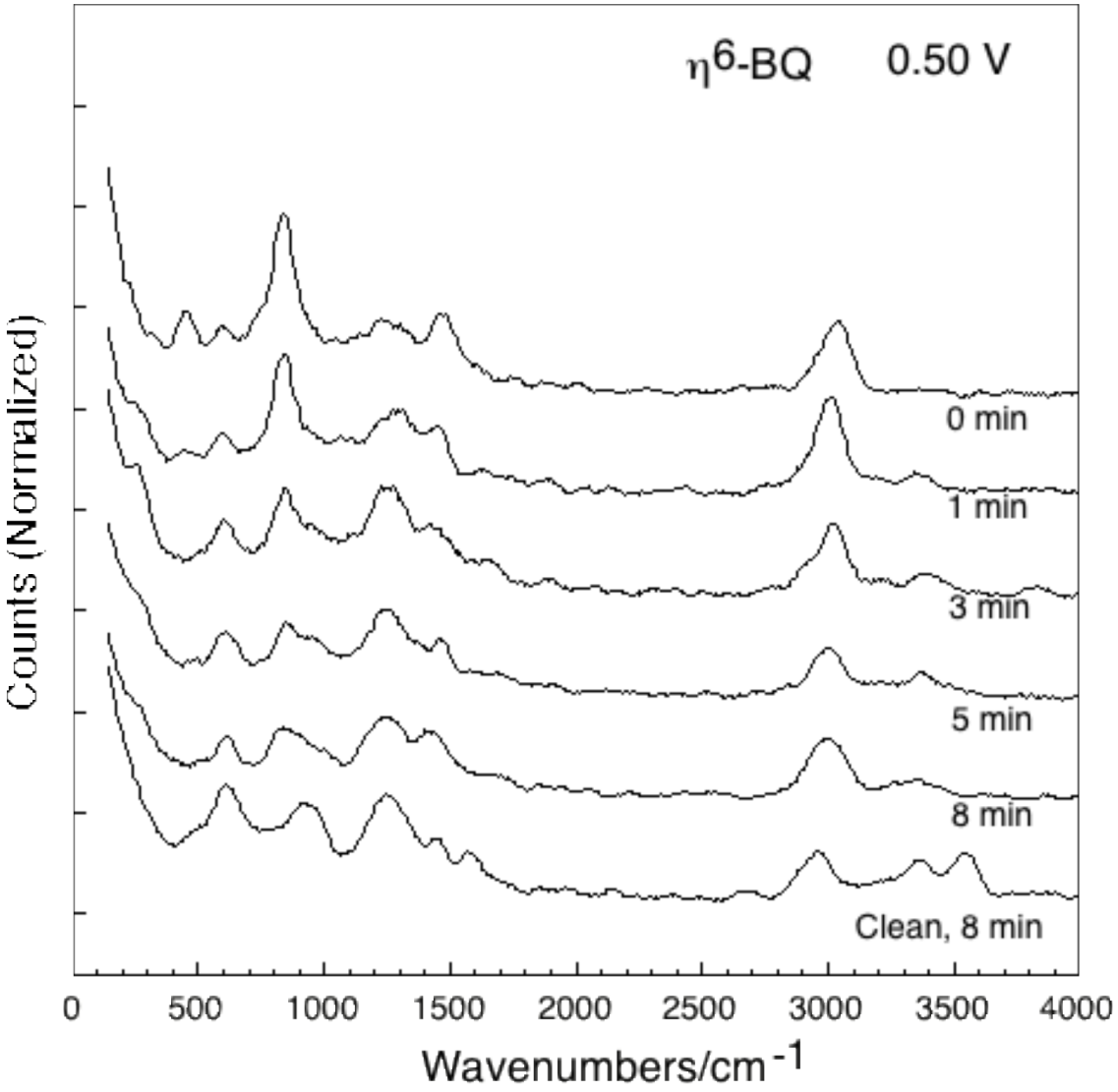

Figure 48. HREEL spectra of Pd(100) surfaces with η^6-BQ surface complexes subjected to anodic oxidation at 0.5 V in 10 m*M* H_2SO_4 for different electrolysis time: 1, 3, 5, and 8 minutes, respectively.

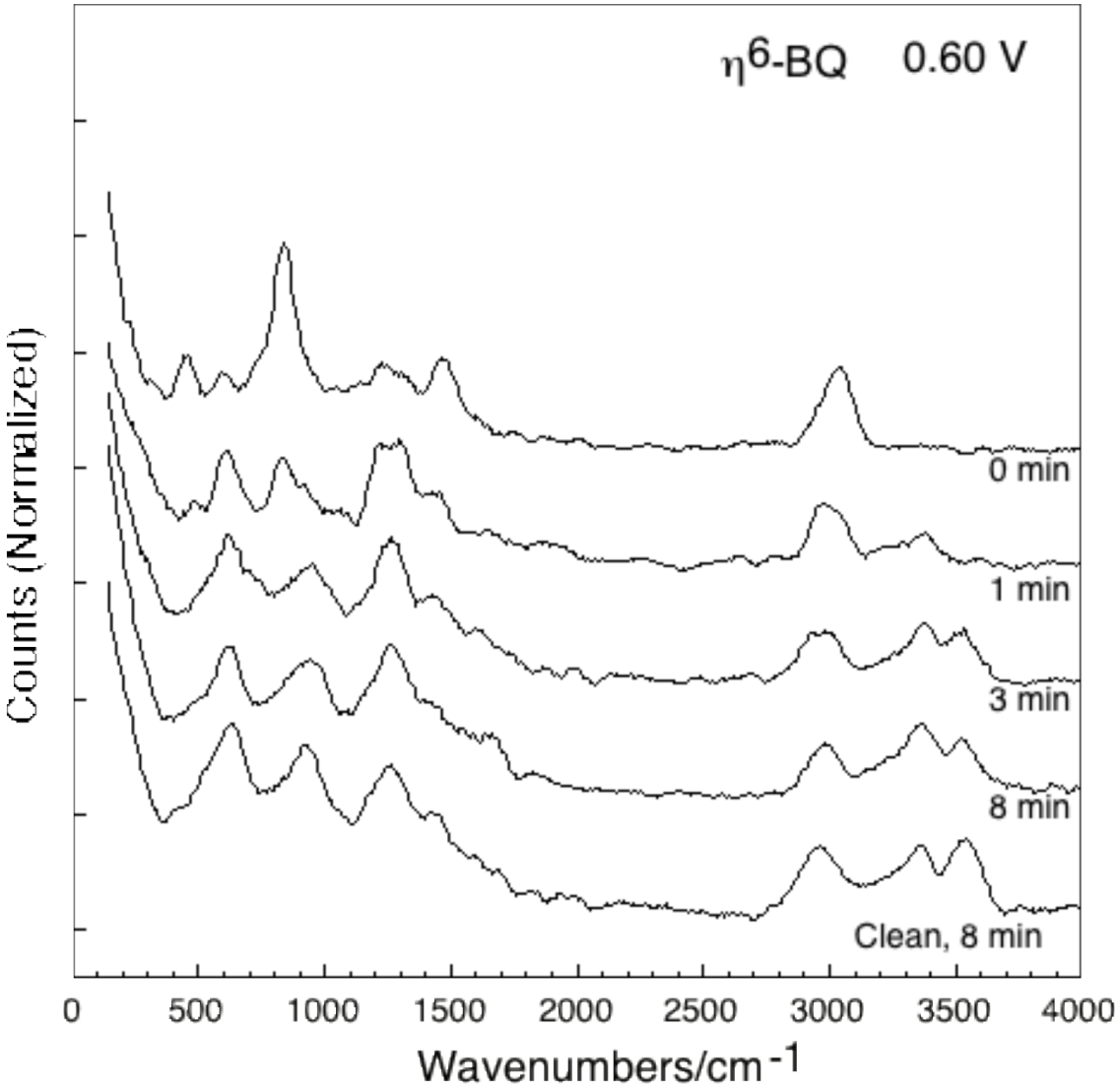

Figure 49. HREEL spectra of Pd(100) surfaces with η^6-BQ surface complexes subjected to anodic oxidation at 0.6 V in 10 m*M* H_2SO_4 for different electrolysis time: 1, 3, and 8 minutes, respectively.

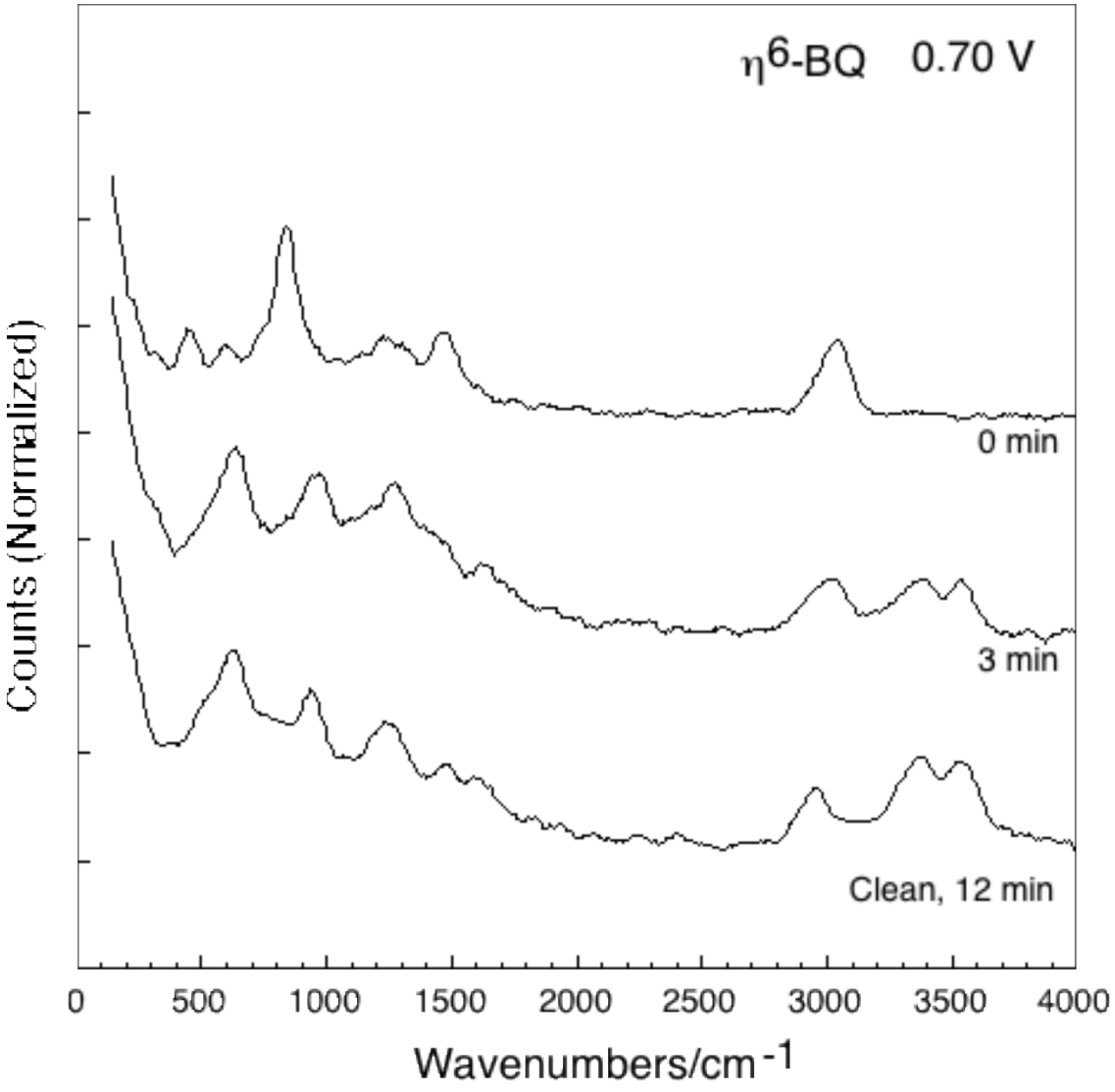

Figure 50. HREEL spectra of Pd(100) surfaces with η^6-BQ surface complexes subjected to anodic oxidation at 0.7 V in 10 m*M* H_2SO_4 for 3 minutes.

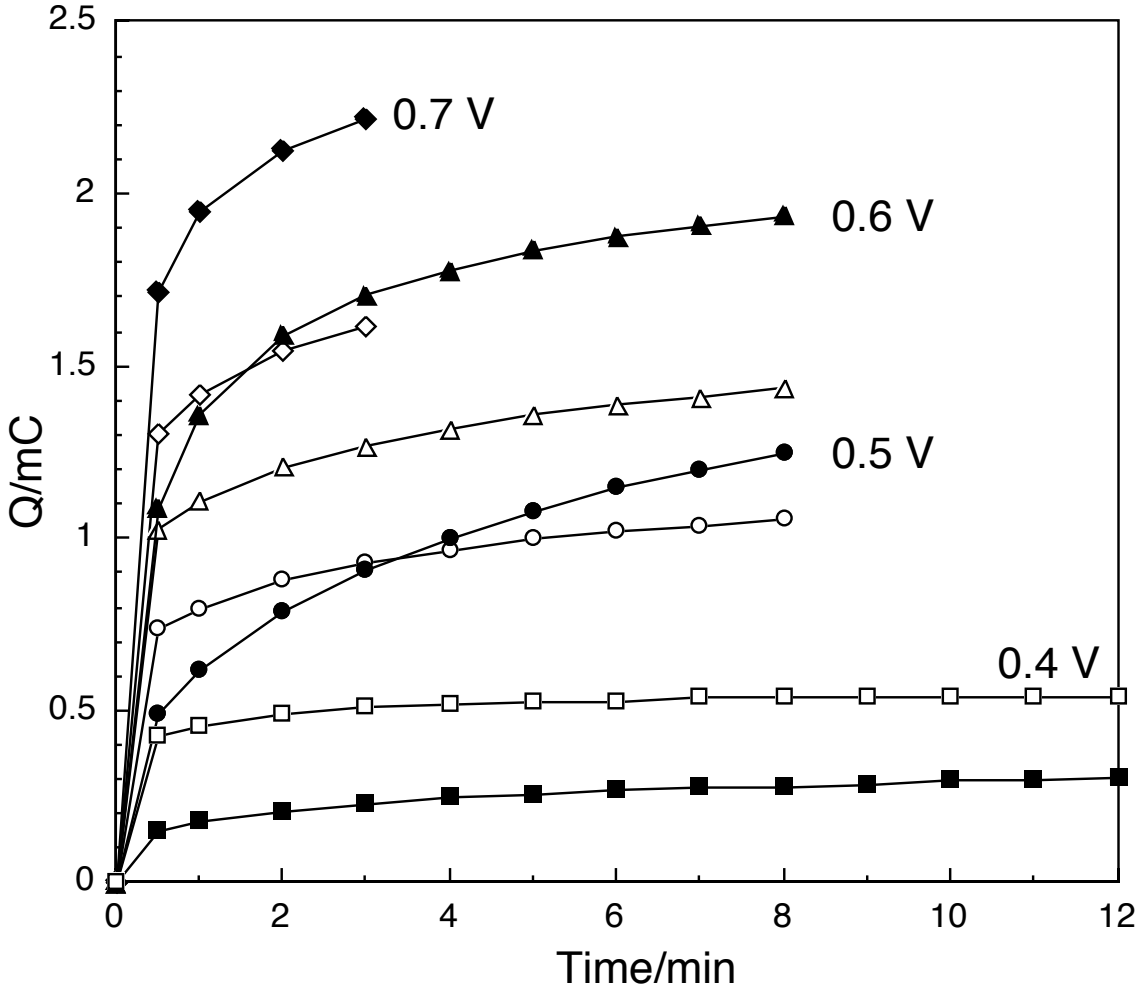

Figure 51. Chronocoulometric data of Pd(100) with η^6-BQ surface complexes oxidized in 10 m*M* H_2SO_4 at different potentials for different electrolysis time. The empty symbols are data collected on a clean Pd(100) electrode; the solid symbols are data obtained on a Pd(100) with η^6-BQ surface complexes.

Table 4. Anodic oxidation rate of Pd-η^2-H_2Q and Pd-η^6-BQ complexes at different potentials.

Rate[a] / min^{-1}	Pd-η^2-H_2Q	Pd-η^6-BQ
0.4 V	258.10	99.11
0.5 V	748.88	381.12
0.6 V	6358.18	2346.22

[a] The rates were determined as described in the text.

CONCLUSIONS

The chemisorption and anodic oxidation of H_2Q on Pd surfaces were investigated using a combination of electrochemistry (EC), Auger electron spectroscopy (AES), high-resolution electron energy loss spectroscopy (HREELS), and electrochemical scanning tunneling microscopy (EC-STM). The results afforded the following conclusions:

(*i*) At low adsorbate concentrations (≤ 0.1 m*M*), H_2Q is oxidatively chemisorbed onto Pd surfaces, forming surface-coordinated benzoquinone (η^6-BQ) oriented parallel to the surface, but with a slight tilt.

(*ii*) The oxidative chemisorption of H_2Q at higher concentrations (≥ 1 m*M*) leads to the formation of an edge-oriented diphenolic species (η^2-H_2Q).

(*iii*) Chemisorption from BQ solutions yields chemisorbed species identical to those obtained from H_2Q solutions.

(*iv*) The possibility exists that a significant fraction of the η^2-chemuisorbed H_2Q is desorbed in ultra-high vacuum at ambient temperatures.

(*v*) Anodic oxidation does not occur unless the organic compound is chemisorbed onto the pure-metal surface; no significant organic chemisorption takes place at an oxide-coated surface.

(*vi*) The rate for the anodic-oxidation reaction is strongly dependent upon the initial adsorbate orientation; the rate for the oxidation of η^2-H_2Q is more than twice that for η^6-BQ.

(*vii*) The extent of the anodic oxidation is profoundly dependent upon the initial orientation of the adsorbed molecules. η^6-oriented species are oxidized completely to carbon dioxide; anodic oxidation of the η^2-coordinated organic yields less extensively oxidized products (which have not been identified).

(*viii*) The chemisorbed species are not oxidized (to the same extent) simultaneously; instead, oxidation occurs one molecule at a time. That is, molecules that survive the anodic oxidation and remain on the surface retain their original identities.

REFERENCES

[1] A. J. Bard, L. R. Faulkner, *Electrochemical Methods,* New York: Wiley, 1980.

[2] K. Itaya, *Progress in Surface Science*, **1998**, *58 (3)*, 121.

[3] G. A. Somorjai. *Introduction to Surface Chemistry and Catalysis* New York: John Wiley, 1994.

[4] K. P.Peterson, R. C. Larock, *J. Org. Chem.* **1998**, *63*, 3185.

[5] T. Nishimura, T. Onoue, K. Ohe, S. Uemura, *Tetrahedron Lett.* **1998**, *39*, 6011.

[6] S. R. Fix, J. L. Brice, S. Stahl, *Angew. Chem. Int. Ed.* **2002**, *41*, 164.

[7] D. R. Lide, ed. *Handbook of Chemistry and Physics*. Boca Raton, FL: CRC Press, 1998.

[8] M. Pourbaix, *Atlas d'Equilibres Electrochimiques 25°C*, Paris: Gutier-Villars, 1963.

[9] T. Matsuzaki, A. Nakamura, *Catal. Surv. Jpn*. **1997**, *1*, 77.

[10] Q. Zhou, C. Zhang, X. Lu, Z. Wu, *Dianhuaxue*, **2000**, *6(3)*, 329.

[11] M. P. Soriaga, A. T. Hubbard, *J. Am. Chem. Soc.* **1982**, *104*, 2735.

[12] M. P, Soriaga, E. B. Soriaga, A. T. Hubbard, J. B. Benziger, K. W. P. Pang, *Inorganic Chemistry*, **1985**, *24(1)*, 65.

[13] L. C. Pauling, *The Nature of the Chemical Bond*, 3rd ed.; Ithaca, NY: Cornell University Press, 1960.

[14] K. W. P. Pang, J. B. Benziger, M. P. Soriaga, A. T. Hubbard, *J. Phys. Chem.* **1984**, *88*, 4583.

[15] M. P. Soriaga, J. L. Stickney, A. T. Hubbard, *J. Electroanal. Chem.* **1983**, *144*, 207.

[16] M. P. Soriaga, J. L. Stickney, A. T. Hubbard, *J. Molecular Catalysis* **1983**, *21*, 211.

[17] T. Mebrahtu, G. M. Berry, M. P. Soriaga, *J. Electroanal. Chem.* **1988**, *239*, 375.

[18] M. P. Soriaga, *Chem. Rev.* **1990**, *90*, 771.

[19] F. Lu, G. N. Salaita, L. Laguren-Davidson, D. A. Stern, E. Wellner, D. G. Frank, N. Batina, D. C. Zapien, N. Walton, A. T. Hubbard, *Langmuir* **1988**, *4*, 637.

[20] J. E. Soto, Y. G. Kim, M. P. Soriaga, *Electrochem. Commun.* **1999**, *1*, 135.

[21] J. F. Rodriguz, T. Mebrahtu, M. P. Soriaga, *J. Electroanal. Chem.* **1987**, *233(1-2)*, 283.

[22] M. P. Soriaga, J. A. Schimpf, J. B. Abreu, A. Carrasquillo, W. Temesghen, R.J. Barriga, J.-J. Jeng, k. Sashikata and K. Itaya. *Surf. Sci*. **1995,** *335,* 273.

[23] Y.-G. Kim, M. P. Soriaga. *J. Phys. Chem. B.* **1998**, *102*, 6188.

[24] G. A. Somorjai, *Chemistry in Two Dimensions*, Ithaca, NY: Cornell University, 1981.

[25] G. Ertl, J. Kuppers, *Low Energy Electrons and Surface Chemistry*, Deerfield Beach, FL: VCH Publishers, 1985.

[26] D. P. Wooddruff and T. A. Delchar, *Modern Techniques of Surface Science*, New York: Cambridge University Press, 1986.

[27] A. T. Hubbard (Ed.), *The Handbook of Surface Imaging and visulization*, Boca Raton, FL: CRC Press, 1995.

[28] A. Zangwill, *Physics at Surfaces*, New York: Cambridge University Press, 1996.

[29] T. H. Rhodin, G. Ertl, *The Nature of the Surface Chemical Bond*, New York: North-Holand, 1979.

[30] K. D. Briggs, M. P. Seah, *Practical Surface Analysis by Auger and X-Ray Photoelectron Spectroscopy*, New York: Wiley, 1983.

[31] L. E. Davis, N. C. MacDonald, P. W. Palmberg, G. E. Riach, R. E. Weber, *Handbook of Auger Electron Spectroscopy*, 2nd Ed., Eden Prairie, MN: Perkin Elmer Corp., 1976.

[32] J. A. Shoeffer, A. T. Hubbard, *Anal. Chem*. **1977**, *49*, 2330.

[33] D. Lin-Vien, N. B. Colthup, W. G. Fately, and J. G. Grasselli, *The Handbook of Infrared and Raman Characteristic Frequencies of Organic Molecules*, San Diego, CA: Academic Press, 1991.

[34] E. Maslowski, *Vibrational Spectra of Organometallic Compounds*, New York: Wiley, 1977.

[35] J. Jungwirthova, L. L. Kesmodel, *J. Phys. Chem. B* **2001**, *105(3)*, 674-680.

[36] A. M. Bradshaw, F. M. Hoffmann, *Surf. Sci*. **1978**, *72*, 513.

[37] D. A. Bonnell (Ed.), *Scanning Tunneling Microscopy and Spectroscopy; Theory, Techniques, and Applications*, New York: VCH Publishers, 1993

[38] J. Tersoff, P. Hansma, *J. Appl. Phys.* **1987**, *R1*, 2.

[39] R. Sonnenfeld, P. K. Hansma, *Science* **1986**, *232*, 211.

[40] J. Clavilier, R. Faure, G. Guinet, R. Durand, *J. Electroanal. Chem.* **1980**, *107*, 205

[41] J. Clavilier, *J. Electroanal. Chem.* **1980**, *107*, 211.

[42] K. Sashikata, Y. Matsui, K. Itaya, M.P. Soriaga, *J. Phys. Chem.* **1996**, *100(51)*, 20027.

[43] X. Chen, J. Sanabria-Chinchilla, M. P. Soriaga, *Electroanalysis*, **2004**, (submitted).

[44] M. P. Soriaga, P. H. Wilson, A. T. Hubbard, *J. Electroanal. Chem.* **1982**, *142*, 317.

[45] M. P. Soriaga, J. H. White, D. Song, V. K. F. Chia, P.O. Arrhenius, A.T. Hubbard, *Inorg. Chem.* **1985**, *24(1),* 73.

[46] J. E. Soto, *Ph.D. dissertation*, College Station, TX: Texas A&M University, 2001.

[47] M. P. Soriaga, *Chem. Rev.*, **1990**, *90*, 771.

[48] Y-G. Kim, J. B. Soriaga, G. Vigh, M. P. Soriaga, J. Col. Inter. Sci. 2000, 227(2), 505-509.

[49] F. C. Nart, T. Iwasita, *J. Electroanal. Chem.* **1991**, *308*, 277-293

[50] F. C. Nart, T. Iwasita, *Electrochim. Acta* **1994**, *39*, 961

[51] F. C. Nart, T. Iwasita, M. Weber, *Electrochimi. Acta* **1994**, *39*, 2093.

[52] F. C. Nart, T. Iwasita, M. Weber, *Electrochimi. Acta* **1995**, *40*, 53.

[53] N. Hoshi, M. Kuroda, O. Koga, Y. Hori, *J. Phys. Chem. B* **2002**, *106*, 9107-9113

[54] S. M. Chackalackal, F.E. Stafford, *J. Am. Chem. Soc.* **1966**, *88*, 723.

[55] K. Stopperka, F. Z. Lilz, *Anorg. Allg. Chem.* **1969**, *370*, 49.

[56] P. E. Hintze, H. G. Kjaergaard, V. Vaida, and J. B. Burkholder, *J. Phys. Chem. A* **2003**, *107*, 1112.

[57] F. R. Hartley, *The Chemisrtry of Platinum and Palladium*, New York: Wiley, 1973.

[58] G. D. Waddill, L. L. Kesmodel, *Phys. Rev. B* **1985**, *32(4)*, 2107.

[59] C. Gregoire, L. M. Yu, F. Bodino, M. Tronc, J. J. Pireaux, *J. Elect. Spectros. and Rel. Phenom.* **1993**, *98-99*, 67.

[60] P. A. Thiry, M. Liehr, J. J. Pireaux, R. Caudano, *Physica Sripta* **1971**, *35*, 229.

[61] L. L. Kesmodel, in: A.T. Hubbard (Ed.), *Surface Imaging and Visualization*, Boca Raton, FL: CRC Press, 1995, Ch. 18.

[62] A. T. Hubbard, *Chem. Rev.* **1988**, *88*, 633.

[63] M. P. Soriaga, *Prog. Surf. Sci.* **1992**, *39*, 325.

[64] J. T. Yates Jr., T. E. Madey (Eds.), *Vibrational Spectroscopy of Molecules on Surfaces*, New York: Plenum, 1987.

[65] F. Lu, G. N. Salaita, L. Laguren-Davidson, D. A. Stern, E. Wellner, D. G. Frank, N. Batina, D. C. Zapien, N. Walton, A. T. Hubbard, *Langmuir* **1988**, *4*, 639.

[66] M. W. Urban, *Vibrational Spectroscopy of Molecules and Macromolecules on Surfaces*, New York: John Wiley & Sons, Inc., 1993, Ch. 4.

[67] M. A. Henderson, S. A. Chambers, *Surf. Sci.* **2000**, *449*, 135-150.

VITA

XIAOLE CHEN

Department of Chemistry
Texas A&M University
TX 77843-3255

Email: xiaole-chen@neo.tamu.edu
Cell: 979-218-6106
Fax: 979-845-9287

EDUCATION

Ph. D., Analytical Chemistry. Texas A&M University, College Station, TX. 2004
Dissertation: "Chemisorption and Anodic Oxidation of Aromatic Molecules on Pd Electrode Surface: Studies by UHV-EC-STM".

M. S., Analytical Chemistry. Beijing Normal University, Beijing, P. R. China. 1998
Thesis: "Electrochemistry and Electrocatalysis with Some Proteins Incorporated in Mimic Biomembrane Thin Film on Pyrolytic Graphite Electrodes".

B. S., Chemistry Education. Hunan Normal University, Changsha, P. R. China. 1995

PUBLICATIONS

1. *"The Chemisorption and Anodic Oxidation of Aromatic Molecules at Smooth Polycrystalline Palladium: Studies by Thin-layer Electrochemistry"* X. Chen, J. Sanabria-Chinchilla, M. P. Soriaga, Electroanalysis, submitted.
2. *"Molecular Adsorption at Well-defined Electrode Surfaces: Benzene on Pd(111) Studied by EC-STM and HREELS"* Y.-G. Kim, J. E. Soto, X. Chen, Y-S Park, M. P. Soriaga, J. Electroanal. Chem., 2003, 554-555, 167-174.
3. *"Self-discharge of Secondary Lithium-ion Graphite Anodes"* C. Wang, X. Zhang, A. Appleby, X. Chen, F. Little., J. Power Sources, 2002, 112, 98-104.
4. *"Direct Electrochemistry of Cytochrome C at Eastman AQ Ionomer Film Electrodes"* X. Chen, N. Hu, Y. Zeng, Journal of Beijing Normal University (Natural Science), 2002, 38 (4), 515-520.
5. *"Molecular Chemisorption at Well-defined Pd(111) Electrode Surfaces: Hydroquinone Sulfonate Studied by UHV-EC-STM"* J. E. Soto, Y-G. Kim, X. Chen, Y-S. Park, M. P. Soriaga, J. Electroanal. Chem., 2001, 500, 374-378.
6. "Ordered Electrochemically Active Films of Hemoglobin, Didodecyldimethylammonium Ions, and Clay" X. Chen, N. Hu, Y. Zeng, J. F. Rusling, and J. Yang, Langmuir, 1999, 15, 7022-7030.